AFFDL-TR-66-220

FRACTURE OF BRITTLE MATERIALS UNDER TRANSIENT MECHANICAL AND THERMAL LOADING

Ralph L. Barnett
Paul C. Hermann
James R. Wingfield
Chester L. Connors

IIT Research Institute

151

NOTICES

When Government drawings, specifications, or other data are used for any purpose other than in connection with a definitely related Government procurement operation, the United States Government thereby incurs no responsibility nor any obligation whatsoever; and the fact that the Government may have formulated, furnished, or in any way supplied the said drawings, specifications, or other data, is not to be regarded by implication or otherwise as in any manner licensing the holder or any other person or corporation, or conveying any rights or permission to manufacture, use, or sell any patented invention that may in any way be related thereto.

Copies of this report should not be returned to the Research and Technology Division unless return is required by security considerations, contractual obligations, or notice on a specific document.

AFLC-WPAFB-MAR 68 1500

Blank pages

IV, VI, 14, 128,
142

AFFDL-TR-66-220

FRACTURE OF BRITTLE MATERIALS UNDER TRANSIENT MECHANICAL AND THERMAL LOADING

Ralph L. Barnett
Paul C. Hermann
James R. Wingfield
Chester L. Connors

IIT Research Institute

TECHNICAL REPORT AFFDL-TR-66-220

March 1967

Air Force Flight Dynamics Laboratory
Research and Technology Division
Air Force Systems Command
Wright-Patterson Air Force Base, Ohio

Unclassified

Security Classification

DOCUMENT CONTROL DATA - R&D

(Security classification of title, body of abstract and indexing annotation must be entered when the overall report is classified)

1. ORIGINATING ACTIVITY (Corporate author)	2a. REPORT SECURITY CLASSIFICATION
IIT Research Institute Chicago, Illinois	Unclassified
	2b. GROUP None

3. REPORT TITLE

Fracture of Brittle Materials Under Transient Mechanical and Thermal Loading

4. DESCRIPTIVE NOTES (Type of report and inclusive dates)

Final Report

5. AUTHOR(S) (Last name, first name, initial)

Ralph L. Barnett Paul C. Hermann
James Wingfield Chester Connors

6. REPORT DATE	7a. TOTAL NO. OF PAGES	7b. NO. OF REFS
March 1967	149	17

8a. CONTRACT OR GRANT NO.	9a. ORIGINATOR'S REPORT NUMBER(S)
AF 33(615)-2468 b. PROJECT NO. 1368 c. Task 136809 d	AFFDL-TR-66-220 9b. OTHER REPORT NO(S) (Any other numbers that may be assigned this report)

10. AVAILABILITY/LIMITATION NOTICES

Unlimited Distribution

11. SUPPLEMENTARY NOTES	12. SPONSORING MILITARY ACTIVITY
	Air Force Flight Dynamics Laboratory, Research and Technology Division, Air Force Systems Command, Wright-Patterson AFB Ohio.

13. ABSTRACT

The integrity of brittle elements subjected to time-dependent thermal and mechanical loads is predicted by means of an algorithm involving three steps: the determination of the temperature distribution, the determination of the thermal and mechanical stresses, and the statistical description of the resistance of the brittle material. Experiments are conducted on beams and disks under transient thermal and mechanical loads. The fracture probability-time curves obtained for these members are very accurately predicted by the fracture algorithm. The sensitivity of the beam and disk response to changes in the elastic, thermal, and statistical strength parameters is investigated. A combined stress fracture theory for brittle elements is developed which accounts for a history of thermal and mechanical loading.

DD FORM 1 JAN 64 1473

Unclassified

Security Classification

14. KEY WORDS	LINK A		LINK B		LINK C	
	ROLE	WT	ROLE	WT	ROLE	WT

INSTRUCTIONS

1. ORIGINATING ACTIVITY: Enter the name and address of the contractor, subcontractor, grantee, Department of Defense activity or other organization *(corporate author)* issuing the report.

2a. REPORT SECURITY CLASSIFICATION: Enter the overall security classification of the report. Indicate whether "Restricted Data" is included. Marking is to be in accordance with appropriate security regulations.

2b. GROUP: Automatic downgrading is specified in DoD Directive 5200.10 and Armed Forces Industrial Manual. Enter the group number. Also, when applicable, show that optional markings have been used for Group 3 and Group 4 as authorized.

3. REPORT TITLE: Enter the complete report title in all capital letters. Titles in all cases should be unclassified. If a meaningful title cannot be selected without classification, show title classification in all capitals in parenthesis immediately following the title.

4. DESCRIPTIVE NOTES: If appropriate, enter the type of report, e.g., interim, progress, summary, annual, or final. Give the inclusive dates when a specific reporting period is covered.

5. AUTHOR(S): Enter the name(s) of author(s) as shown on or in the report. Enter last name, first name, middle initial. If military, show rank and branch of service. The name of the principal author is an absolute minimum requirement.

6. REPORT DATE: Enter the date of the report as day, month, year; or month, year. If more than one date appears on the report, use date of publication.

7a. TOTAL NUMBER OF PAGES: The total page count should follow normal pagination procedures, i.e., enter the number of pages containing information.

7b. NUMBER OF REFERENCES: Enter the total number of references cited in the report.

8a. CONTRACT OR GRANT NUMBER: If appropriate, enter the applicable number of the contract or grant under which the report was written.

8b, 8c, & 8d. PROJECT NUMBER: Enter the appropriate military department identification, such as project number, subproject number, system numbers, task number, etc.

9a. ORIGINATOR'S REPORT NUMBER(S): Enter the official report number by which the document will be identified and controlled by the originating activity. This number must be unique to this report.

9b. OTHER REPORT NUMBER(S): If the report has been assigned any other report numbers *(either by the originator or by the sponsor)*, also enter this number(s).

10. AVAILABILITY/LIMITATION NOTICES: Enter any limitations on further dissemination of the report, other than those imposed by security classification, using standard statements such as:

(1) "Qualified requesters may obtain copies of this report from DDC."

(2) "Foreign announcement and dissemination of this report by DDC is not authorized."

(3) "U. S. Government agencies may obtain copies of this report directly from DDC. Other qualified DDC users shall request through _____."

(4) "U. S. military agencies may obtain copies of this report directly from DDC. Other qualified users shall request through _____."

(5) "All distribution of this report is controlled. Qualified DDC users shall request through _____."

If the report has been furnished to the Office of Technical Services, Department of Commerce, for sale to the public, indicate this fact and enter the price, if known.

11. SUPPLEMENTARY NOTES: Use for additional explanatory notes.

12. SPONSORING MILITARY ACTIVITY: Enter the name of the departmental project office or laboratory sponsoring *(paying for)* the research and development. Include address.

13. ABSTRACT: Enter an abstract giving a brief and factual summary of the document indicative of the report, even though it may also appear elsewhere in the body of the technical report. If additional space is required, a continuation sheet shall be attached.

It is highly desirable that the abstract of classified reports be unclassified. Each paragraph of the abstract shall end with an indication of the military security classification of the information in the paragraph, represented as *(TS), (S), (C), or (U)*.

There is no limitation on the length of the abstract. However, the suggested length is from 150 to 225 words.

14. KEY WORDS: Key words are technically meaningful terms or short phrases that characterize a report and may be used as index entries for cataloging the report. Key words must be selected so that no security classification is required. Identifiers, such as equipment model designation, trade name, military project code name, geographic location, may be used as key words but will be followed by an indication of technical context. The assignment of links, roles, and weights is optional.

FOREWORD

This report was prepared by the Solid Mechanics Division, IIT Research Institute, Chicago, Illinois under Air Force contract AF 33(615)-2468. This contract was initiated under Project No. 1368, "Structural Design Concepts", Task No. 136809, "Design Techniques for Brittle Materials." The work was administered under the direction of the Flight Dynamics Laboratory with James F. Nicholson as Air Force Project Engineer.

The research was performed during the period April 1965 to November 1966. Mr. Ralph L. Barnett was program manager for this project. The authors would like to acknowledge the efforts of Seymour A. Bortz of the Ceramics Division in the area of experimental supervision and Walter D. Pilkey of the Solid Mechanics Division in the area of thermal stress analysis.

Manuscript released by authors November 1966 for publication as an AFFDL Technical Report.

This technical report has been reviewed and is approved.

HOLLAND B. LOWNDES, Actg Chief
Applied Mechanics Branch
Structures Division

ABSTRACT

The integrity of brittle elements subjected to time-dependent thermal and mechanical loads is predicted by means of an algorithm involving three steps: the determination of the temperature distribution, the determination of the thermal and mechanical stresses, and the statistical description of the resistance of the brittle material. Experiments are conducted on beams and disks under transient thermal and mechanical loads. The fracture probability-time curves obtained for these members are very accurately predicted by the fracture algorithm. The sensitivity of the beam and disk response to changes in the elastic, thermal, and statistical strength parameters is investigated. A combined stress fracture theory for brittle elements is developed which accounts for a history of thermal and mechanical loading.

CONTENTS

ILLUSTRATIONS

ILLUSTRATIONS (Contd)

ILLUSTRATIONS (Contd)

SECTION I

INTRODUCTION

Culminating several years of research in the application and development of statistical fracture theory, this report addresses itself to the problem of predicting the structural integrity of ceramic elements which are subjected to transient thermal and mechanical loading. Our specific objectives were fourfold:

(1) Develop an analysis procedure for the "thermal shock response" of brittle materials.

(2) Verify the analysis procedure using simple ceramic elements.

(3) Develop a combined stress theory for brittle materials.

(4) Describe the inadequacies or shortcomings of the analysis procedure.

For reasons that will be made clear, we were unable to respond to the latter objective.

Before we describe our general method of attack, a few comments appear to be in order concerning the term "thermal shock." The sudden cooling, which takes place when a very hot solid is plunged into a relatively cool liquid, creates tensile stresses on the surface of the solid which frequently cause cracking. The expression "thermal shock," which is usually associated with this rapid cooling process, seems to be sort of a biological description of the solid's reaction. In the jargon of the physical sciences, the term shock has come to represent a stationary or propagating discontinuity across some surface in a continuum. This is not what is experienced by a quenched solid which does not, for example, develop a shock wave. The complications which attend the study of shock conditions fortunately do not arise in the rapid heating or cooling of solids. Furthermore, the heating rates normally associated with leading edges and nose cones are of a lower order of magnitude than those associated with quenching.

The behavior of brittle bodies under transient thermal loadings has been treated historically as a distinct material property called thermal shock resistance. With continuing study it has become increasingly clear that such behavior is really a composite of more basic physical phenomena. In particular, the broad problem of strength prediction under thermal loading can almost be viewed as a classic problem in continuum strength analysis. It is now customary to divide the problem into the following parts:

(a) Determination of the thermal and mechanical boundary conditions

(b) Determination of the time-dependent temperature distribution

(c) Determination of the time-dependent thermal stress distribution

(d) Assessment of the temperature-dependent strength or resistance of the body.

In the first three cases the physical description of the processes involved and the methods of approach are well known; however, there are many analytical and computational difficulties which make the general problem very complicated. On the other hand, the latter case is concerned with a failure theory for brittle materials and the physics of this problem becomes a research subject, quite apart from any possible computational difficulties. For this reason, we have directed most of our attention to the strength aspect of the response problem.

An experimental program was designed to minimize the uncertainties which might arise in the temperature and stress determinations. For example, rather than calculate the temperature distribution and expose ourselves to possible imprecision in the characterization of the boundary conditions, we measured the distribution with thermocouples. To reduce the thermal and mechanical stress analysis to the simplest possible form, elements were sought for which a one-dimensional stress analysis was possible;

we choose a beam subjected to terminal couples and heated along the bottom surface and a circular disk which was heated around the inside edge of a concentric hole.

A high purity alumina was selected for our experiments because of the wide experience accumulated with such materials. This experience manifests itself in a consistent manufacturing capability and in plentiful data for both mechanical and thermal properties. Some 60 beams and 60 disks were fabricated using Wesgo Al 995 and each member was exposed to a time varying temperature input. The beam was subjected, in addition, to monotonically nondecreasing terminal couples.

The time to failure for every test was recorded and the distribution of these times was displayed for each element by a cumulative distribution curve. The resulting two curves described the tradeoff between the fracture probability and the failure time for the beam and disk. The analytical prediction of these curves required as input the mechanical loading and the temperature distribution as functions of time. The following scalar functions of temperature were also required: modulus of elasticity, Poisson's ratio, the thermal strain, and the statistical strength parameters for pure tension. These curves were integrated into a statistical thermal and mechanical response algorithm which embraced the conservative assumption that alumina is a series or weakest link material. It was further assumed that the tensile distribution curves for the temperatures of interest do not depend explicitly on time or load history, so that, the effects of creep, static fatigue, or general fatigue are not taken into account.

The original program strategy required that all of the temperature dependent properties be obtained from the literature with the exception of the statistical strength parameters which we wanted to develop ourselves. Unfortunately, the tension members ordered for this purpose were badly warped and had to be disregarded. Since it was not expedient to correct or reorder

the tension specimens, we set out to find the "tension behavior" that would predict the fracture-time distributions that were obtained experimentally.

Indeed, we found a set of Weibull parameters which made our predictions for both the beam and the disk coincide almost exactly with the measured results. This seemed remarkable considering that the beam stresses were uniaxial and mostly mechanical and that the disk stresses were biaxial and entirely thermal. Furthermore, the tensile strength distribution that we assumed was similar to the stronger results described in the literature.

While this report was being prepared, we obtained a set of tension data from Southern Research Institute that was generated for a 99.5 percent alumina using a gas bearing machine. Our assumed tension distribution fits this data precisely.

The agreement between the theoretical and experimental results for the beam, disk and tension specimen is so close that it precludes the error analysis alluded to in our fourth objective. Instead, we have presented a variation of parameters study which illustrates the effects on the fracture-time curve of a $\pm$ 10 percent variation in any physical property used in our prediction scheme.

In view of the remarkable results obtained in this investigation, we feel justified in claiming to have established the potential of the statistical fracture theory approach to the thermal shock problem. It should be clearly understood that establishing a method's potential and "proving" its applicability are very different accomplishments.

SECTION II

THERMALLY AND MECHANICALLY INDUCED FRACTURE

1. INTRODUCTION

Procedures for predicting the performance of a structure composed of a brittle material have been presented in our previous work (References 1 and 2). In this section these procedures are extended to account for time varying mechanical and thermal loading and temperature dependent material properties. The general concept of a generalized stress is replaced by an approximate biaxial Weibull type formulation for the "risk of rupture." This is a more restrictive statement and that this is a proper assumption must be justified in each application of the procedure. Also, new attention is drawn to the role of the volume of the basic tensile strength distribution specimen and to the fact that care is necessary to ensure that the procedure is always yielding at least conservative predictions.

2. ASSUMPTIONS

The applicability of the statistical analysis procedure or fracture algorithm in a given situation rests entirely upon the accuracy of the basic assumptions employed in the algorithm. For this reason it is desirable to state and examine all the assumptions that enter into the fracture algorithm.

It is assumed that the probability of failure of a subvolume of a brittle structure depends only upon its temperature, state of stress and volume. Effects such as creep, strain rate dependance, stress gradient dependance, static fatigue and cyclic fatigue are assumed to be insignificant if not entirely absent. Surface effects such as surface finish are assumed to be insignificant and thus the strength of a subvolume does not depend upon whether or not it is located on the surface of the structure. All the material in the basic tension specimens and in the brittle structure being analyzed is assumed to come from the same statistical population. The mechanical and

thermal loadings are assumed to be known deterministically. Also, in the stress analysis of the brittle structure, it is assumed that the material is homogeneous at uniform temperature, isotropic and linearly elastic.

The earlier fracture algorithms are very general with regard to describing the strength distribution of a subvolume of material under arbitrary temperature and state of stress. In fact they are so general as to render them virtually impossible to directly apply in all but the simplest situations. The governing generalized stress has to be determined and then the strength distribution must be determined for each temperature with no requirement that the distributions be of any particular form or that the same form be preserved throughout the temperature range of interest.

In this formulation of the fracture algorithm, it is assumed that the behavior of the material under a general two-dimensional state of stress can be adequately described by the approximate biaxial statistical fracture theory developed in Appendix I. In this theory, the probability of failure of a subvolume with volume ΔV under a biaxial state of stress σ_1, σ_2 is given by

$$F = 1 - \exp\left\{ - \frac{\Delta V}{V} \left[f(\sigma_1) + f(\sigma_2) \right] \right\} \qquad (1)$$

where

$$f(\sigma) = \left(\frac{\sigma - \sigma_u}{\sigma_o} \right)^m \quad \text{for } \sigma > \sigma_u$$

$$f(\sigma) = 0 \quad \text{for } \sigma \leq \sigma_u \qquad (2)$$

This formulation has the desirable property that, for the case of uniaxial tension ($\sigma_2 = 0$), it reduces to the familiar Weibull form. Consequently all the procedures developed for determining the Weibull parameters can be utilized - providing that all the strength distributions are of the Weibull form with perhaps the parameters varying with temperature. It should be noted that the assumption expressed by Equation (1) does not automatically imply that the material is a pure series material.

When a material is not known to be a pure series material some additional care must be exercised regarding the size of the subvolumes into which a structure is divided. The reason for this is that if a material is not pure series, then a non-conservative step is performed if the volume of the subvolumes ΔV are made smaller than the tensile strength distribution specimen volume $\bar{v}$ in that the strength of the subvolume is overestimated. In order to avoid this problem we suggest that all subvolumes be made equal to or larger than the tensile specimen volume, i.e., $V \geq \bar{v}$ for all subvolumes.

3. FRACTURE ALGORITHM

The following statement of the fracture algorithm, along with the aforementioned assumptions has been devised specifically for the analysis of the structures tested on this program.

(1) At each temperature obtain the strength distribution curve $F_{\bar{v}}(\sigma)$ for a tension specimen of volume $\bar{v}$. Fit the distribution curve with the form

$$F_{\bar{v}}(\sigma) = 1-\exp\left\{ - \frac{\bar{v}}{v} \left[\frac{\sigma-\sigma_u}{\sigma_o} \right]^m \right\} \text{ for } \sigma \geq \sigma_u \qquad (3)$$

In this manner the parameters are determined as functions of temperature: $m = m(T)$, $\sigma_u = \sigma_u(T)$ and $\sigma_o = \sigma_o(T)$.

(2) For each mechanical loading and thermal loading (temperature distribution) determine the stress distribution throughout the structure: $\sigma_i = \sigma_i(x,y,z,t)$, $i = 1,2$

(3) Divide the structure into n convenient subvolumes $V_1, V_2, \ldots V_n$. No subvolume should be smaller than the gage volume of the tension specimen; $V_j \geq \bar{v}$, $j = 1,2,\ldots n$. Subvolumes should be selected with approximately homogeneous stress states.

(4) For each value of time t determine the "worst" risk of rupture for each subvolume V_j:

$$B_{ij}(t) = \frac{V_j}{v}\left\{\max_{D_j} f\left[\sigma_i(x,y,z,t);\ m(T),\ \sigma_u(T),\ \sigma_o(T)\right]\right\}, i=1,2 \qquad (4)$$

$$\text{where } f = \left[\frac{\sigma_i(x,y,z,t) - \sigma_u(T)}{\sigma_o(T)}\right]^{m(T)} \quad \text{for } \sigma_i > \sigma_u \qquad (5)$$

$$= 0 \quad \text{for } \sigma_i \leq \sigma_u$$

and where $T = T(x,y,z,t)$ and D_j is the region in space occupied by V_j.

(5) Determine the maximum value of each $B_{ij}(t)$ in the interval $0 \leq t \leq \tau$:

$$B^*_{ij}(\tau) = \max_{0 \leq t \leq \tau} B_{ij}(t) \qquad (6)$$

(6) The probability that the entire structure will survive the entire environmental history up to $t = \tau$ is given by

$$1 - F(\tau) = \exp\left\{-\sum_{j=1}^{n}\left[B^*_{ij}(\tau) + B^*_{2j}(\tau)\right]\right\} \qquad (7)$$

or

$$1 - F(\tau) = \prod_{j=1}^{n} \exp\left\{-\left[B^*_{ij}(\tau) + B^*_{2j}(\tau)\right]\right\} \qquad (8)$$

where the term

$$\exp\left\{-\left[B^*_{ij}(\tau) + B^*_{2j}(\tau)\right]\right\}$$

represents the reliability of the j^{th} subvolume, $1-F_j$.

4. EXAMPLE

Consider the problem of calculating the reliability of the circular plate shown in Figure 1 . Although the plate is assumed to be at uniform temperature and the mechanical loading does not vary with time, the problem should still illustrate several of the facets in the application of the fracture algorithm. Following the algorithm we proceed as follows.

(1) For the purposes of this example, the tensile strength distribution is assumed to be of the Weibull type with parameters: m=3.0, σ_u = 4,130 psi and σ_o = 5,610 psi and the tension gage volume is $\bar{v}$ = 0.0125 in.^{3}

(2) Assuming a linearly elastic, homogeneous and isotropic material, the radial and circumferential stresses are found from elasticity theory to be

$$\sigma_r = S_i\left[\frac{r_o^2 - r^2}{r_o^2 - r_i^2}\right]\left(\frac{r_i}{r}\right)^2 + S_o\left[\frac{r^2 - r_i^2}{r_o^2 - r_i^2}\right]\left(\frac{r_o}{r}\right)^2 \qquad (9)$$

$$\sigma_\theta = -S_i\left[\frac{r_o^2 + r^2}{r_o^2 - r_i^2}\right]\left(\frac{r_i}{r}\right)^2 + S_o\left[\frac{r^2 + r_i^2}{r_o^2 - r_i^2}\right]\left(\frac{r_o}{r}\right)^2$$

For S_o = 4,956 psi
S_i = 4,460 psi
r_o = 4.0 in.
r_i = 1.0 in.
h = 1.0 in.
these expressions reduce to

$$\sigma_r = 4.99 - \frac{0.495}{r^2} \qquad (10)$$

$$\sigma_\theta = 4.99 + \frac{0.495}{r^2}$$

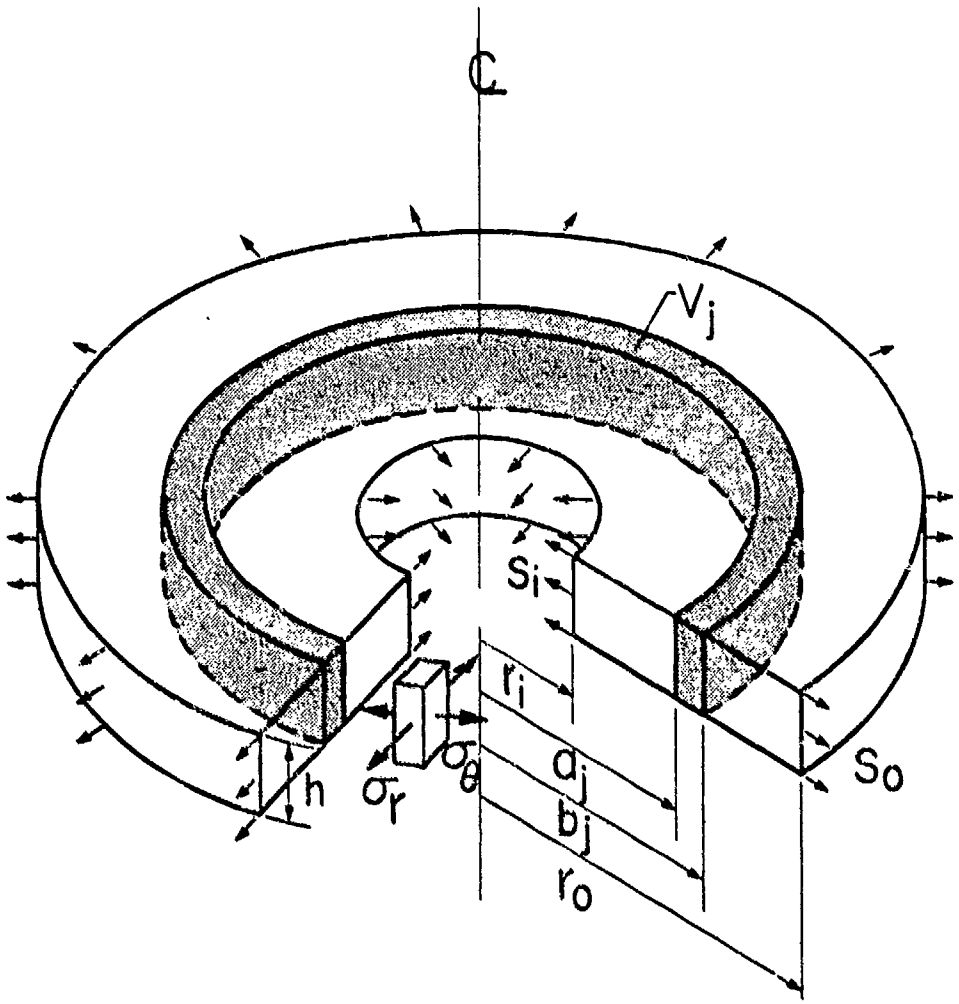

Figure 1 Circular Plate with Central Hole Loaded by Both Inside and Outside Tensile Stresses

(3) The plate is divided into five concentric rings with the dimensions indicated in Table I .

(a) Note that each ring volume is greater than the gage volume $\bar{v} = 0.125$ in.^{3}

(b) The stress state in each ring becomes more homogeneous when the number of rings is increased.

(4) Due to the fact that the temperature distribution is uniform, the "worst" risk of rupture is computed using the maximum stresses in the subvolume. The largest radial stress in the j^{th} ring occurs at its outside radius b_j

$$\sigma^*_{rj} = 4.99 - \frac{0.495}{b_j^2} \tag{11}$$

The largest circumferential stress is found at the inside radius a_j

$$\sigma^*_{\theta j} = 4.99 + \frac{0.495}{a_j^2} \tag{12}$$

Thus the components of the "risk of rupture" for the j^{th} ring are given by

$$B_{rj} = \frac{V_j}{v}\left[\frac{\sigma^*_{rj} - \sigma_u}{\sigma_o}\right]^m \tag{13}$$

$$B_{\theta j} = \frac{V_j}{v}\left[\frac{\sigma^*_{\theta j} - \sigma_u}{\sigma_o}\right]^m$$

The values of the stresses and "risks of rupture" are tabulated in Table I .

Table I

PLATE EXAMPLE RELIABILITY CALCULATIONS

Ring No. j	Inside Radius a_j (in)	Outside Radius b_j (in)	Volume V_j (in^3)	Maximum Radial Stress σ_r (ksi)	Maximum Circumferential Stress σ_θ (ksi)	Radial "Risk of Rupture" B_{rj}	Circumferential "Risk of Rupture" $B_{\theta j}$	Ring Reliability $1-F_j$
1	1.0	1.5	3.927	4.76	5.48	0.00556	0.05472	0.94148
2	1.5	2.0	5.498	4.86	5.21	0.01211	0.03923	0.94996
3	2.0	2.5	7.069	4.91	5.11	0.02045	0.04056	0.94090
4	2.5	3.0	8.639	4.94	5.06	0.02600	0.03936	0.93674
5	3.0	4.0	21.991	4.95	5.04	0.06868	0.09386	0.85015

(5) Due to the fact that there is no variation with time, we have

$$B^{*}_{rj} = B_{rj}$$
$$B^{*}_{\theta j} = B_{\theta j} \qquad (14)$$

(6) Computing the ring reliabilities

$$1-F_j = \exp\left[- B^{*}_{rj} - B^{*}_{\theta j} \right] \qquad (15)$$

and tabulating the results in Table I , the reliability of the plate is computed to be

$$1-F = \prod_{j=1}^{5} (1-F_j)$$
$$= (0.94148)\ (0.94996)\ (0.94090)\ (0.93674)\ (0.85015) \qquad (16)$$
$$= 0.670$$

If the material in the plate is known to be a series material, we can drop the restriction that $V_j \geq \bar{v}$. This enables us to use infinitesimal rings which leads to a reliability prediction of 0.696. Thus, in this example, the partitioning of the plate into only five unit volumes results in a fair estimate of the total reliability.

SECTION III

EXPERIMENTAL PROGRAM

1. BEAMS: THERMAL AND MECHANICAL LOADING

a. General Discussion

The specimen selected for flexural testing under thermal and mechanical loading was a beam 1/2 in. wide, 1 in. deep, and 10 in. long - made of Wesgo Al 995 material. The test mode was four point bending with a gage span of 4 in. Because of the additional condition of thermal loading it was necessary to construct a loading fixture which would bridge the heating apparatus (Figure 2). Further, loading was done through a point contact and roller scheme to compensate for any initial misalignment in the specimen (see detail in upper corners of Figure 2).

The thermal loading was obtained through the use of two strip heaters (R I Controls model number 5305-5A). The units consisted of parabolic reflectors which were focused to concentrate the heat flux onto the tension side of the beam. This arrangement necessitated protecting the quartz heating element from broken beam debris with a piece of heavy screen. Anticipating some change in heat flux, all temperature distributions were obtained with this screen in place. When preparations were complete, several beams were broken without the thermal loading as part of a general check on the system, and the flexural strengths were found to be in the expected range.

b. Temperature Distribution

The temperature distribution as a function of time was obtained with the use of rapid response iron constantan thermocouples and an electronic multiple channel millivolt recording instrument, (each channel prints every 12 seconds). Six 1/16-in. diameter holes were drilled into the depth of the beam from the top side at varying depths of 0.179, 0.314, 0.451, 0.552, 0.727, and 0.863 in. (Figure 5). The temperatures were monitored with

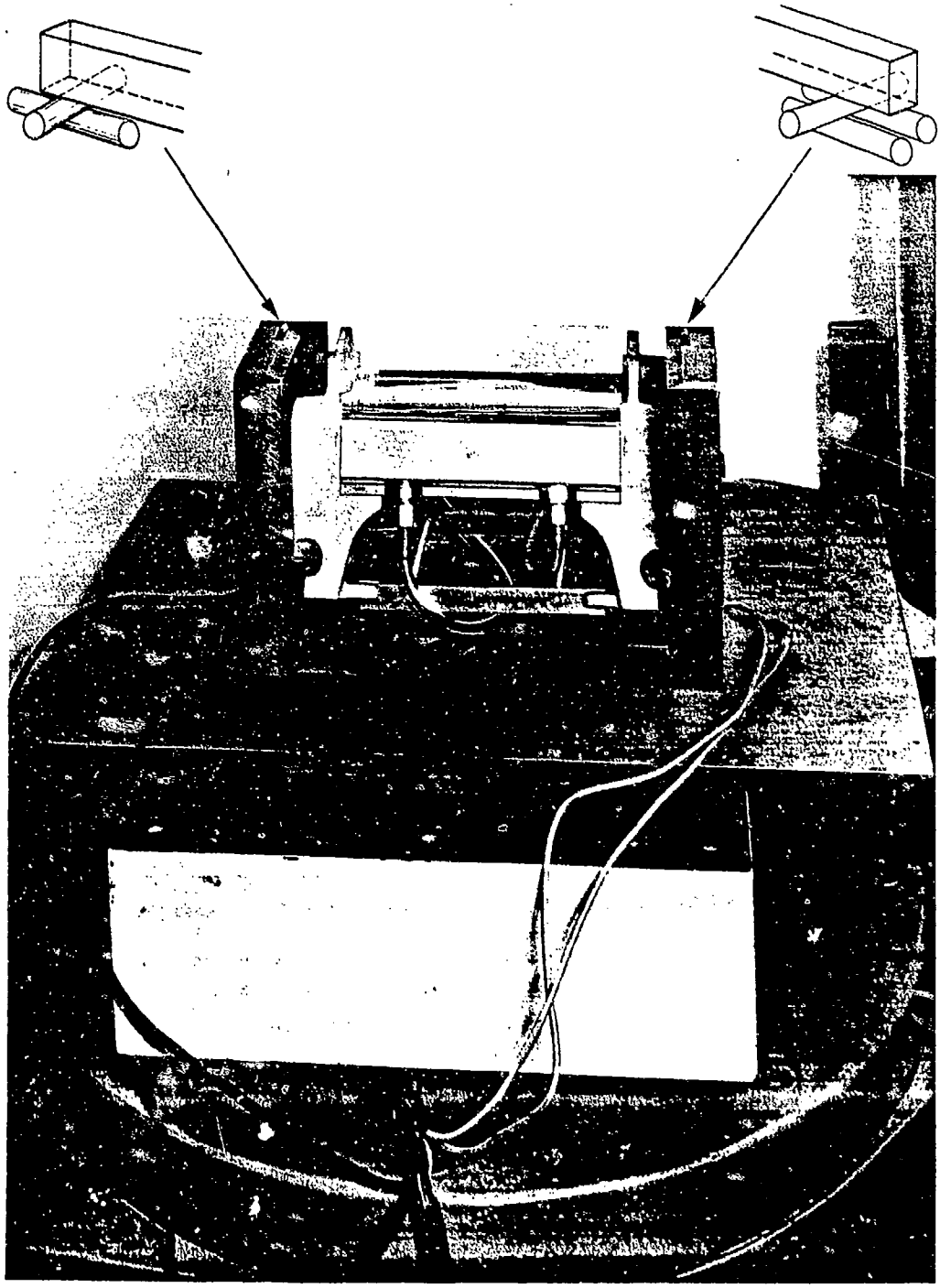

Figure 7 Beam Loading Support and Strip Heater Arrangement

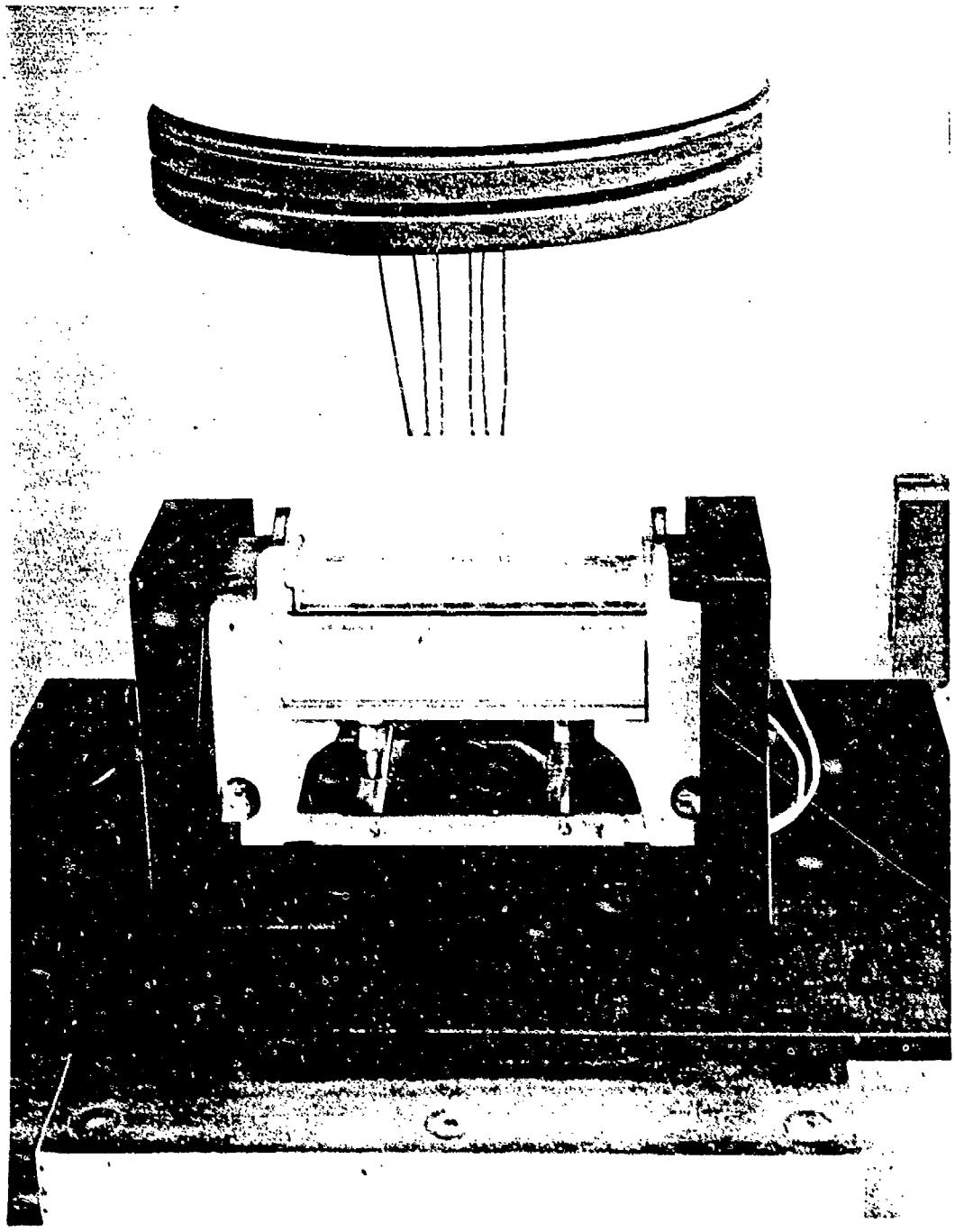

Figure 3 Arrangement of Beam and Thermocouples for Temperature Monitoring Purposes

the beam in place in the test fixture duplicating the conditions which would be encountered during the actual testing of the specimens. A refractory brick was notched to the width of the beam to provide the insulation and shielding required to discourage all but a pure one-dimensional heat flow through the beam depth (Figure 4). The recording instrument was calibrated and the thermocouples were checked in a water bath at boiling point.

Initial trials revealed that the Al_2O_3 material exhibited some transparency to thermal radiation which distorted the reading of those thermocouples nearest the hot interface. This problem was dealt with by coating this surface with a thin even layer of nickel silicate. Four sets of data, each determining a temperature distribution, were obtained. Each set was checked against the other to ascertain reproducibility. The temperature distribution curves are shown in Figure 5.

c. Test Procedure

The test procedure consisted of applying an initial load of 50 lb and energizing the strip heaters at a controlled level of 190 volts for 8 min. After 8 min. the mechanical load was increased at an approximate rate of 500 lb per min. until fracture occurred. The time to failure is taken to be 8 min. plus the duration of increasing load. The initial 50 lb loading served to preserve initial alignment and eliminate backlash during change from thermal to thermal-mechanical loading. A total of 48 beams were tested in this manner. The test machine was equipped with a load pacer device which enabled the operator to approximate a predetermined load rate. To compute the actual load rate, the time from the start of the load increase to final fracture was recorded for each test and loading rates were determined by dividing the final load minus 50 lb by the duration of the increase. Consequently, there was a loading rate associated with each test which deviated somewhat from the target number of 500 lb per min.

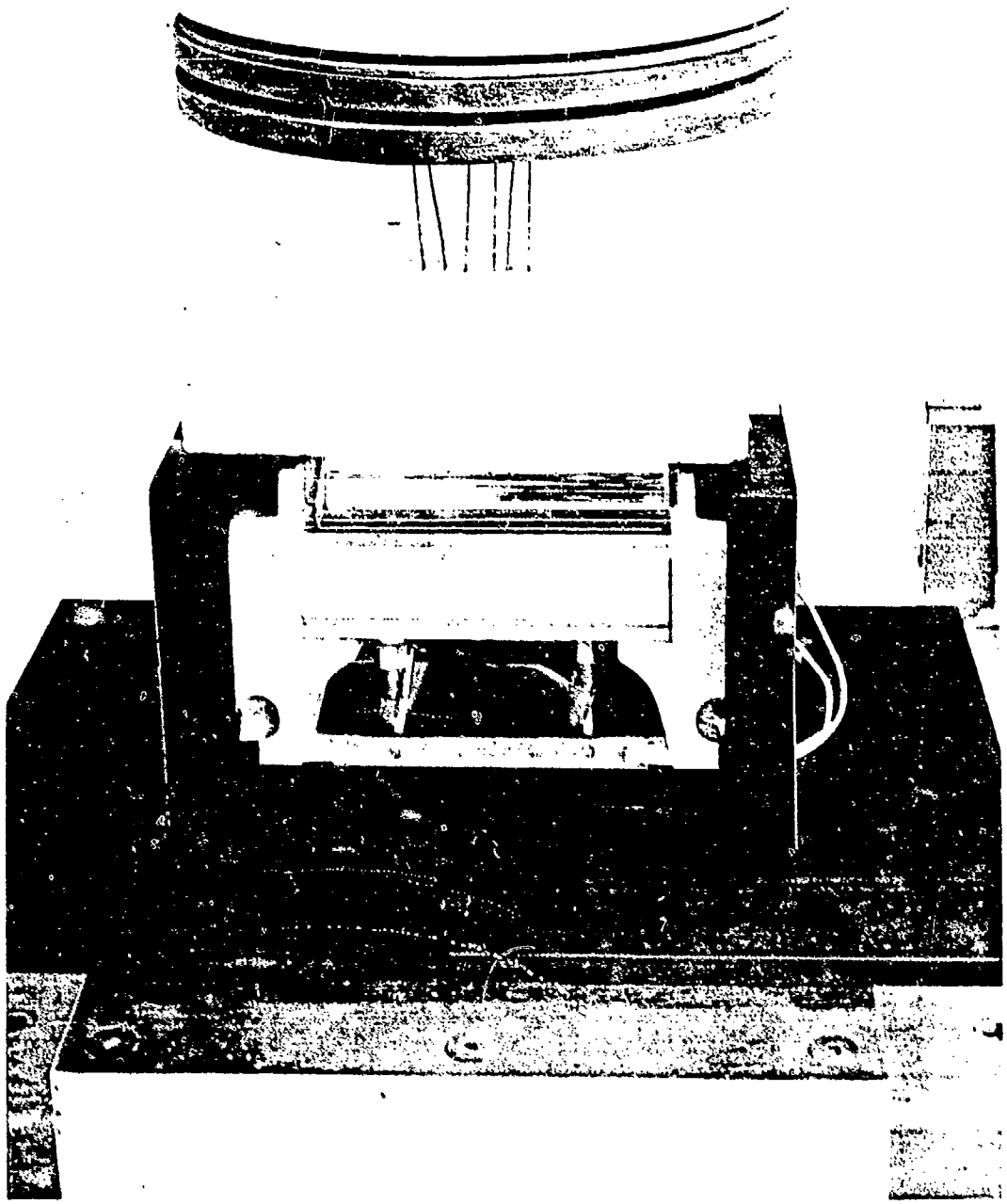

Figure 4 Refractory Brick Used as Insulating Shield to Protect the Beam Sides From Radiant Heat

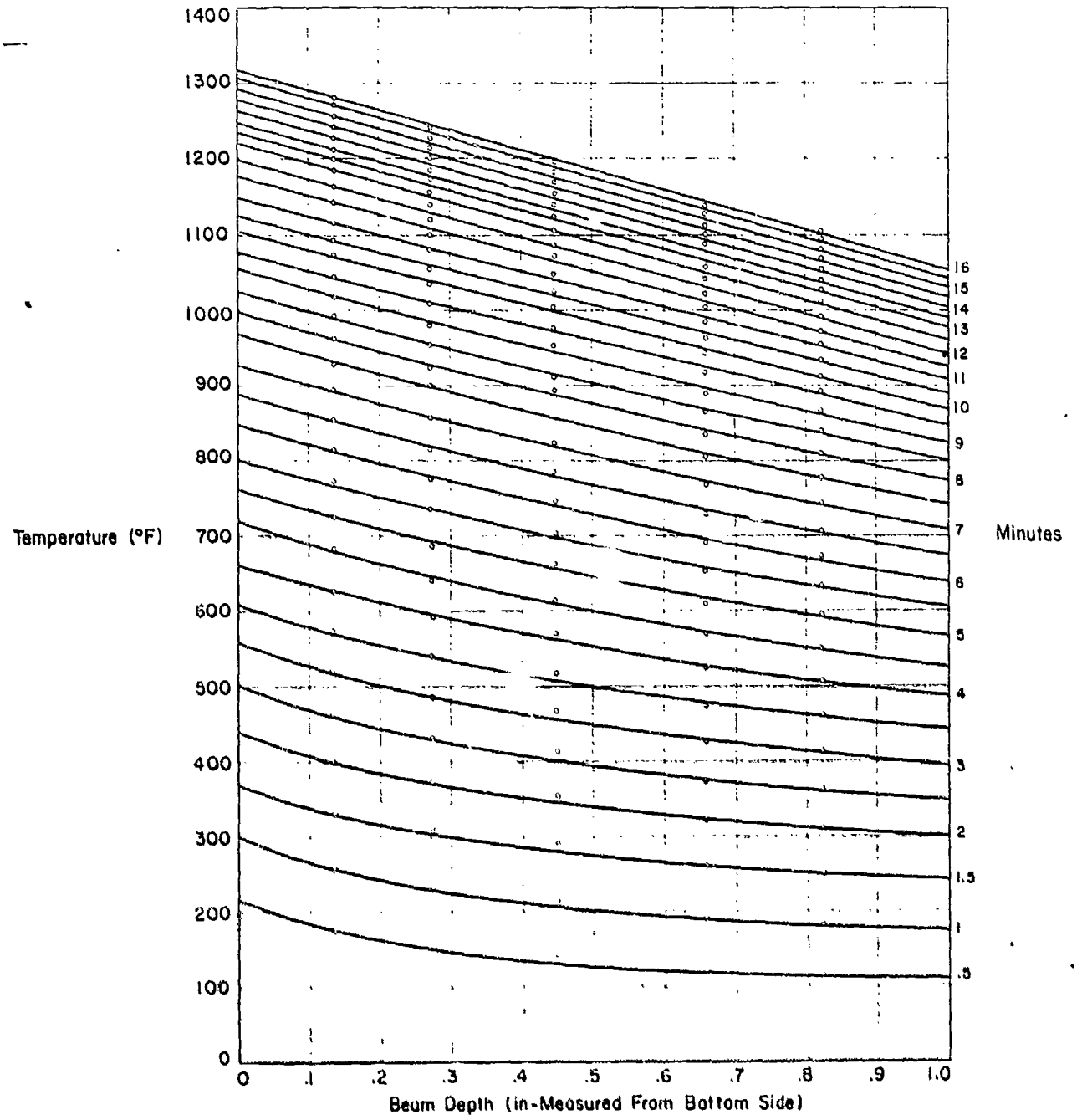

Figure 5 Temperature Distribution through Beam Depth

From this data an estimate of the average loading rate for all tests was determined as 492.9 lb per min. This number was in turn used to determine a corrected time to failure.

The statistical significance of these operations is based on our hypothesis that the mechanical and thermal load histories are the same for all specimens; this requires that the mechanical loading rate be the same for each beam. The actual load rates are not constant and do not, therefore, exactly conform to our hypothesis. To account for the small variations in loading rate, we used the average load rate to compute a corrected time to failure which would reflect the actual failure load. This correction is possible only because the thermal stresses in the beam do not significantly contribute to its probability of failure. (See Section IV-4).

The beam fracture data is presented in Table II. Column 1 tabulates in ordered form the fracture time recorded for each test. The loading rate for each test is listed in column 5 and the average of column 5 which is the average loading rate is determined to be 492.9 lb per min. The corrected time to failure is found by dividing column 4 by 492.9 and adding 8.0 min. Table III presents the corrected and ordered data and Figure 6 illustrate the resulting cumulative distribution.

2. PLATES: THERMAL LOADING

a. General Discussions

The plate specimen was made of Wesgo Al 995. The configuration was circular with a concentric 1-in. diameter hole. The overall diameter was 6 in., and the thickness dimension was 1/4 in.

The thermal loading was produced by means of a 3/4-in. diameter silicon carbide heating element (Globar) positioned perpendicular to the plate through its center hole. A purely two-dimensional heat flow was encouraged by insulating both the top and bottom of the plate so that the principal heat loss would be through the outer plate edge. Pictures of this setup are shown in Figures 7 and 8.

Table II

TEST DATA - Al_2O_3 BEAM

1	2	3	4	5	6
TIME TO FAILURE (MIN.)	FAILURE LOAD (LBS.)	TIME TO FAILURE MINUS 8 MIN.	FAILURE LOAD MINUS 50 LB.	LOADING RATE COL 4 / COL 3	CORRECTED TIME TO FAILURE MINUS 8 MIN. COL 4 / 492.9
11.283	1680	3.283	1630	496	3.307
11.283	1670	3.283	1620	493	3.29
11.384	1755	3.384	1705	504	3.459
11.6	1820	3.6	1770	491	3.692
11.75	1940	3.75	1890	504	3.834
11.784	1920	3.784	1870	494	3.780
11.95	2000	3.95	1950	494	3.956
11.95	2010	3.95	1960	496	3.976
11.95	2040	3.95	1990	504	4.037
12.0167	2020	4.0167	1970	491	3.997
12.033	2040	4.033	1990	495	4.0373
12.033	2085	4.033	2035	505	4.128
12.05	2030	4.05	1980	489	4.107
12.083	2110	4.082	2060	504	4.179
12.1	2060	4.1	2010	490	4.078
12.117	2020	4.117	1970	490	3.997
12.133	2090	4.133	2040	494	4.139
12.15	2120	4.15	2070	498	4.199
12.167	2095	4.167	2045	493	4.149
12.2	2190	4.2	2140	510	4.342
12.2	2140	4.2	2090	498	4.240
12.25	2110	4.25	2060	496	4.179
12.266	2200	4.266	2150	505	4.362
12.38	2175	4.3	2125	494	4.311
12.34	2080	4.34	2030	467	4.118
12.416	2190	4.416	2140	484	4.341
12.45	2090	4.45	2040	458	4.138
12.484	2270	4.484	2220	495	4.504
12.534	2240	4.534	2190	484	4.443
12.534	2320	4.534	2270	502	4.605
12.584	2360	4.584	2310	504	4.686
12.584	2215	4.584	2165	473	4.392
12.667	2360	4.667	2310	495	4.686
12.7	2360	4.7	2310	492	4.686
12.75	2380	4.75	2330	490	4.727
12.766	2370	4.766	2320	486	4.707
12.8	2405	4.8	2355	490	4.778
12.816	2405	4.816	2355	488	4.778
12.834	2400	4.834	2350	486	4.768
12.933	2460	4.933	2410	490	4.889
12.933	2480	4.933	2430	493	4.93
12.95	2525	4.95	2475	500	5.021
12.966	2530	4.966	2480	497	5.031
13.0	2540	5.0	2490	498	5.051
13.0167	2490	5.0167	2440	477	4.949
13.0167	2530	5.0167	2480	493	5.011
13.05	2530	5.05	2480	492	5.031
13.2	2640	5.2	2590	498	5.255
				AVG. = 492.9	

Table III

Al_2O_3 BEAM DATA - CORRECTED TIME TO FAILURE AND ASSOCIATED PROBABILITY

CORRECTED TIME TO FAILURE (MIN)	$F = \frac{i}{N+1}$
11.290	.0204
11.307	.0408
11.459	.0612
11.692	.0816
11.780	.102
11.834	.122
11.956	.143
11.976	.163
11.997	.184
11.997	.204
12.017	.224
12.037	.245
12.037	.265
12.078	.286
12.118	.306
12.128	.326
12.138	.347
12.139	.367
12.149	.387
12.179	.407
12.179	.428
12.199	.449
12.240	.469
12.311	.49

CORRECTED TIME TO FAILURE (MIN)	$F = \frac{i}{N-1}$
12.341	.51
12.342	.53
12.362	.55
12.392	.572
12.443	.592
12.489	.613
12.504	.633
12.560	.653
12.605	.673
12.686	.694
12.686	.714
12.707	.734
12.727	.754
12.768	.775
12.778	.796
12.778	.816
12.889	.836
12.93	.857
13.011	.876
13.021	.897
13.031	.918
13.031	.938
13.225	.978
13.255	.98

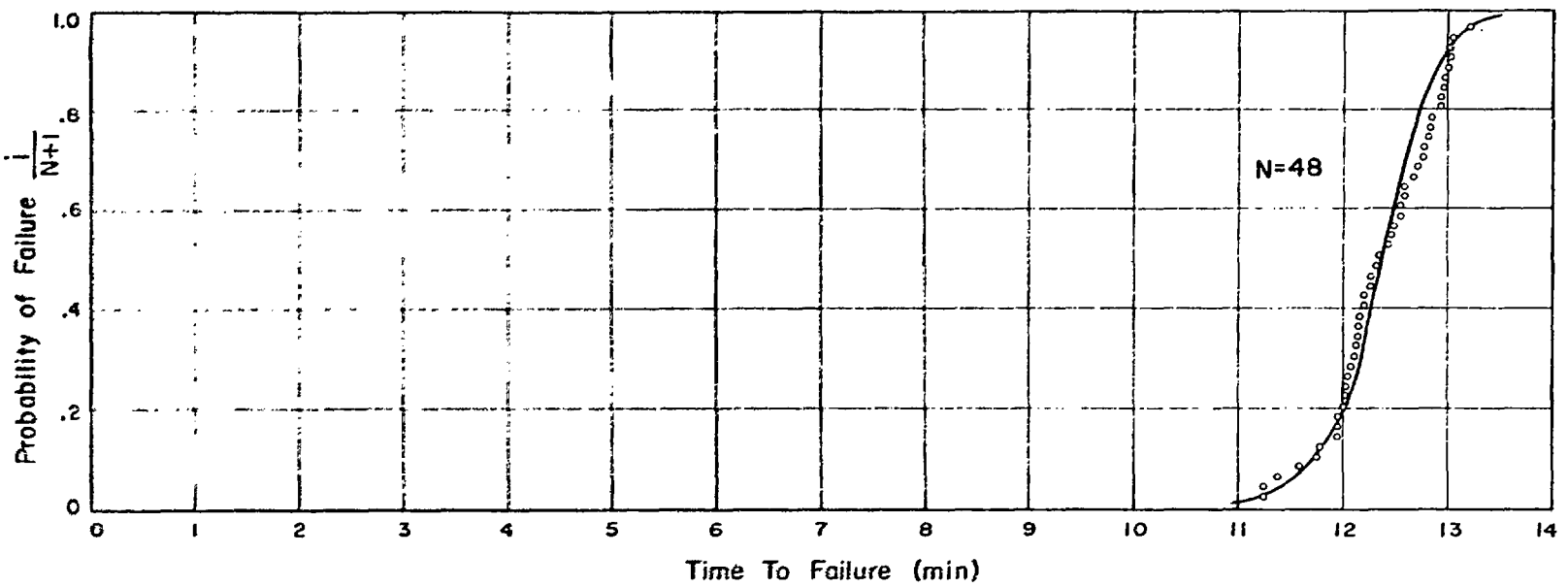

Figure 6 Cumulative Distribution of $A\ell_2O_3$ BEAM DATA

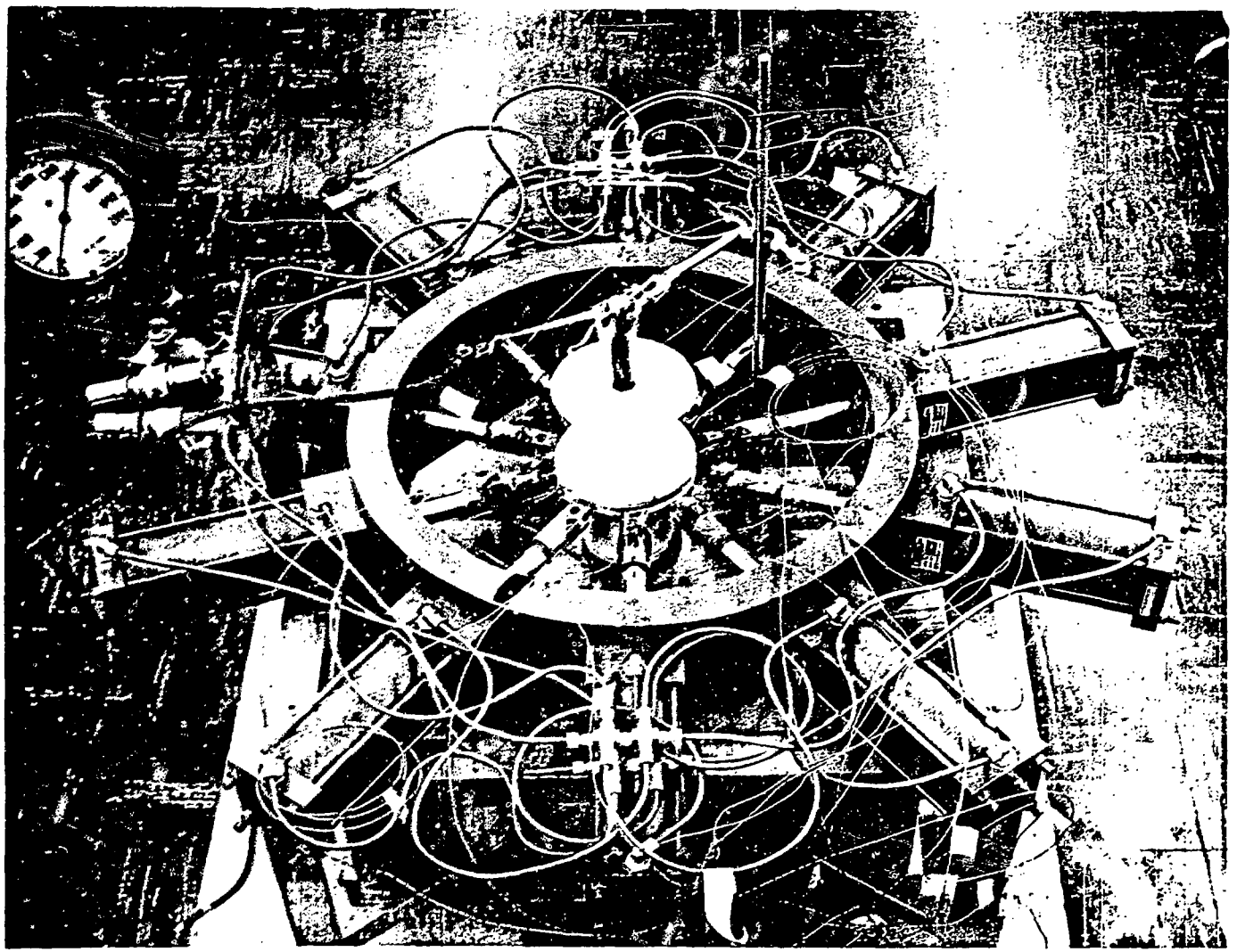

Figure 7 Plate Test Arrangement Showing Relationship of Loading Fixture, Insulation, and Heating Element

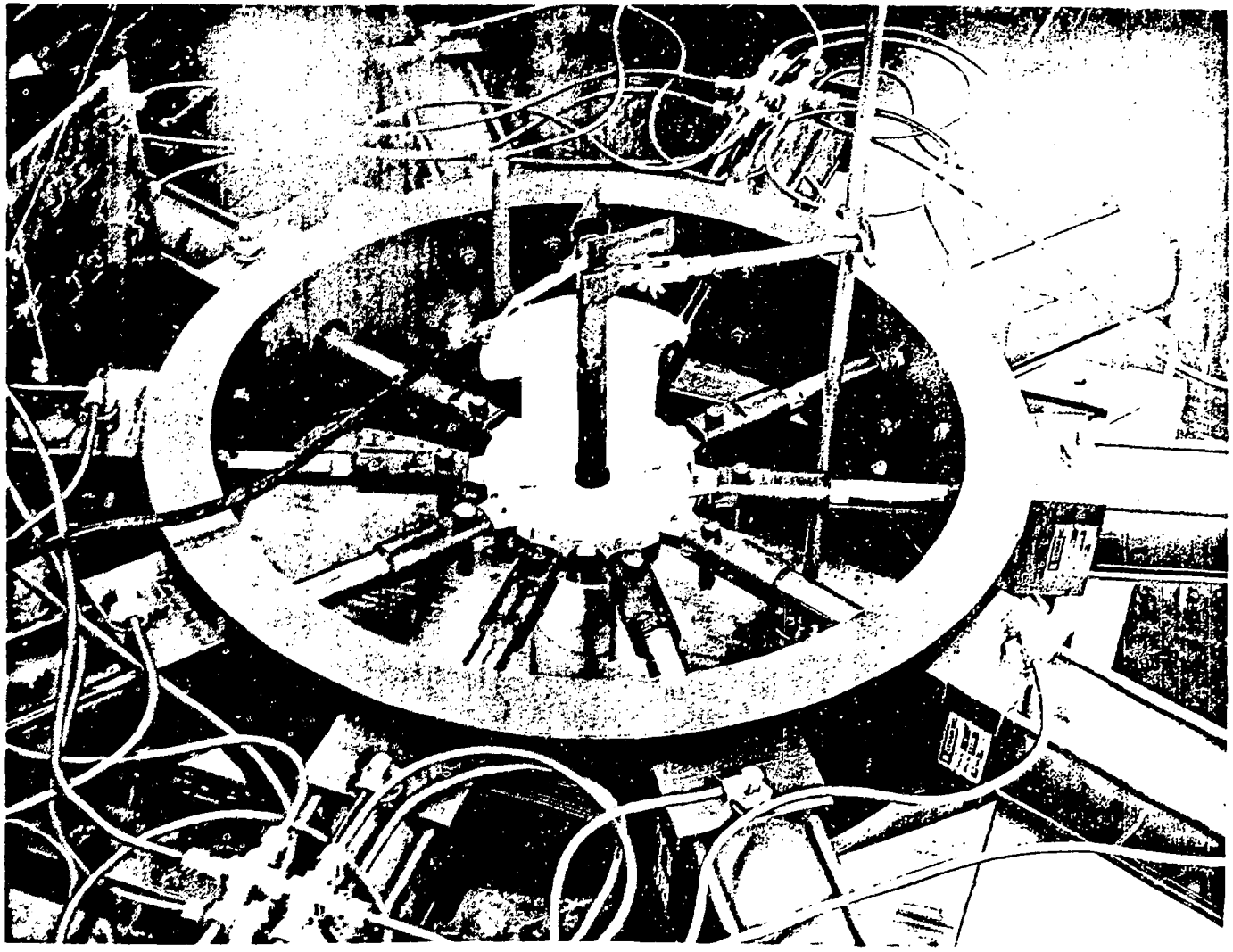

Figure 8 Cross Section Showing Detail of Various Test Components

The radial loading fixture which appears in all of these photographs is present only for the mechanical aspect of the loading which is disucssed under part 3 of this section. The power input to the heating element was measured and controlled by the use of a watt meter and rheostat. The test was completed when catastrophic failure of the disk occurred. The time to failure in each test was the interval between the instant of power application and the instant of failure. The gross heat flux incident upon the disk as computed using the temperature distribution and material properties will be presented later in Section IV-3.

b. Temperature Distribution

As in the case of the beam it was necessary to obtain a temperature distribution throughout the disc as a function of time and location. Because of the axisymmetric character of the thermal loading, the location is specified by radius only. A very satisfactory way of monitoring temperatures through the disk consisted of implanting thermocouples at strategic locations on the plate (Figures 9 and 10). This precluded the possibility of instrumenting each plate tested. Hence it was necessary to obtain a definitive set of measurements from one fully instrumented disk to infer the temperature distribution which existed during all successive tests. As in the case of the beam, some transparency near the inside hole was in evidence and a graphite coating was applied to the inside edge of all plates to minimize "see through."

It should be recalled that failure is catastrophic (Figure 11) in these tests and that the time to failure is variable. Hence, the problem arises of obtaining a representative set of temperature data for a duration of time greater than the greatest time to failure expected for all tests without having the instrumented disk fail during this period. The only solution that presented itself was to "prefail" the instrumented disk. Two pieces were formed by cracks along the radial direction. See Figures 12 and 13 for explanatory diagrams showing location of the cracks and thermocouple implants. Several preliminary tests on plate specimens gave an indication of what to expect as a time to failure duration.

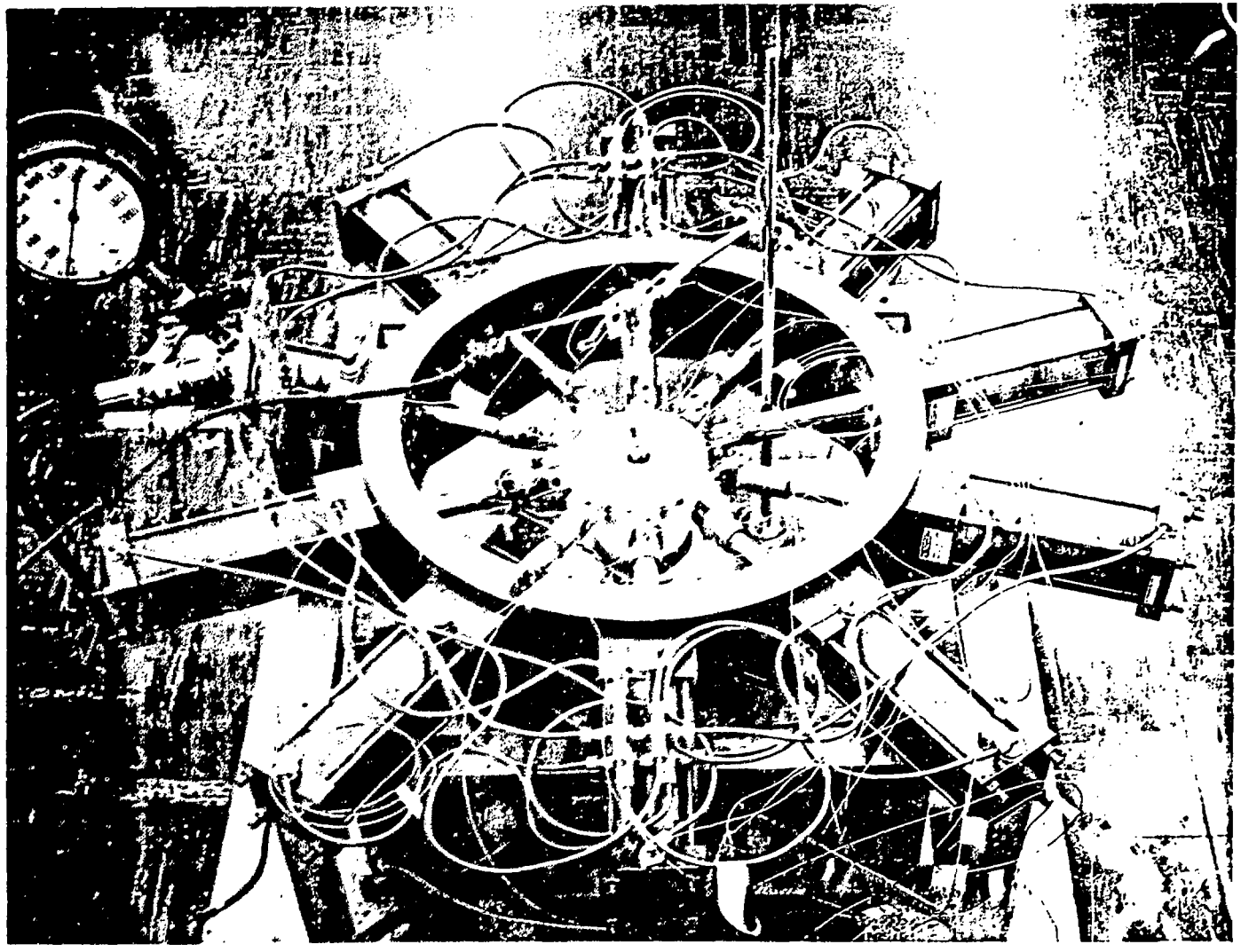

Figure 9 General View of the Instrumented Plate in Test Mode

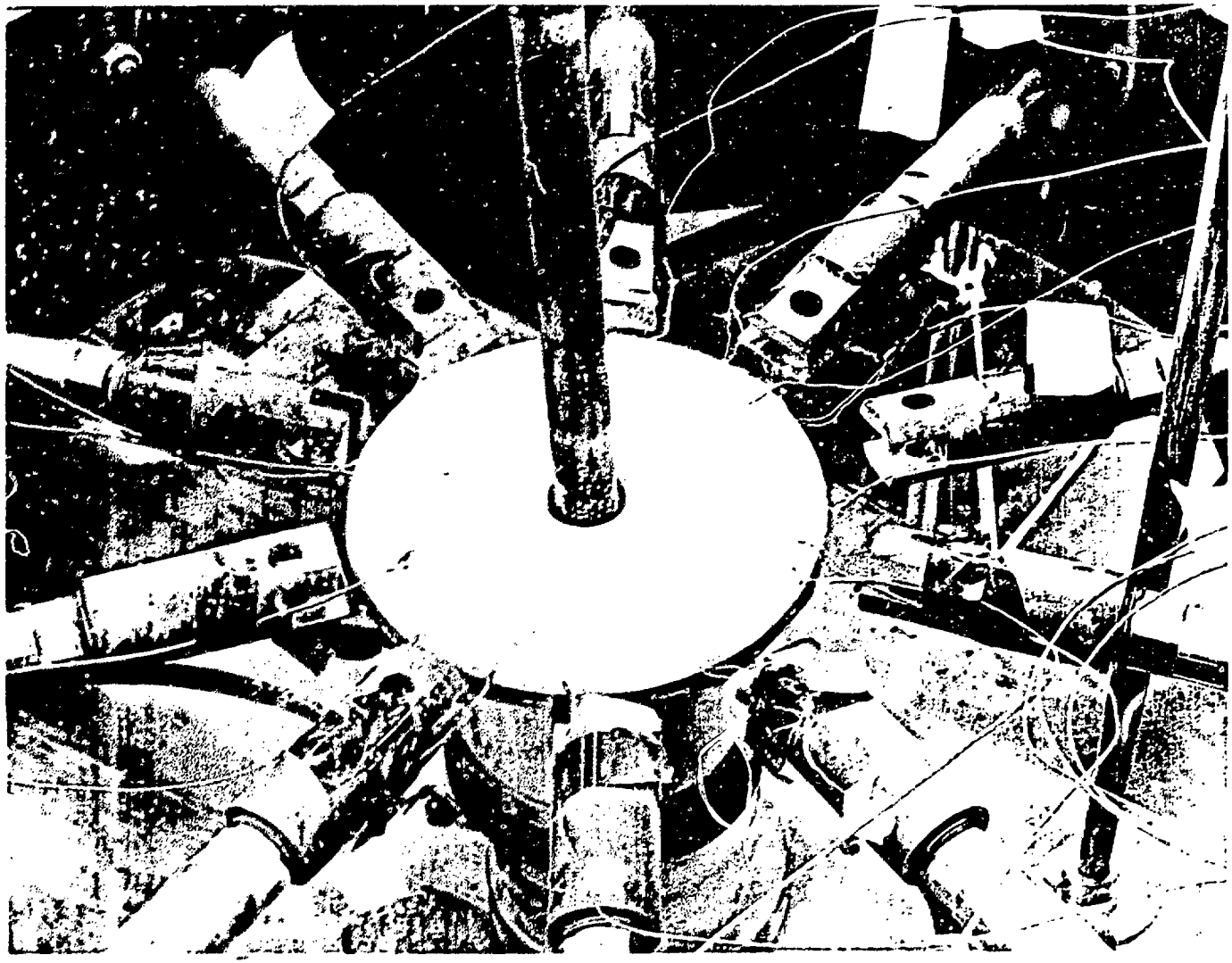

Figure 10 Detailed View of Instrumented Plate with Insulation Removed to Show Thermocouple Implants

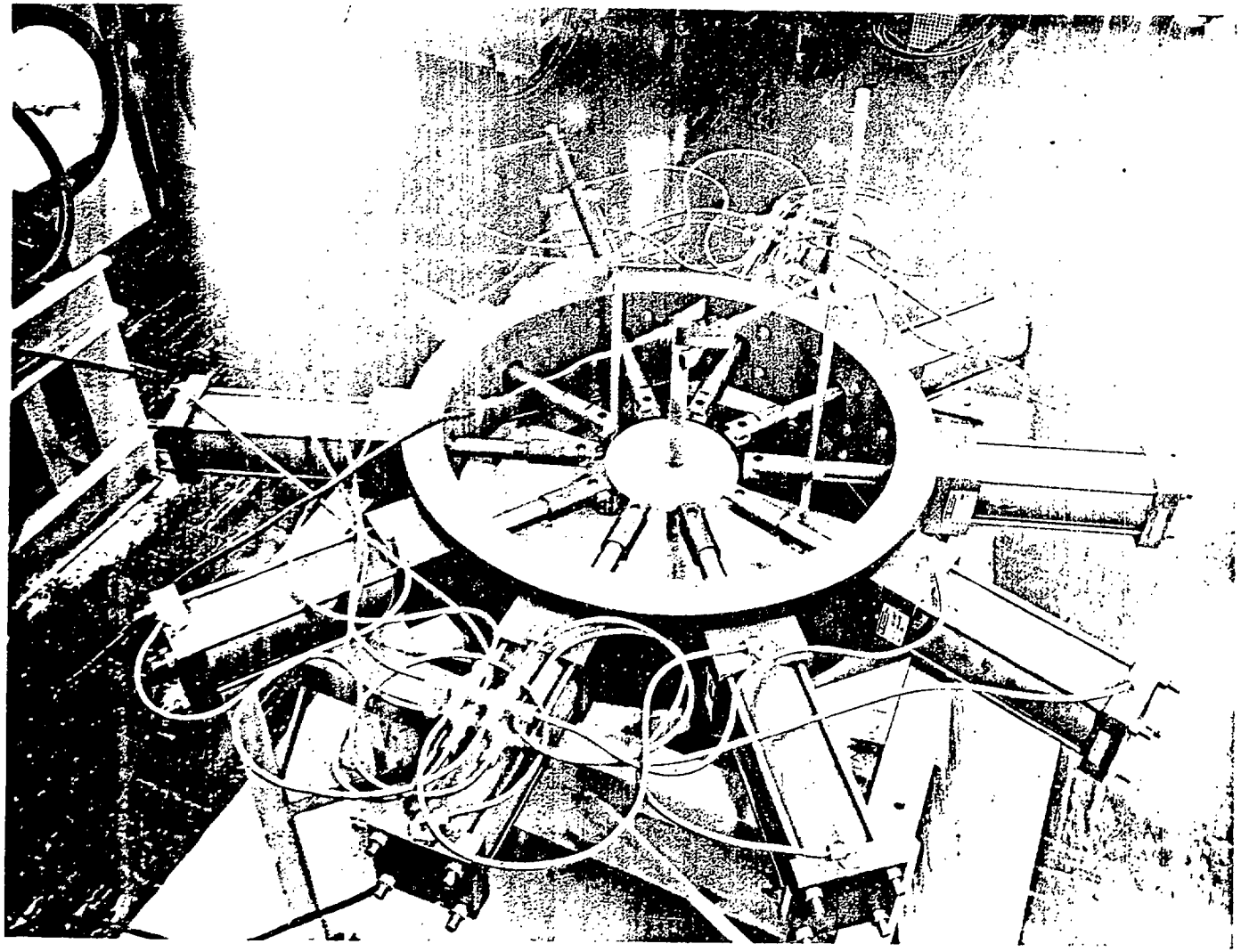

Figure 11 Typical Failure Mode After Application of Thermal Load

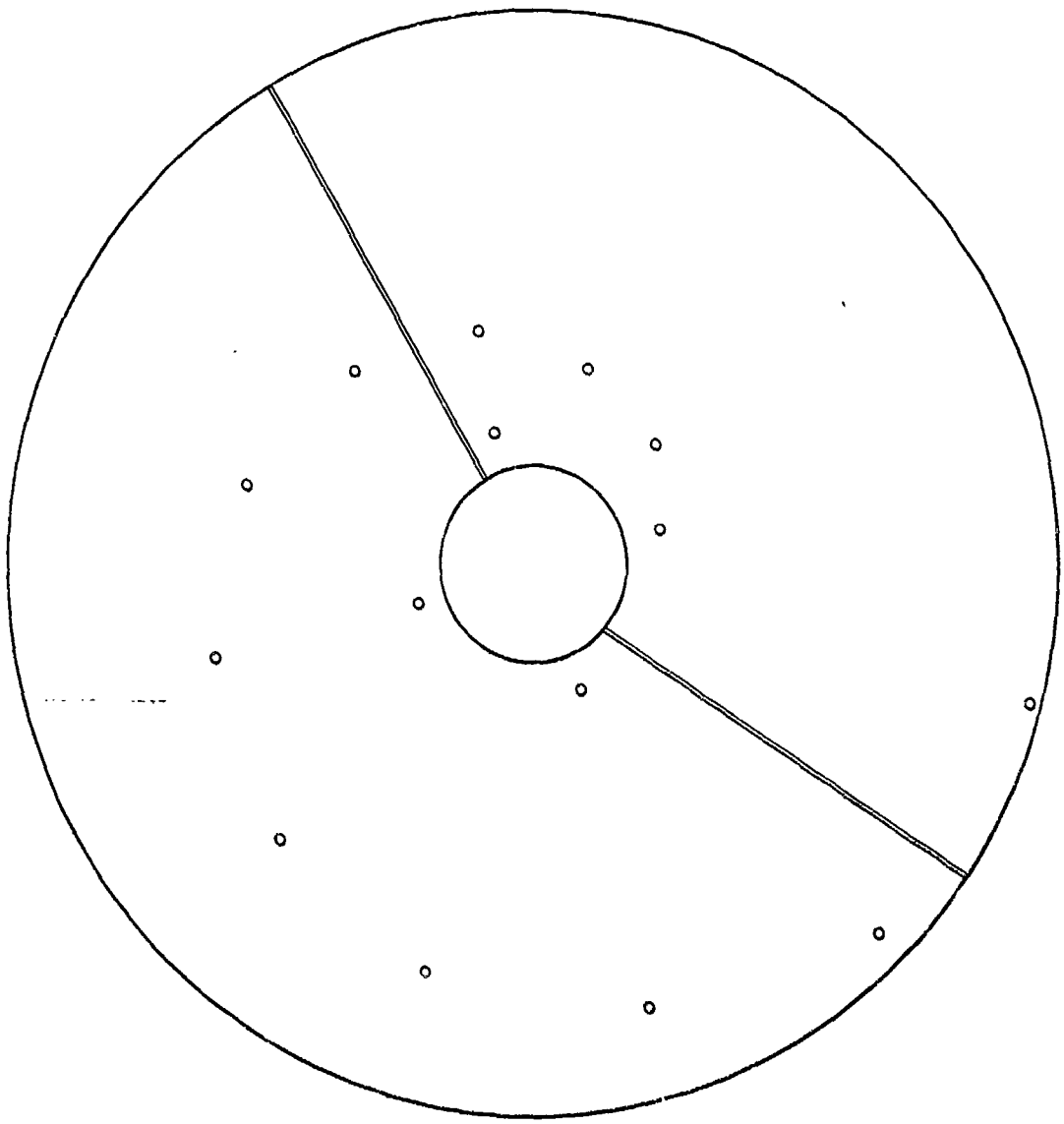

Figure 12 Diagram Showing Relative Locations of Thermocouples and Prefail Cracks

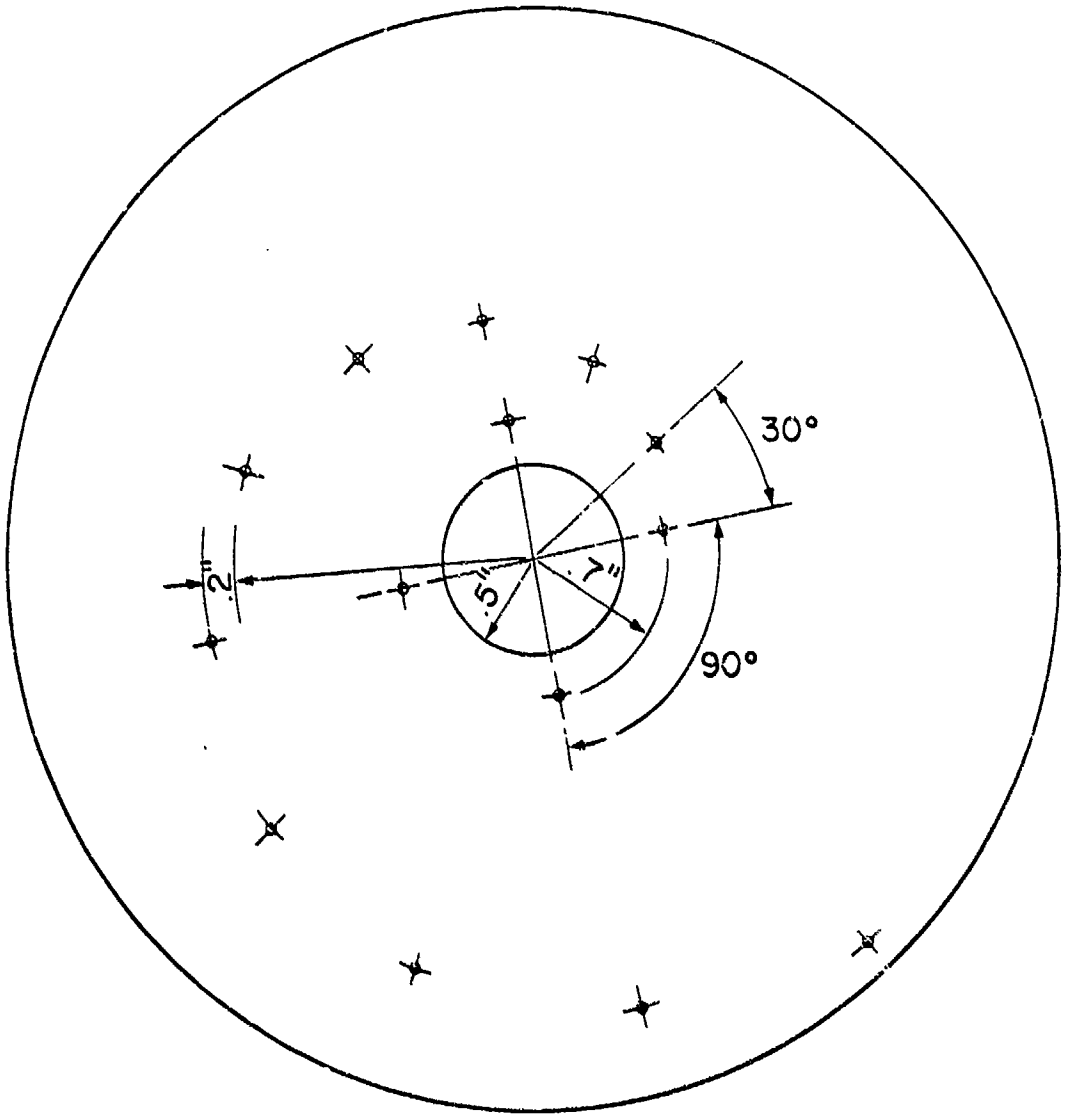

Figure 13 Diagram Showing Locations of Thermocouples

Using this as a guide, the instrumented disk was monitored for a time period almost twice that expected. Finally, many tests were run with this instrumented disk under a variety of circumstances which served two primary interests. First, that of obtaining a temperature distribution which, with a degree of confidence, will accurately represent the actual distribution in each test specimen. Secondly, planned differences such as dismantling setup and reassembling, immediate reruns without any disturbance and rotational reorientation of the disk with respect to the heating element gave the technicians experience which was a valuable asset in conducting the unmonitored disk experiments.

The temperature data was obtained as a millivolt reading at a particular time and position. This information has been converted to temperature-time-position measurements and replotted in a manner more useful in the program. The results of these temperature distribution tests are shown in Figure 14.

c. Fracture Testing

Results of these tests are shown in Table IV and the resulting cumulative distribution is illustrated in Figure 15.

3. PLATES: THERMAL AND MECHANICAL LOADING

a. General Discussion

When we formulated our original program strategy, it was contemplated that the disk element would be subjected to an axisymmetric thermal loading and a mechanical radial tensile loading. Unfortunately, the required magnitude for the tensile loading could not be achieved with the gripping scheme that we visualized. For this reason, it seemed expedient to consider a radial compressive loading which would not present special gripping problems.

Using the radial load fixture shown in Figures 16 and 17, compressive loads were applied to the disk through various types of bearing devices. We attempted to approach, as close as possible, a uniform peripheral loading. Our efforts were simply not good enough as shown by the photoelastic results in Figure 18.

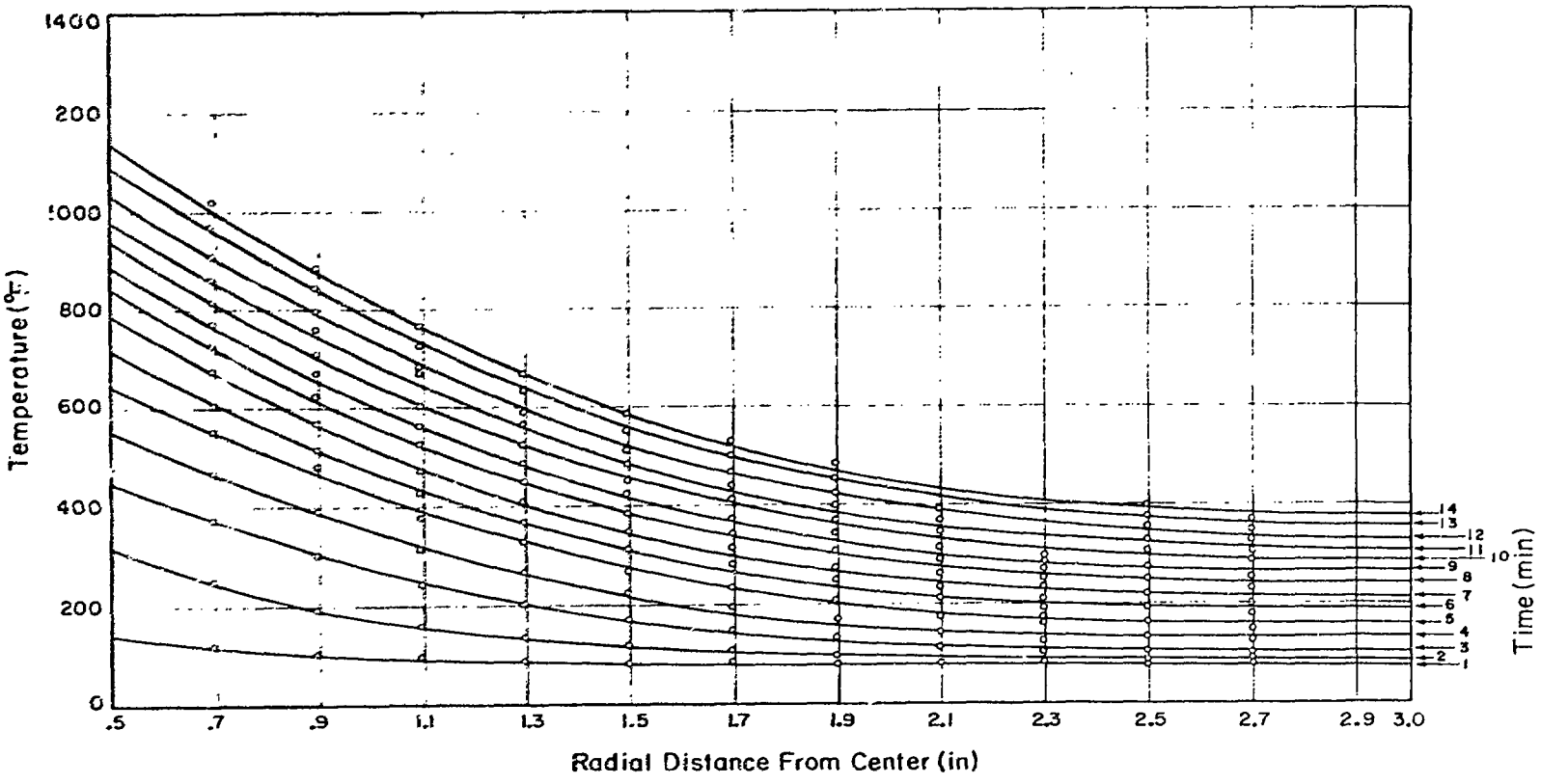

Figure 14 Temperature Distribution through Plate (Influence of Heat Sink Absent)

Table IV

Al_2O_3 DISK DATA - TIME TO FAILURE AND ASSOCIATED PROBABILITY
(Thermal Loading Only)

TIME TO FAILURE (MIN.)	$F = \frac{i}{N+1}$
6.984	.0244
7.766	.0488
7.9	.0732
7.967	.0986
8.150	.122
8.516	.146
8.667	.171
8.766	.195
8.850	.219
9.000	.244
9.017	.268
9.067	.293
9.216	.317
9.266	.341
9.266	.366
9.284	.390
9.300	.425
9.300	.439
9.384	.463
9.467	.488

TIME TO FAILURE (MIN.)	$F = \frac{i}{N+1}$
9.750	.512
9.817	.536
9.934	.561
9.967	.585
10.083	.610
10.217	.634
10.266	.655
10.316	.683
10.334	.707
10.400	.731
10.716	.755
10.750	.780
10.833	.804
10.866	.829
10.917	.853
11.083	.877
11.750	.902
12.350	.926
12.367	.951
12.415	.975

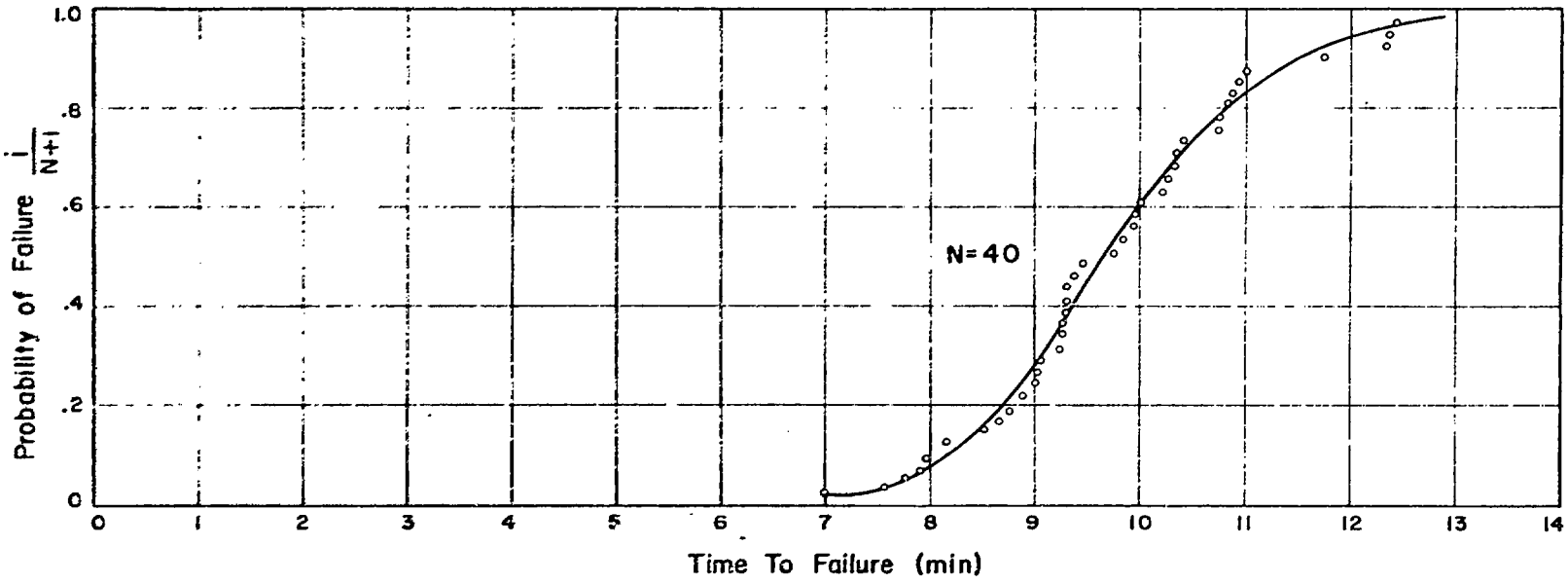

Figure 15 Cumulative Distribution of Al_2O_3 Disk Data (Thermal Load Only)

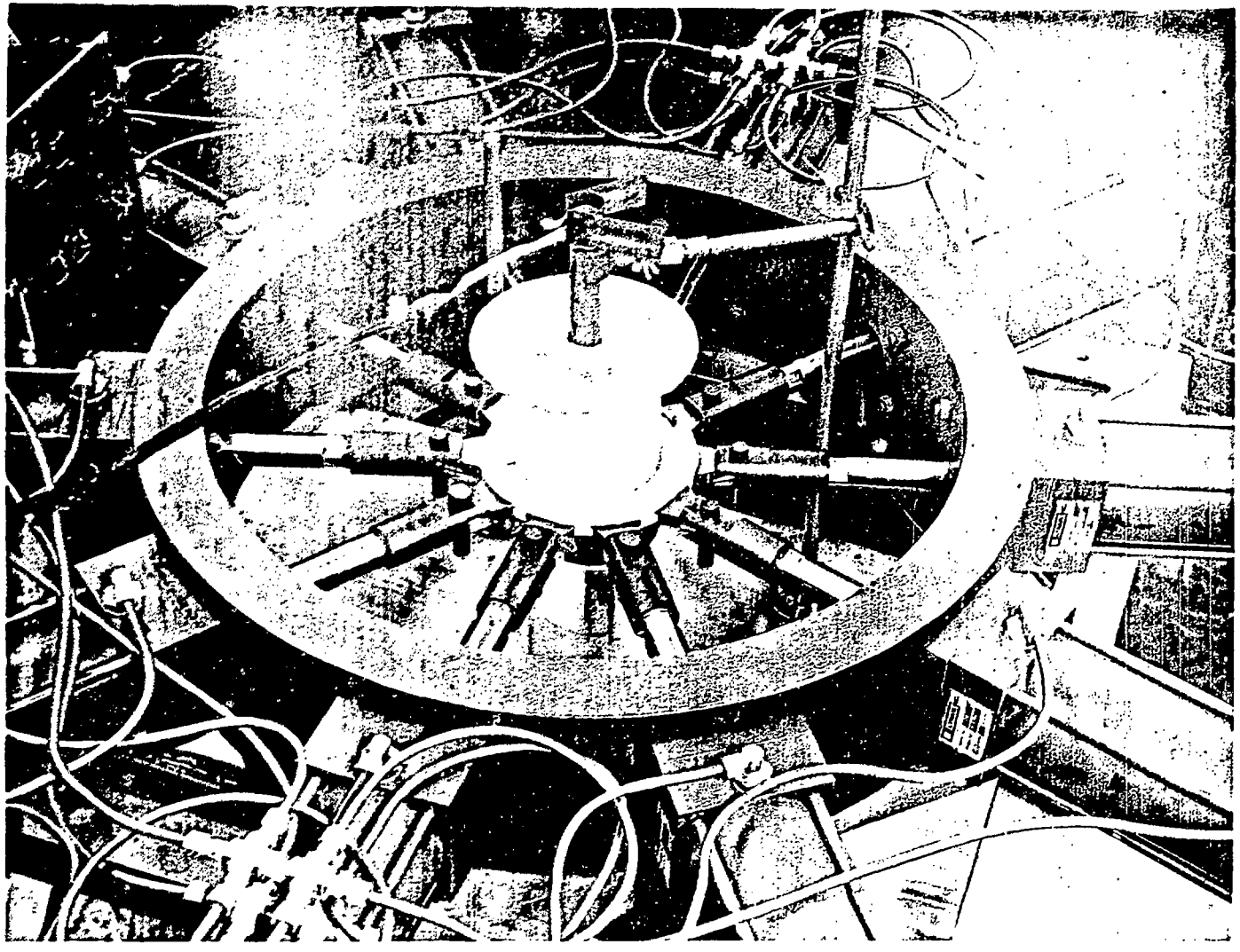

Figure 16 Plate During Application of Both Mechanical and Thermal Load

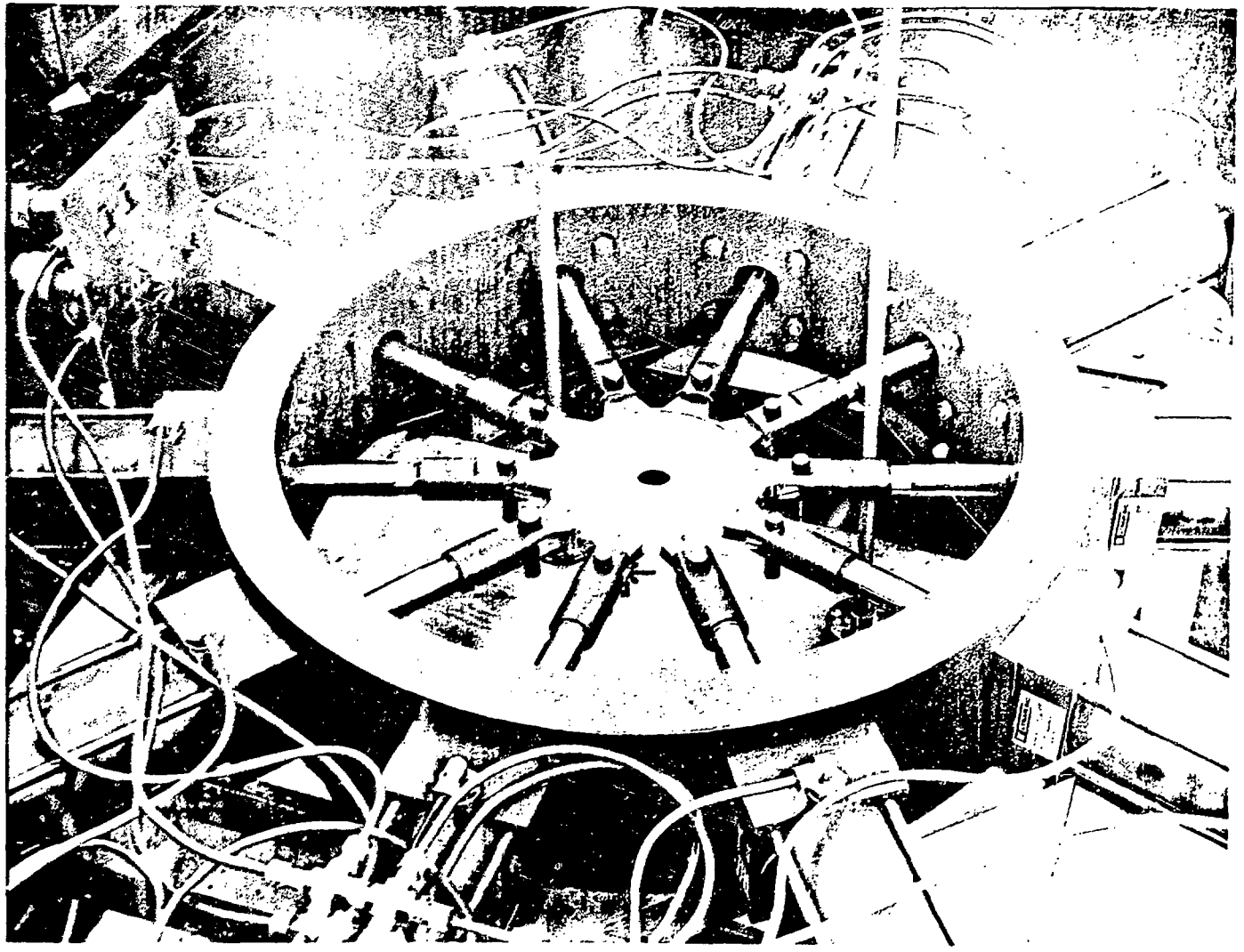

Figure 17 Mechanically Loaded Plate (Compression)

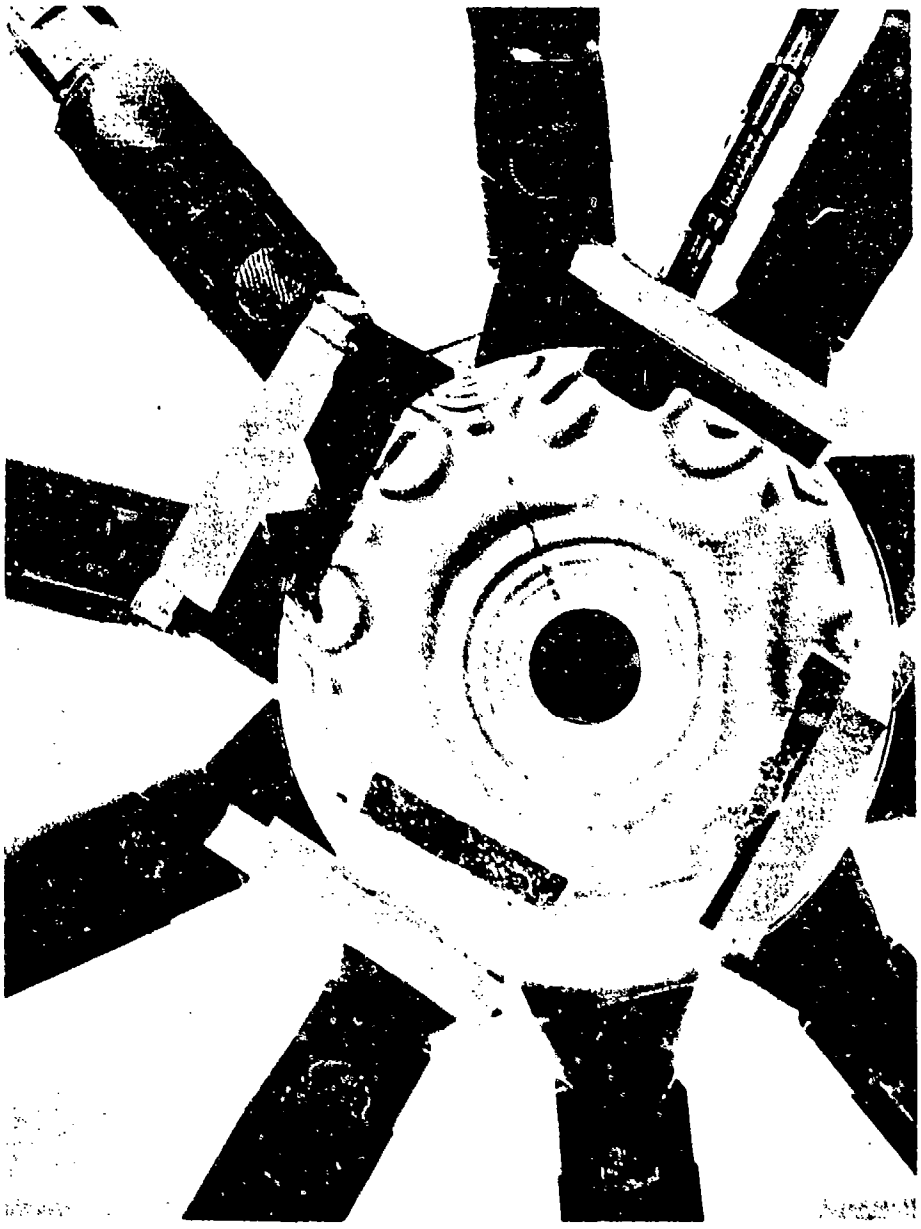

Figure 18 Fringe Patterns Produced in Photoelastic Specimen Subjected to Compressive Mechanical Loading

Here, we observe not only that the stress distribution is not axisymmetric; but, that significant tensile stresses are present. As we shall see, these tensile stresses cause the disk to fail sooner than the disks without this compressive loading. This illustrates quite clearly that a compressive prestress will not necessarily strengthen a brittle element. We hasten to point out that a uniform compressive prestress would not have introduced tensile stresses and would have resulted in an increase in the plate's integrity.

b. Temperature Distribution

The temperature distribution for the disk with compressive grips in place, was obtained in the same manner previously described in part 2b of this section. The temperature distribution curves are shown in Figure 19. Because 90 percent of the periphery was used to approach a uniform mechanical loading, the effective heat sink was appreciable. Comparison with the previously obtained temperature distribution shows a strong shift to lower temperatures for the same time intervals, as expected.

c. Fracture Testing

The disks were placed in the loading fixture as shown in Figure 16 and subjected to a mechanical loading and thermal loading, the latter being superposed on the mechanical loading when it reached a prescribed level. The time to failure was recorded for each test and is given in Table No. V. Failure was defined by the first audible sound of cracking. The cumulative probability distribution is shown in Figure 20.

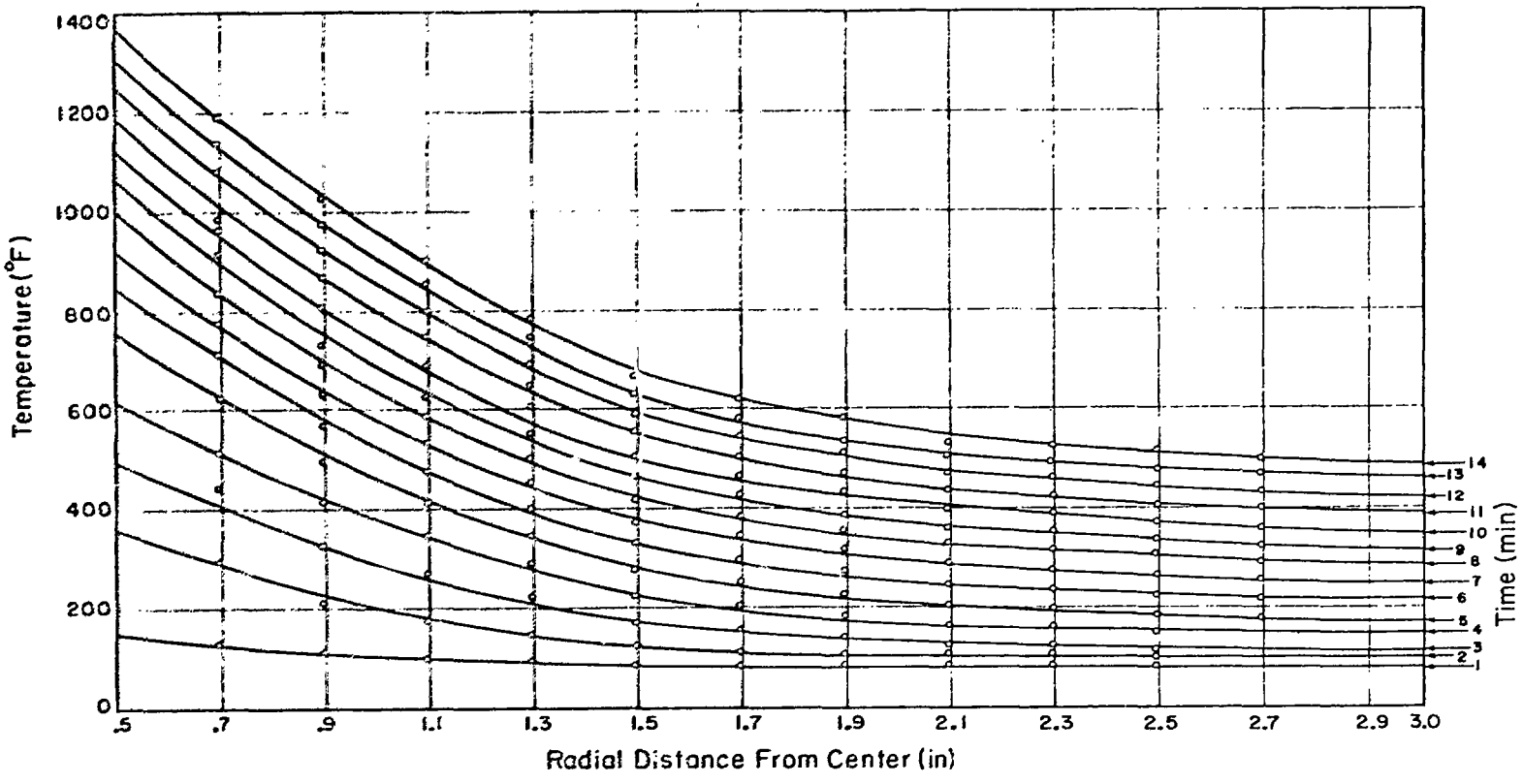

Figure 19 Temperature Distribution through Plate (Influence of Heat Sink Present)

Table V

Al_2O_3 DISK DATA - TIME TO FAILURE AND ASSOCIATED PROBABILITY (Mechanical and Thermal Loading)

TIME TO FAILURE (MIN.)	$F = \frac{i}{N+1}$
3.566	.091
3.583	.182
3.600	.272
3.917	.364
4.033	.455
4.083	.545
4.233	.636
4.583	.727
4.784	.818
4.800	.91

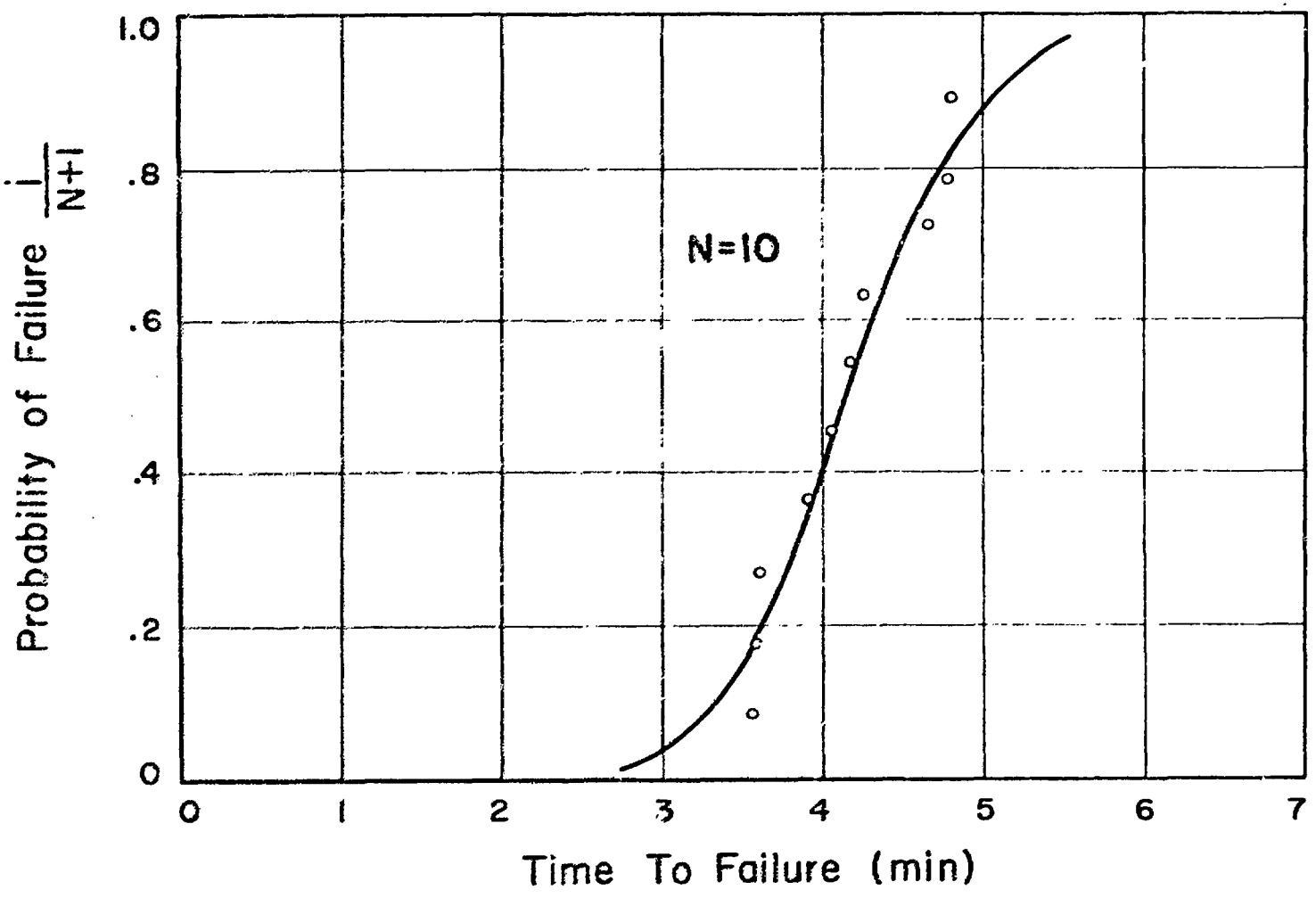

Figure 20 Cumulative Distribution of Al_2O_3 DISK DATA (Thermal and Mechanical Loading)

SECTION IV

RESPONSE PREDICTIONS

1. APPROACH

The central question to which this research effort addresses itself is: "Can the statistical analysis algorithm be successfully applied in the case of brittle structures exposed to thermal and mechanical loadings and, if not, why not?" Specifically, on this program we seek to explain the results of the beam and disk experiments described in Section III with the aid of the fracture algorithm presented in Section II.

There are many possible avenues of approach on this question. The straightforward approach is the most logical and involves using experimentally obtained basic material property data in conjunction with the fracture algorithm to attempt to "predict" the results of the beam and disk experiments. The difficulty with this approach is that the tensile strength distribution for alumina, at room temperature and especially at elevated temperatures, has not yet been satisfactorily defined. Each available strength distribution is probably an underestimate of the true distribution for alumina. Even if alumina were a pure series material of the Weibull type and the algorithm was performed using infinitesimal subvolumes, the use of the available strength distributions should result in conservative and not exact results. Thus, the achievement of conservative predictions is not a very sensitive test of the applicability of fracture algorithm - especially if the material is close to being of the pure series type as in fact we hoped alumina would be.

The approach which was selected begins by making an additional assumption that the tensile strength distribution for alumina is independent of temperature in the range from R.T. to 1500°F. At moderate temperatures some investigators (References 3,4,5,6 and 7) do measure a slight degradation of strength with increasing temperature. However, our experience with elevated temperature

testing suggests that the experiments cannot be performed with the same precision as they can at room temperature. Thus, since a measured degradation of strength at moderate temperatures may be explained by experimental limitations, the assumption of the strength distribution being temperature independent may not be unreasonable.

Since the strength distribution is assumed to be of the Weibull type, the assumption of temperature independence requires that the parameters m, σ_u, σ_o are independent of temperature. In this approach these parameters are left as open parameters. A trial and error procedure employing the fracture algorithm in conjunction with the stress analysis is used to attempt to simultaneously "fit" both the beam and disk experiments using a single set of values for the parameters. Using this method, a deficiency in the algorithm, experimental procedure, or the temperature independent strength assumption may be observed in two ways. First, it is entirely possible that the beam and disk experiments cannot be "fitted" satisfactorily using a single set of parameters. Second, assuming that it is possible to fit both the beam and disk experiments, it is very likely that the resulting strength distribution may be unreasonably different from the data obtained from the best strength tests.

2. MATERIAL PROPERTIES

The approach just described was successfully employed. Using the single set of Weibull parameters m = 3.3, σ_u = 19,700 psi, σ_o = 7,000 psi with a tension gage volume of $\bar{V}$ = 0.0982 $in.^3$, both the beam and disk experiments were satisfactorily "fitted." Using these values the strength distribution is plotted in Figure 21. The mean strength can be computed to be approximately 32,400 psi. This value tends to be somewhat higher than most available tension data and begins to approach the flexural strength data. However, very recent gas-bearing data by Pears and Starrett (Reference 8) achieves some high mean strengths in tension for alumina.

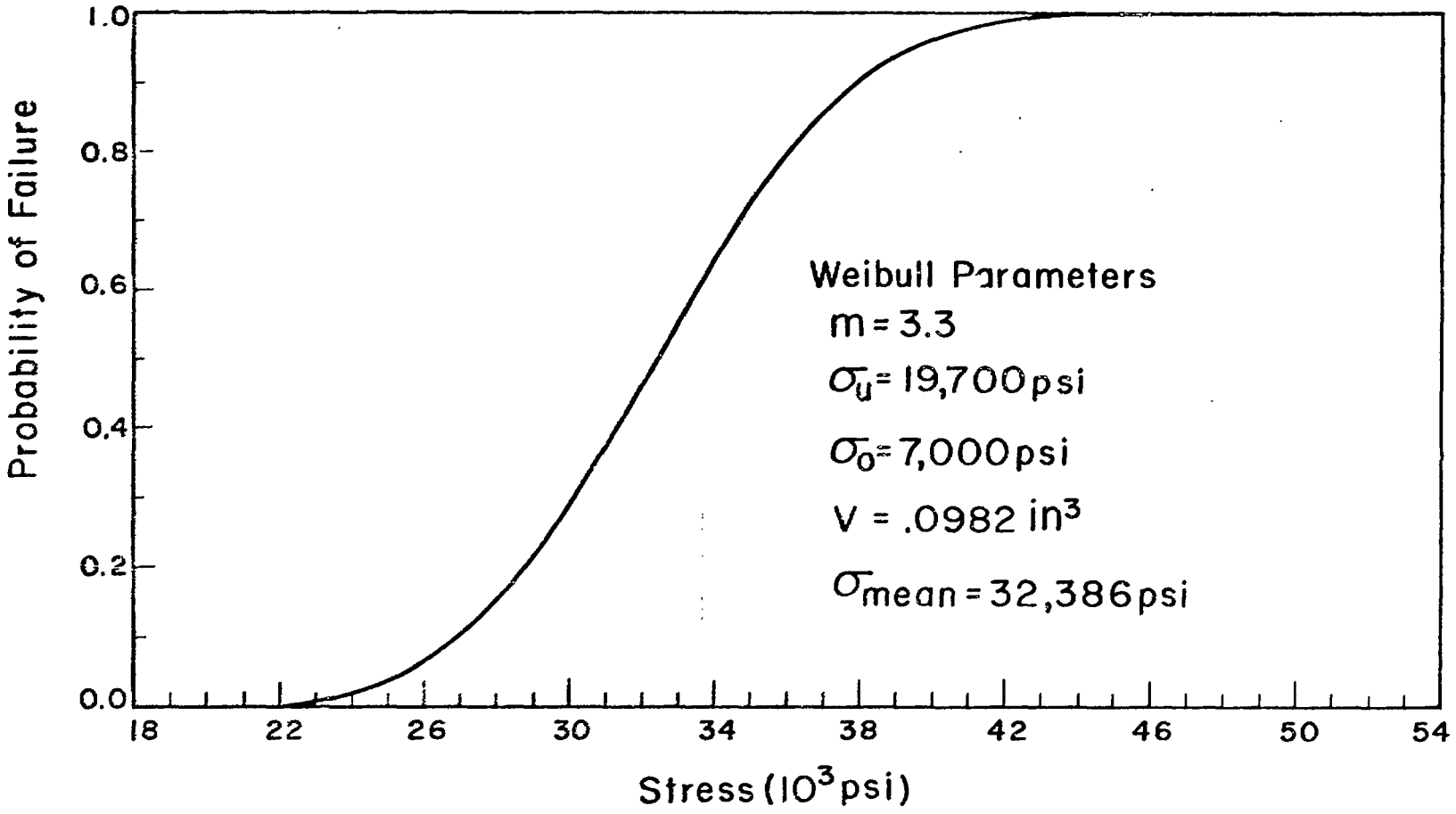

Figure 21 Cumulative Tensile Strength Distribution of Alumina for a Tension Specimen with Gage Volume of 0.0982 in.^{3}

When the comparison is made between this excellent data for a gage volume of 0.031 $in.^3$ to the derived Weibull type strength distribution for the same volume, Figure 22 , the agreement is seen to be quite remarkable.

For the remainder of this report the tensile strength distribution, in the range from R.T. to 1500° F, shall be assumed to be given by the Weibull formulation with parameters m = 3.3, σ_u = 19,700 psi and σ_o = 7,000 psi. Furthermore, for the purpose of illustrating the general application of the fracture algorithm, the distribution curve shall be pretended to come from tests on a tensile specimen of gage volume $\bar{v}$ = 0.0982 $in.^3$

The other material properties entering into the stress analysis and thermal analysis have been obtained from the literature. Thermal strain as a function of temperature after Goldsmith, Hirschhorn and Waterman (Reference 9) is shown in Figure 23. Modulus of elasticity as a function of temperature after Dally (Reference 10) is illustrated in Figure 24. Poisson's ratio as a function of temperature after Coble and Kingery (Reference 11) is shown in Figure 25. Finally the thermal conductivity as a function of temperature after Goldsmith, Hirschhorn and Waterman (Reference 9) is illustrated in Figure 26.

3. THERMAL ANALYSIS

Assuming black body radiation, the heat flux Q impingent upon the surface of the beam or disk may be expressed as

$$Q = - k \frac{\partial T}{\partial n} + \sigma T^4 \qquad (17)$$

where k is the thermal conductivity of alumina, $\frac{\partial T}{\partial n}$ is the normal derivative of the temperature distribution into the body evaluated on the surface, σ is the Stefan-Boltzman constant and T is the absolute temperature on the surface. Using the temperature distribution curves for the beam and disk from Section II, Figures 5 and 13 , and Figure 26 for the thermal conductivity, the heat flux Q can be computed using Equation (17). The results of these computations are plotted in Figure 27.

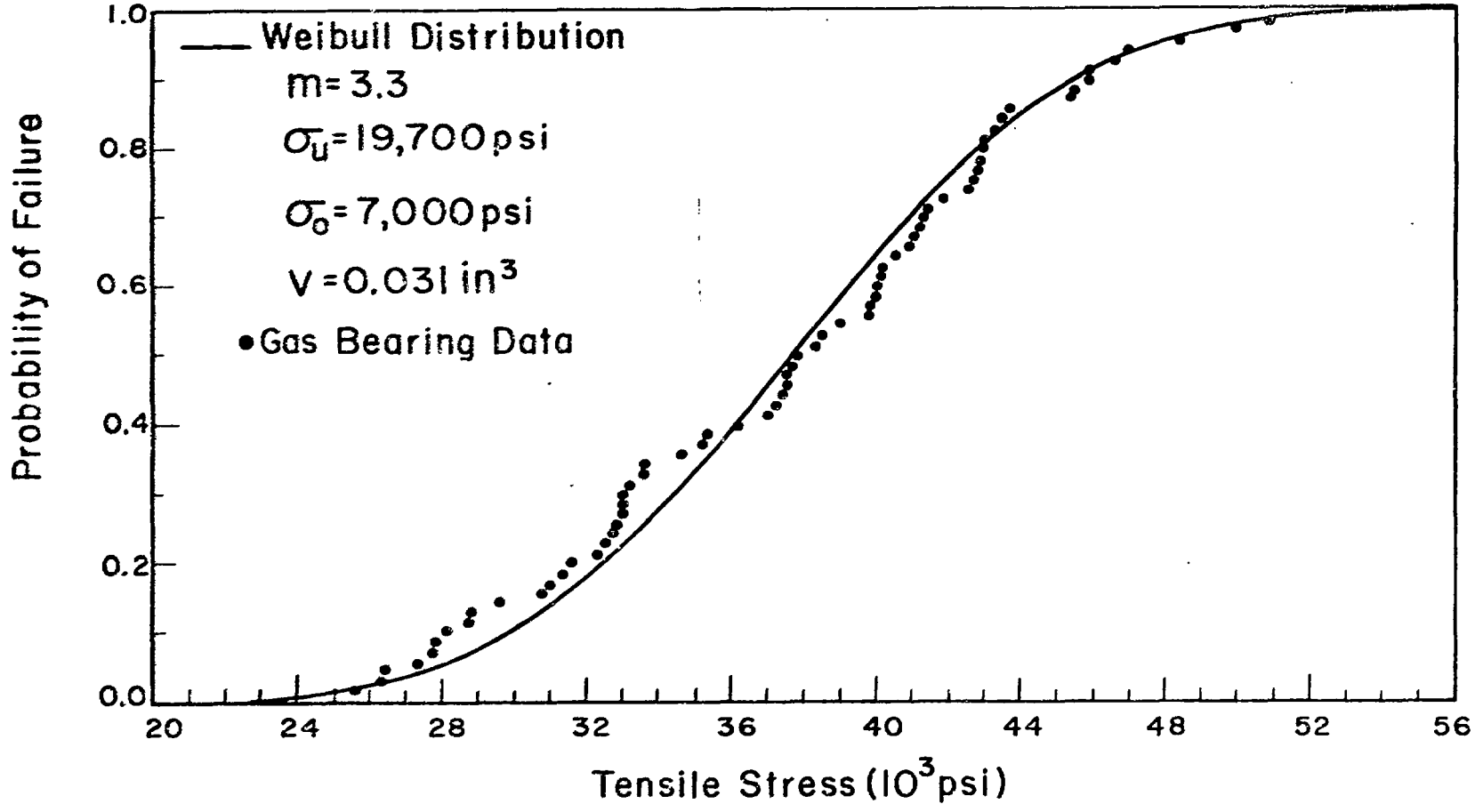

Figure 22 Comparison of Tensile Strength Cumulative Distribution for Alumina to Gas-Bearing Data of C. D. Pears

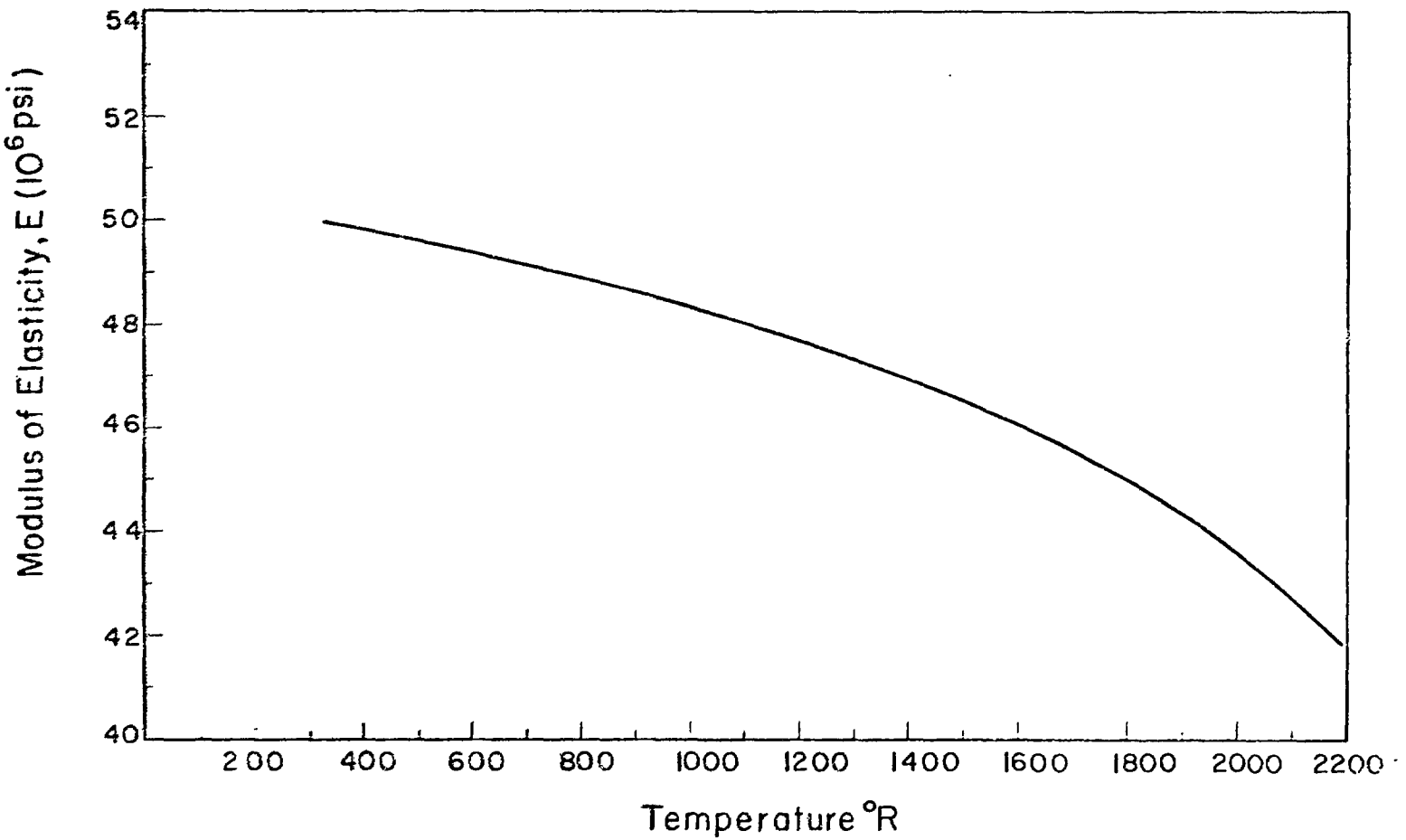

Figure 21 Modulus of Elasticity of Alumina as a Function of Temperature (After Dally)

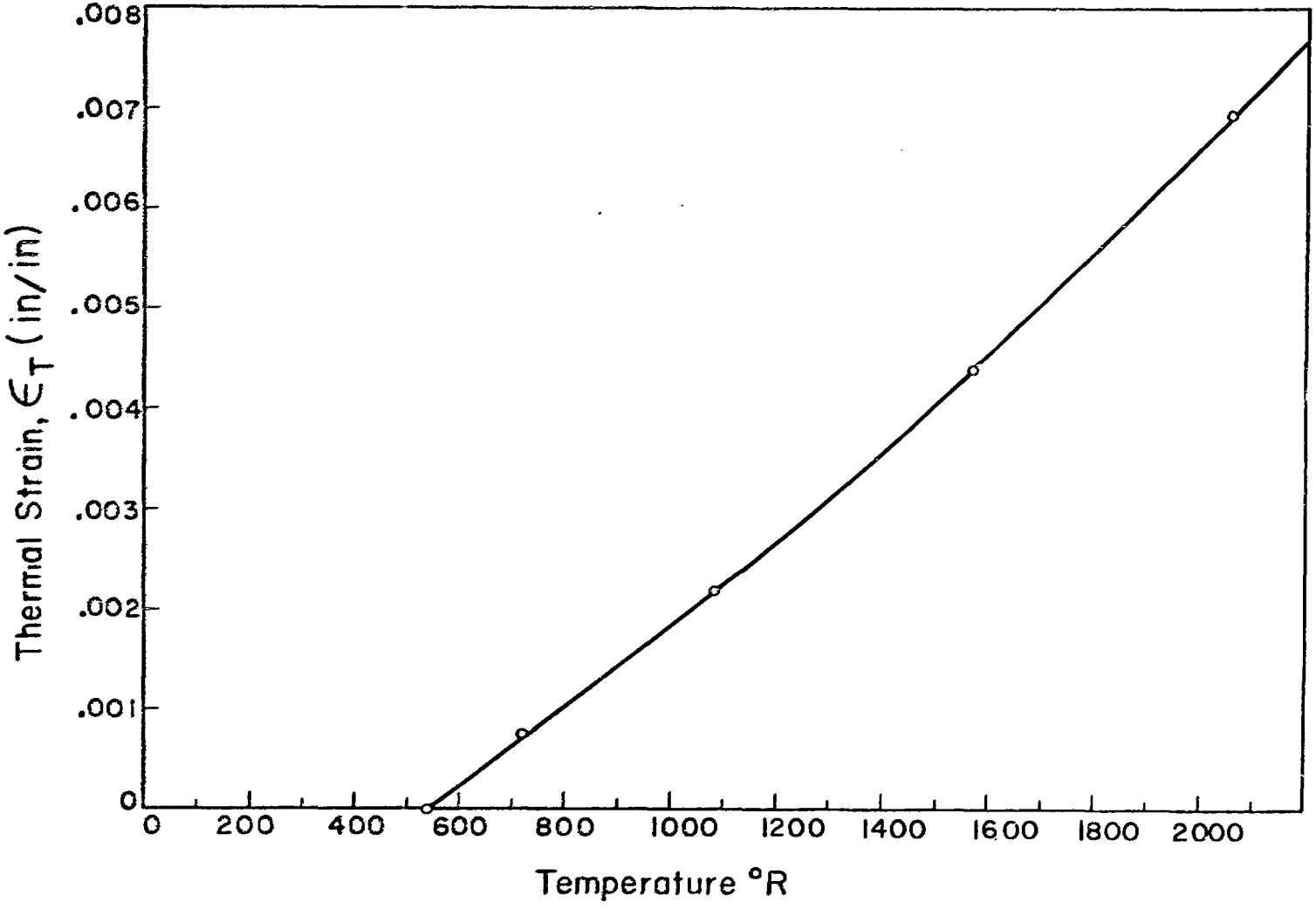

Figure 24 Thermal Strain of Alumina as a Function of Temperature (After Goldsmith, Hirschhorn and Waterman)

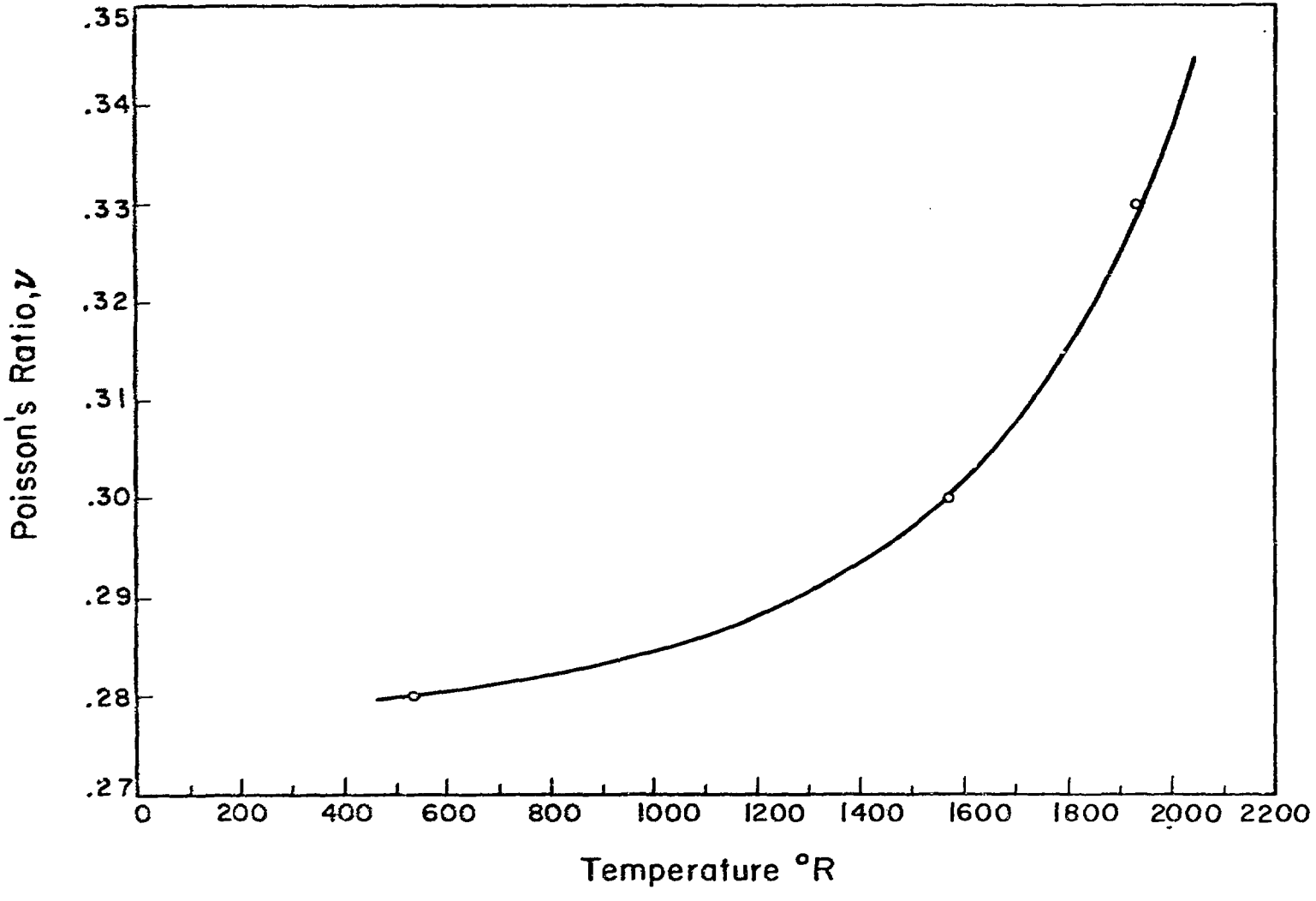

Figure 25 Poisson's Ratio of Alumina as a Function of Temperature (After Coble and Kingery)

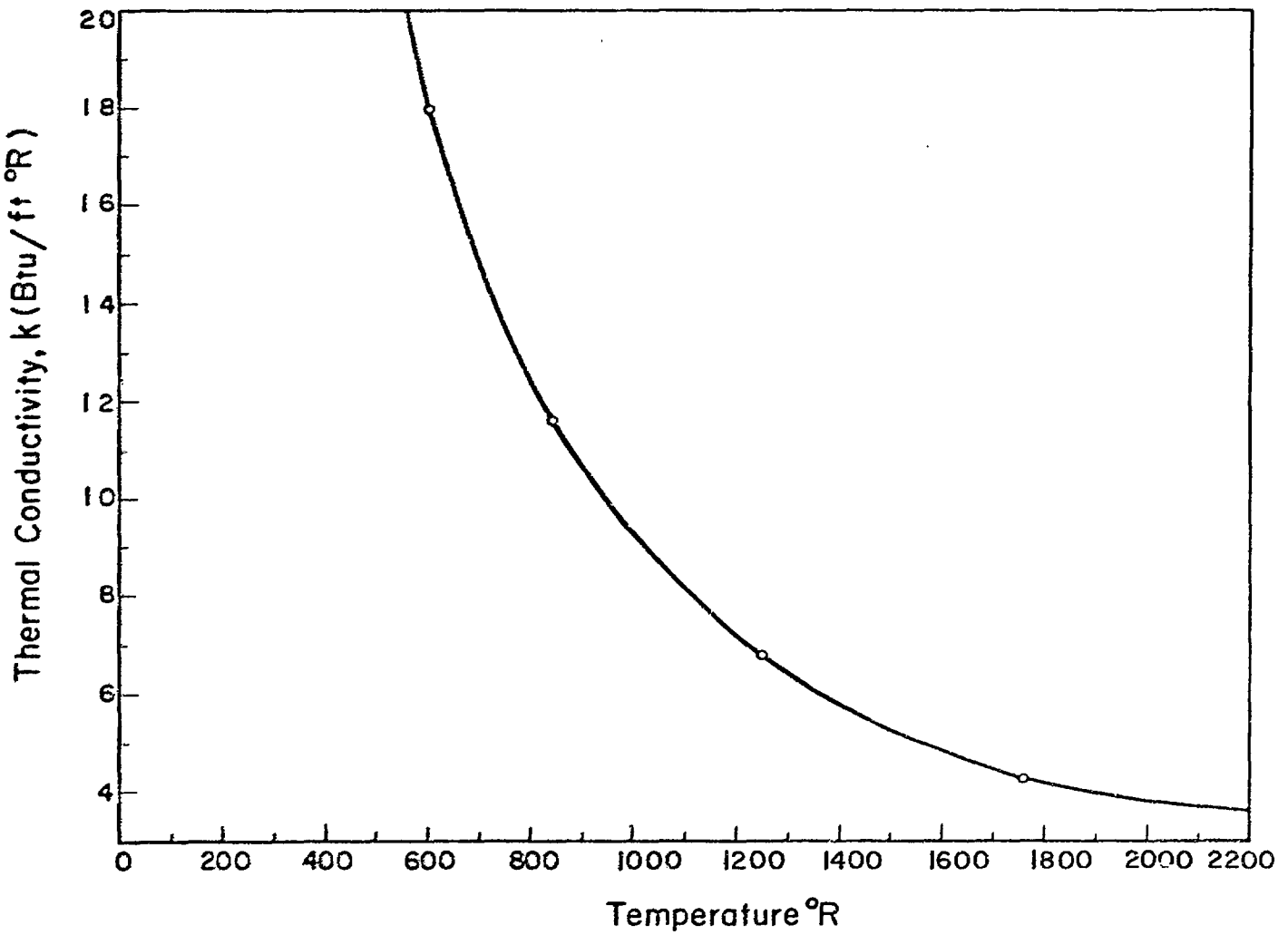

Figure 26 Thermal Conductivity of Alumina as a Function of Temperature
(After Goldsmith, Hirshhorn and Waterman)

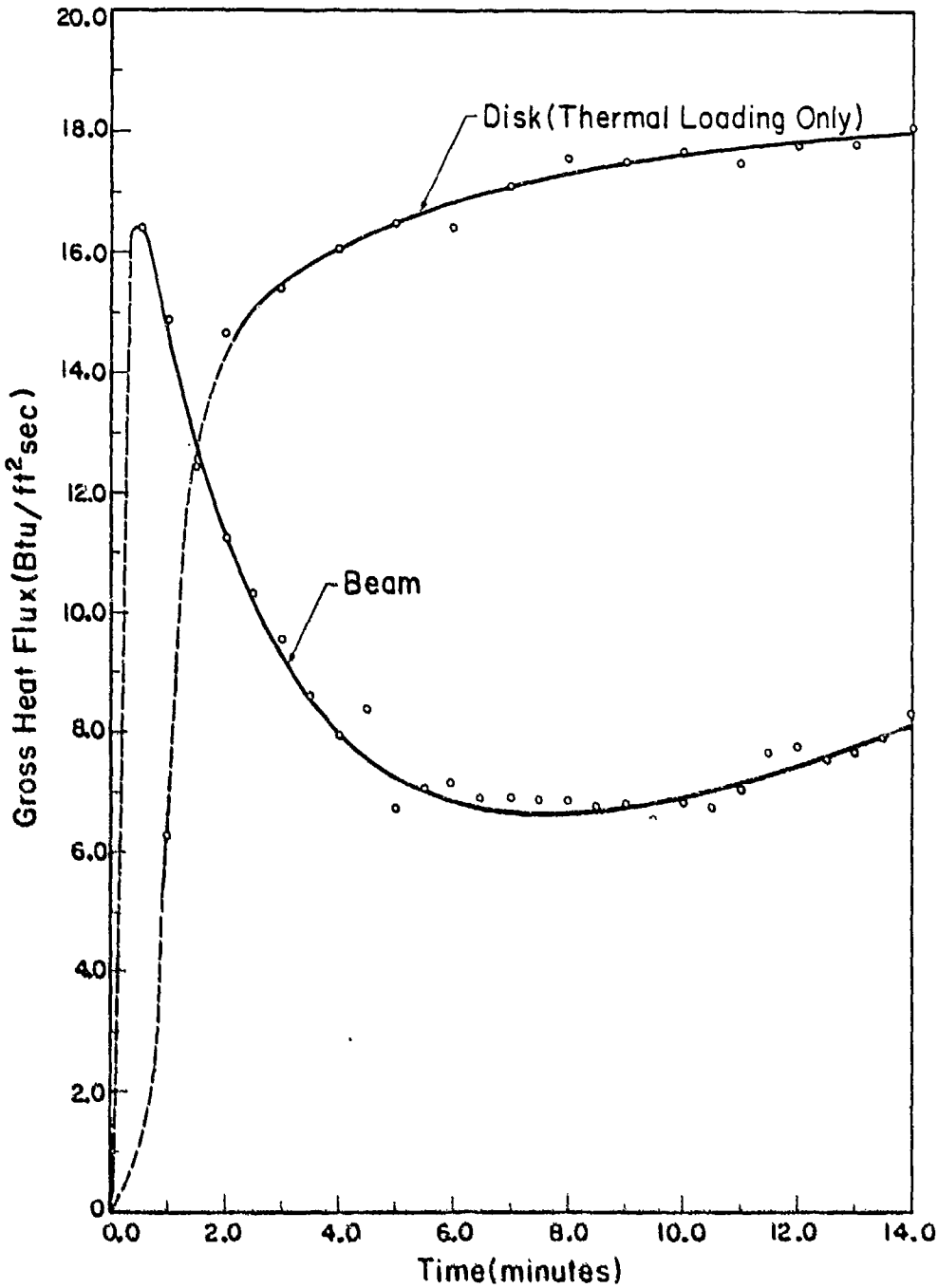

Figure 27 Gross Heat Flux Incident Upon Beam and Disk as a Function of Time

4. BEAM STRESS ANALYSIS

The beam prototype structure is loaded, as shown in Figure 28, by terminal couples M(t) and by the temperature distribution T(z,t) induced by the heat flux Q(t) impinging on the bottom surface. The general solution of the thermal stresses in a beam with temperature dependent mechanical and thermal properties using strength-of-materials type assumptions is well known (Reference 12). By replacing the term αT everywhere by ε_T, the thermal strain, and introducing the mechanically induced bending moment distribution M(t), the stress distribution $\sigma_x(z,t)$ is found to be given by

$$\sigma_x(z,t) = -\varepsilon_T E + \frac{P_T(t)}{A} + \frac{M_{T_z}(t)\, y}{I_z} + \frac{\left[M_{T_y}(t) + M(t)\right] z}{I_y} \qquad (18)$$

where

$$P_T(t) = \int_A \varepsilon_T E \, dA \qquad (19)$$

$$M_{T_y}(t) = \int_A \varepsilon_T E z \, dA \qquad (20)$$

$$M_{T_z}(t) = \int_A \varepsilon_T E y \, dA \qquad (21)$$

It is observed that, in this formulation with ε_T replacing αT, the dependence of the solution upon the temperature distribution is now entirely implicit.

Due to the fact that the temperature distribution is independent of y the following simplifications result:

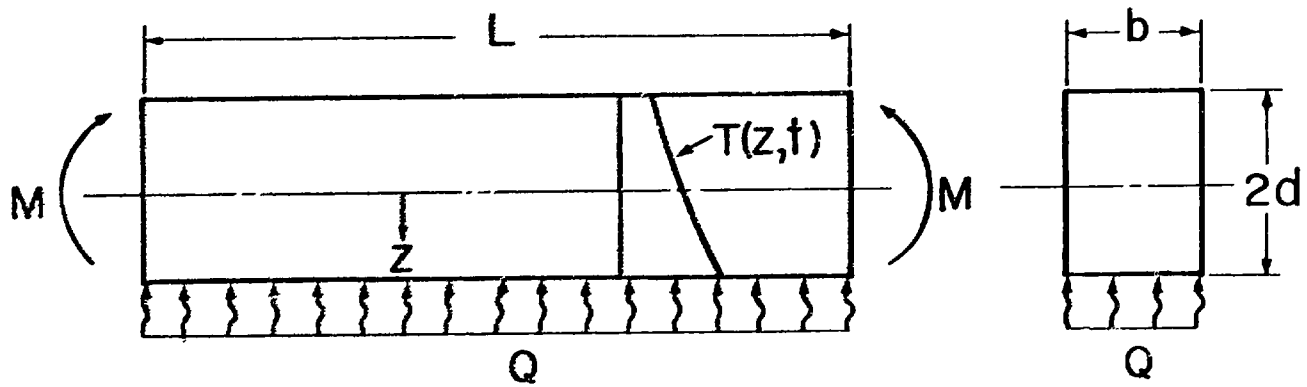

Figure 28 Geometry for Beam Analysis

$$M_{T_z}(t) = 0$$

$$P_T(t) = b \int_{-d}^{d} \varepsilon_T E \, d\, z \qquad (22)$$

$$M_{T_y}(t) = b \int_{-d}^{d} \varepsilon_T E \, z \, d\, z$$

Noting that $A = 2bd$ and $I_y = (2/3)bd^3$, the expression for the stress distribution becomes

$$\sigma_x(z,t) = \frac{3M(t)\, z}{2bd^3} - \varepsilon_T E + \frac{1}{2d} \int_{-d}^{d} \varepsilon_T E dz + \frac{3z}{2d^3} \int_{-d}^{d} \varepsilon_T E \, z \, d\, z \qquad (23)$$

Thus, given $\varepsilon_T = \varepsilon_T(T)$, $E = E(T)$, $T(z,t)$ and $M(t)$, Equation (23) will yield the stresses in the beam.

The solution of Equation (23) has been accomplished using a digital computer (Appendix II). Using the temperature distribution curves, Figure 5 , the material property curves, Figures 23 and 24, and the relationship

$$M(t) = 59.4 \text{ in-lbs for } 0 \leq t \leq 8.0 \text{ min}$$
$$= 59.4 + 535.3\ (t-8.0) \text{ in. lbs for } t \geq 8.0 \text{ min} \qquad (24)$$

the stress distribution is found to be as shown in Figure 29. It is observed that the stresses are small until after the mechanical load begins to increase at the 8.0 min point. Also, another consequence of the dominating mechanical loading is that the stress distribution is very nearly linear after the 9.0 min point.

Figure 30 illustrates the maximum tensile stress distribution. It is interesting to note that, using the mean tensile strength of approximately 32,400 psi, the deterministic maximum stress theory predicts failure at about 12.6 min. From the experimental data, Figure 6, the earliest failure occurs at about 11.3 min and the median time to failure is about 12.3 min.

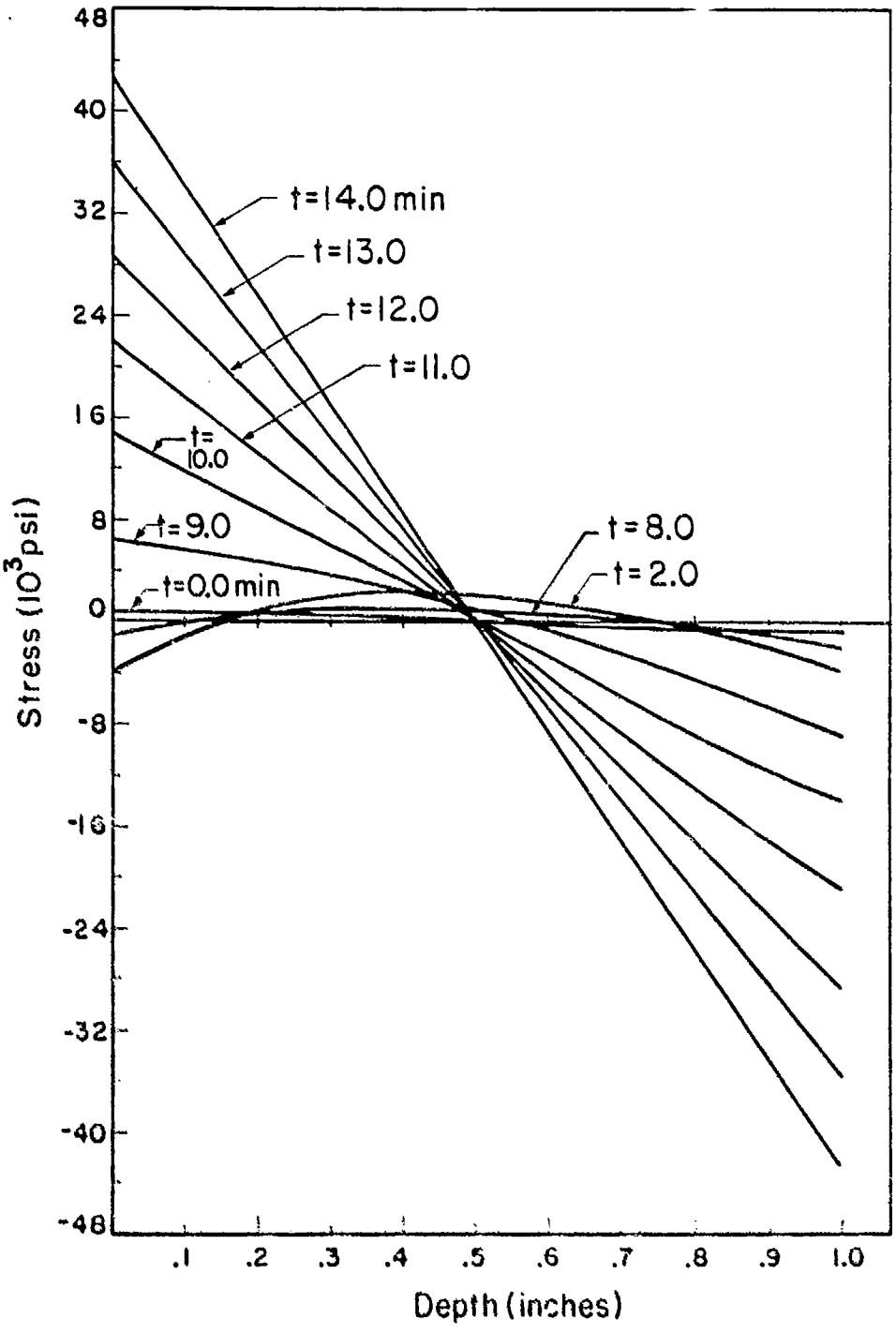

Figure 29 Stress Distributions in Beam Under Thermal and Mechanical Loading

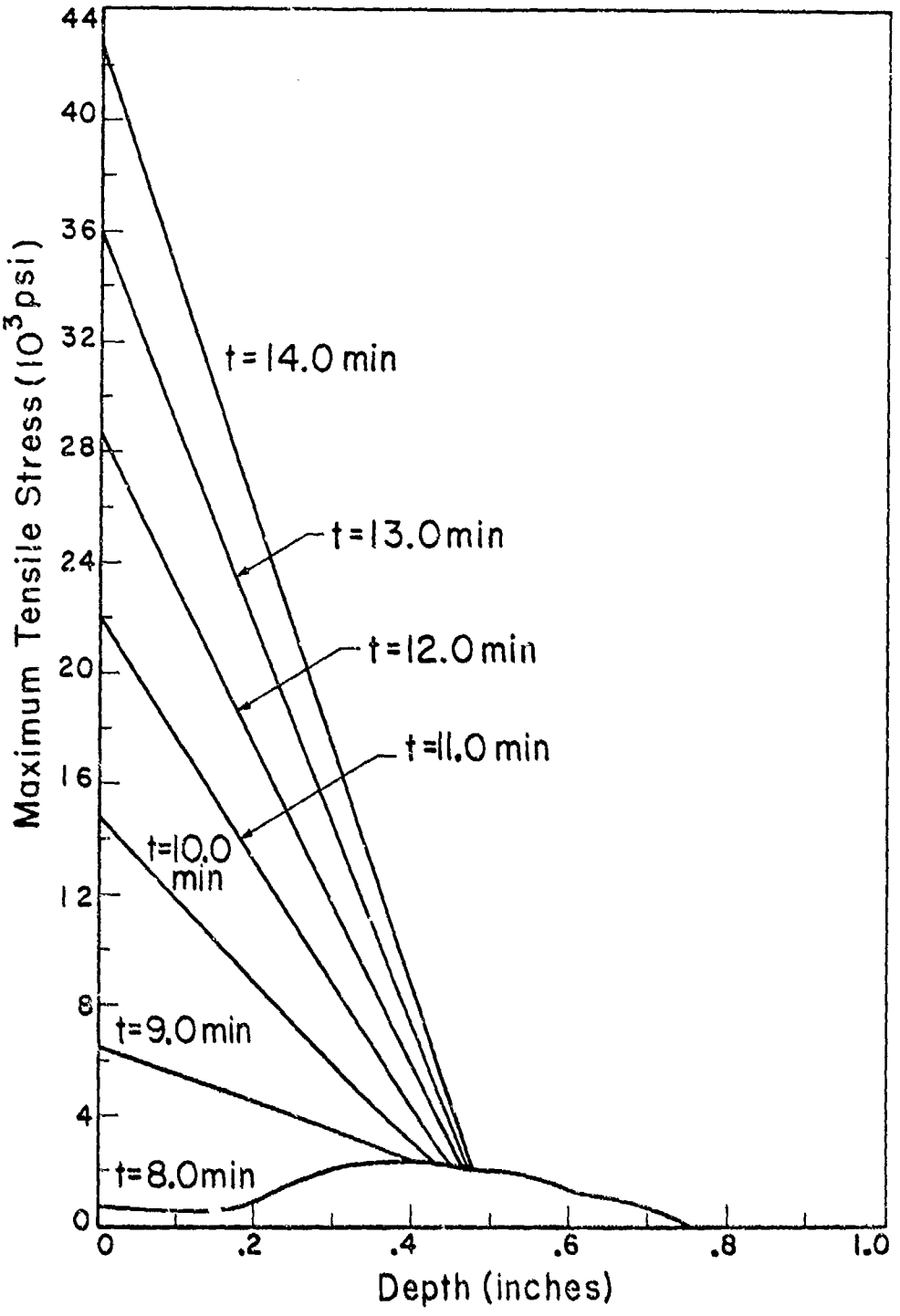

Figure 30 Maximum Tensile Stresses in Beam Under Thermal and Mechanical Loading

5. DISK STRESS ANALYSIS

The disk prototype structure is loaded, as shown in Figure 31, by a tensile radial stress S on the outside surface and by the temperature distribution T(r,t) produced by the heat flux Q(t) on the inside surface. The plane stress solution in the case where the mechanical and thermal properties of the material are independent of temperature is well known (Reference 12). One method of accounting for temperature dependent properties is to represent the disk as a composite structure of concentric rings where each ring is thin enough so that the material properties within the ring can be assumed to be constant.

The analysis of the concentric rings can be readily accomplished using the Method of Initial Parameters or Transfer Matrix Method (Reference 13) due to the fact that the geometric and equilibrium conditions which must be satisfied at each interface between rings are automatically fulfilled. In addition to those parameters defined in Figure 31, the parameters and variables entering into the problem are:

ε_T = thermal strain

E = modulus of elasticity

ν = Poisson's ratio

$T(r,t)$ = temperature distribution

$u(r,t)$ = radial displacement distribution

$\sigma_r(r,t)$ = radial stress distribution

$\sigma_\theta(r,t)$ = circumferential stress distribution

Using a matrix form of this method, the stress distribution in the disk is given by

$$\sigma_r(r,t) = \frac{N_r(r,t)}{h}$$

$$\sigma_\theta(r,t) = \frac{N_\theta(r,t)}{h} \qquad (25)$$

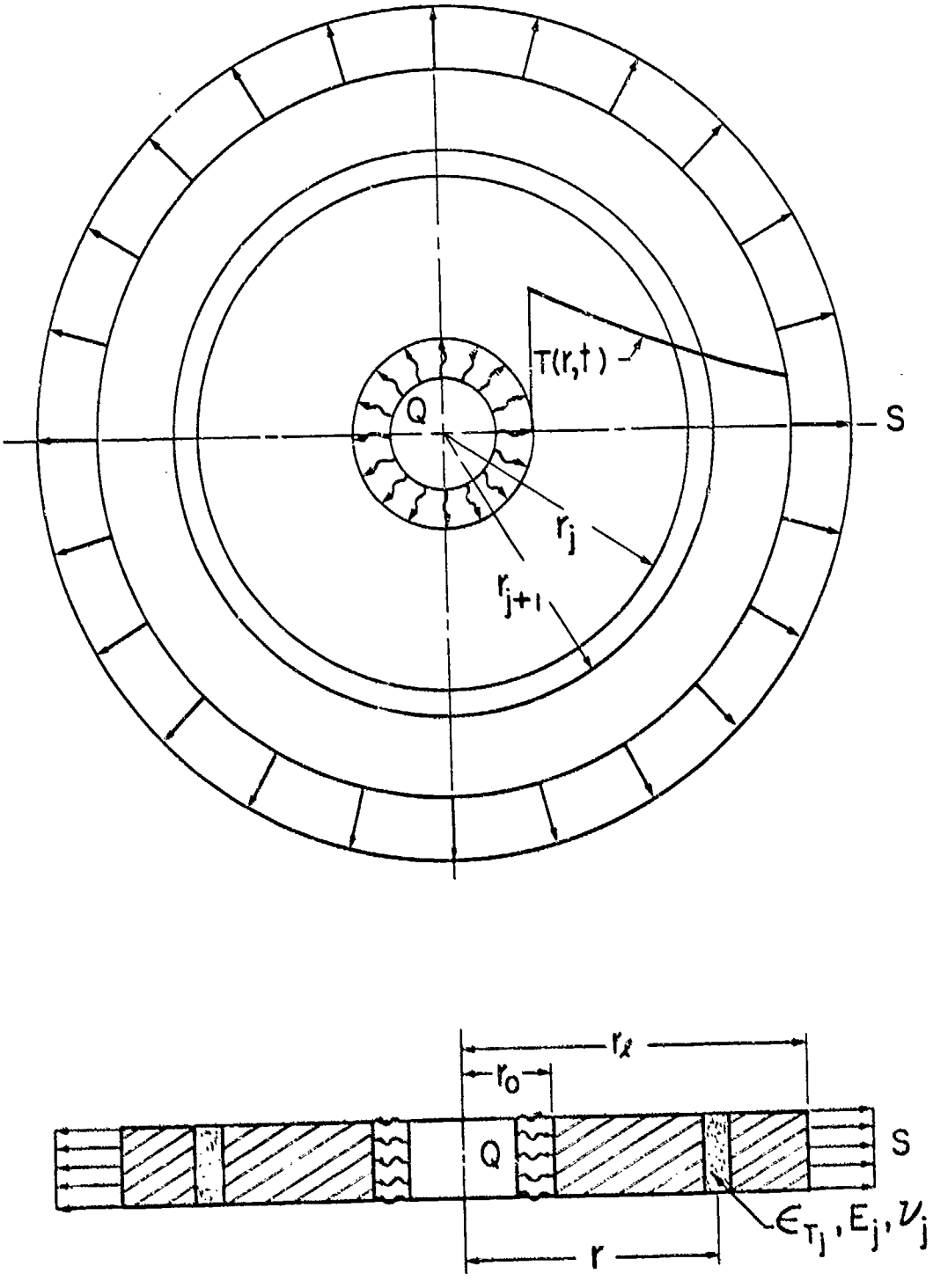

Figure 31 Concentric Ring Geometry for Disk Analysis

where

$$\bar{N}(r,t) = \bar{M}_j(r,t)\,\bar{M}_{j-1}(r_j,t)\,\bar{M}_{j-2}(r_{j-1},t)\ldots\bar{M}_1(r_2,t)\,\bar{M}_o(r_1,t)\bar{I}_o(t) \tag{26}$$

and

$$\bar{N}(r,t) = \begin{bmatrix} u(r,t) \\ N_r(r,t) \\ 1 \end{bmatrix} \tag{27}$$

$$\bar{I}_o(t) = \begin{bmatrix} u(r_o,t) \\ N_r(r_o,t) \\ 1 \end{bmatrix} \tag{28}$$

$$N_\theta(r,t) = \begin{bmatrix} \frac{E_j h}{r} & \nu_j & 0 \end{bmatrix} \bar{N}(r) \tag{29}$$

$$\bar{M}_j(r,t) = \begin{bmatrix} \frac{r}{r_j}\left\{1 - \frac{(1+\nu_j)}{2}\Psi_j(r)\right\} & \frac{r(1-\nu_j^2)}{2E_j h}\Psi_j(r) & \frac{(1+\nu_j)\varepsilon T_j}{r\,T(r,t)}\int_{r_j}^{r}\eta T(\eta,t)\,d\eta \\ \frac{E_j h}{2r_j}\Psi_j(r) & 1 - \frac{(1-\nu_j^2)}{2}\Psi_j(r) & -\frac{hE_j\varepsilon T_j}{r^2 T(r,t)}\int_{r_j}^{r}\eta T(\eta,t)\,d\eta \\ 0 & 0 & 1 \end{bmatrix} \tag{30}$$

$$\Psi_j(r) = 1 - \left(\frac{r_j}{r}\right)^2 \tag{31}$$

In general Equation (26) leads to two nontrivial relationships which may be expressed as

$$u(r,t) = u_o(t)\,F_1(r,t) + N_o(t)\,F_2(r,t) + F_3(r,t)$$
$$N_r(r,t) = u_o(t)\,G_1(r,t) + N_o(t)\,G_2(r,t) + G_3(r,t) \tag{32}$$

where $u_o(t) = u(r_o,t)$ and $N_o(t) = N_r(r_o,t)$ and where $F_i(r,t)$ and $G_i(r,t)$, $i = 1,2,3$, represent the cumbersome expressions that could be obtained from Equation (26). Now since the boundary conditions are

$$N_r(r_o,t) = 0$$
$$N_t(r_\ell,t) = Sh \tag{33}$$

the two constants of integration $u_o(t)$ and $N_o(t)$ are found from Equation (32) to be

$$N_o(t) = 0$$
$$u_o(t) = \frac{Sh - G_3(r_\ell,t)}{G_1(r_\ell,t)} \tag{34}$$

The system of equations, Equations (25) through (34), has been programmed on a digital computer (Appendix III). Using the temperature distribution in the disk, Figure 13, and the curves for the material properties, Figures 23, 24 and 25, the stress distribution has been computed as depicted in Figures 32 and 33. It is observed that the radial stress is always compressive and hence, according to the fracture algorithm does not contribute to the probability of failure. The circumferential stress distribution is observed to be compressive near the inside radius and tensile over most of the remainder of the disk.

The maximum tensile circumferential stress distribution is illustrated in Figure 34. Using the mean tensile strength of approximately 32,400 psi, the deterministic maximum stress theory predicts that no disk will fail up to the end of the test at 14.0 min. From the experimental data, Figure 14, the earliest failure occurs at just under 7.0 min, the median is at about 9.6 min and all specimens have failed by the 12.4 min point.

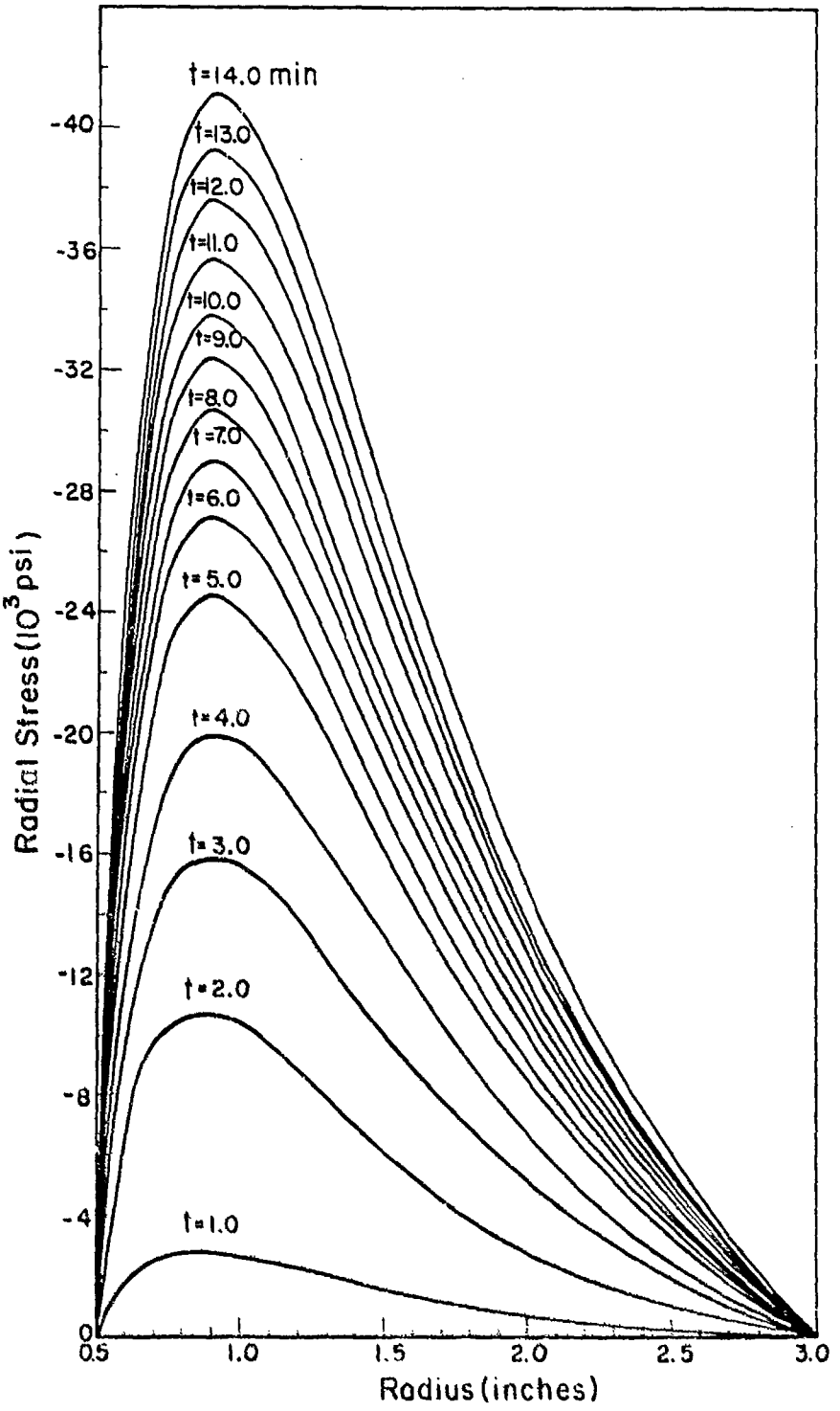

Figure 32 Radial Stress Distributions in Disk Under Thermal Loading

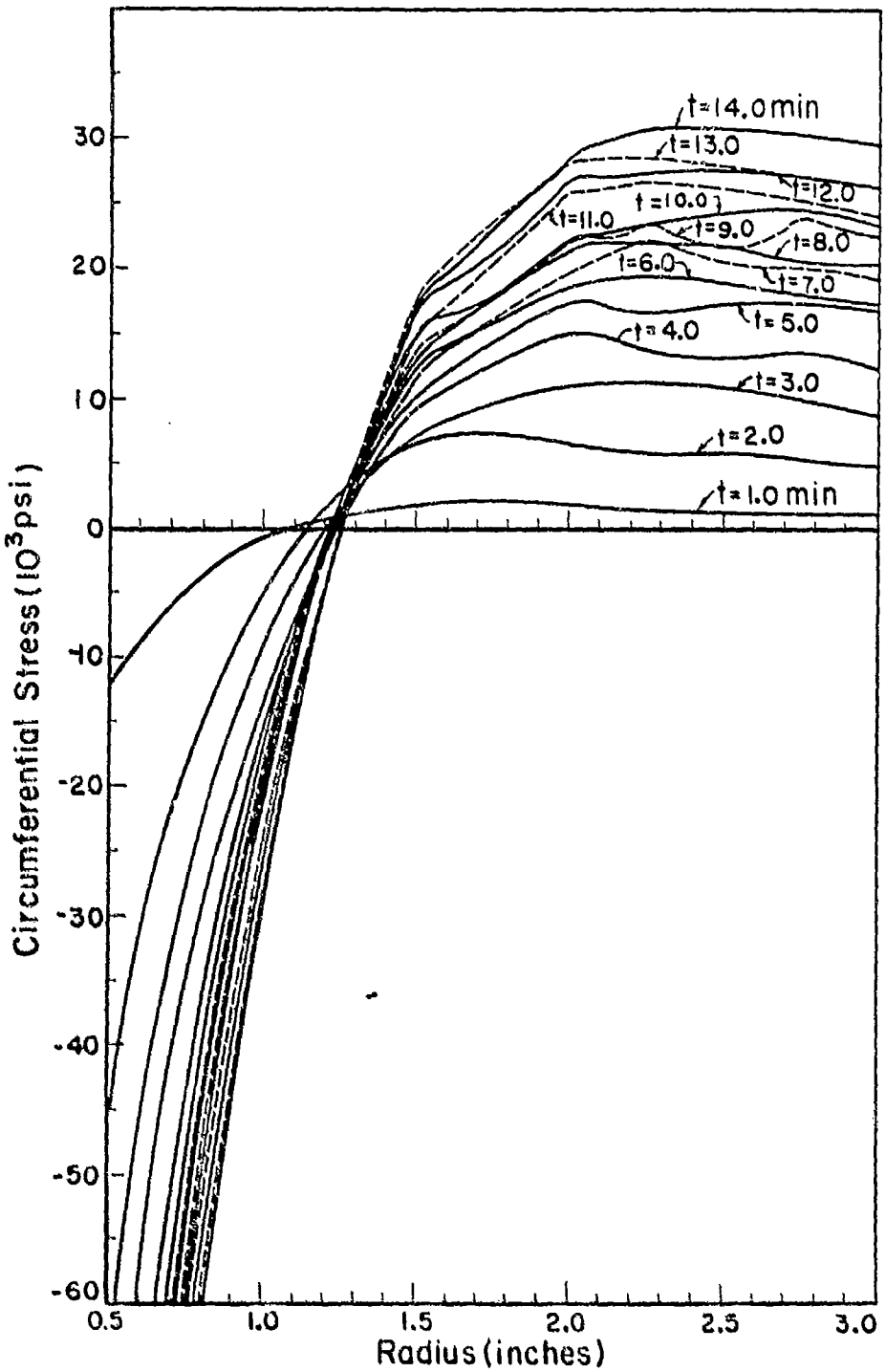

Figure 33 Circumferential Stress Distributions in Disk Under Thermal Loading

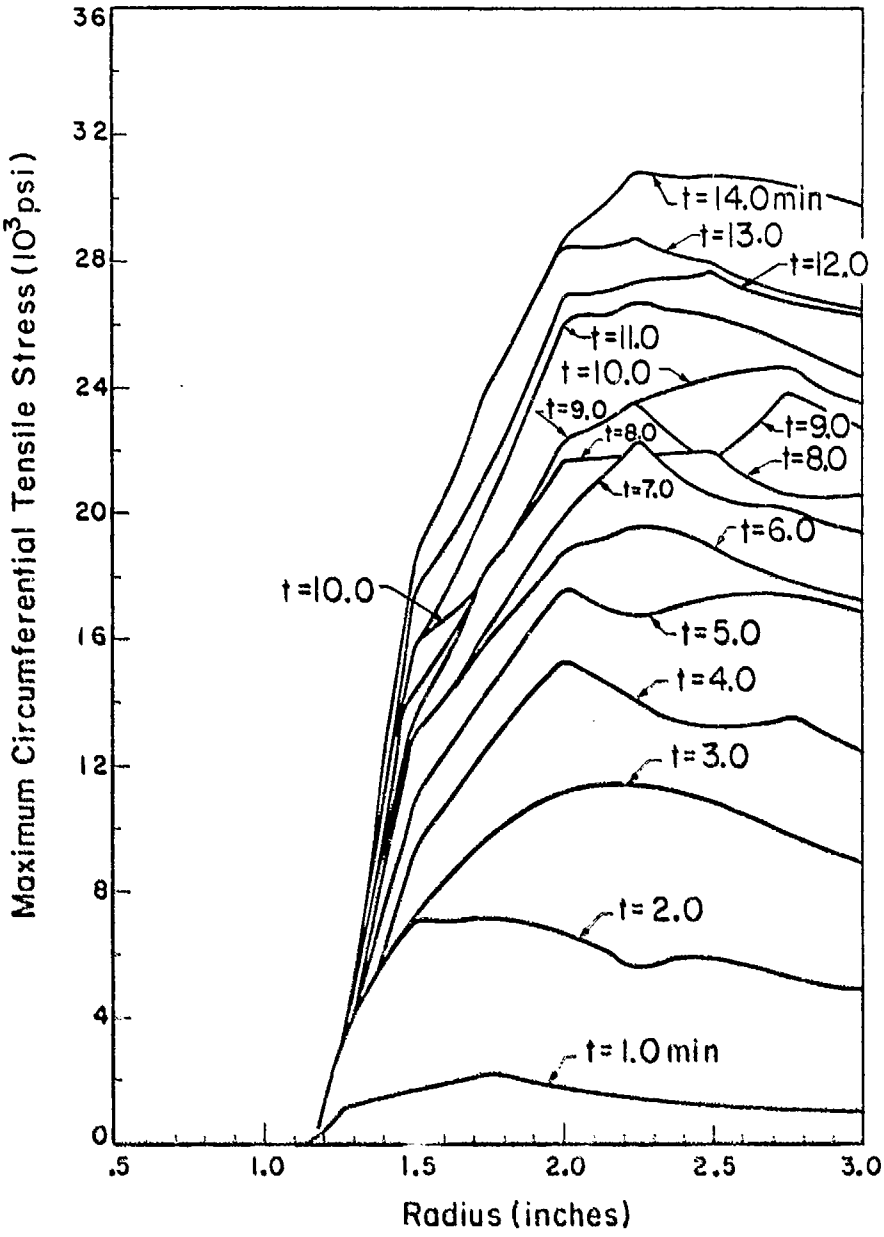

Figure 34 Maximum Tensile Circumferential Stresses in Disk Under Thermal Loading

6. APPLICATION OF THE FRACTURE ALGORITHM

Separate, but similar, computer programs were written for the analysis of the beam and disk prototype structures (see Appendices II and III). Each program did the complete analysis of its prototype structure, including thermal analysis, stress analysis and the statistical analysis employing the fracture algorithm.

The fracture algorithm described in Section II was designed especially for the analysis of the beam and disk experiments and thus no major modifications were necessary in incorporating it into the computer programs. Steps (3), (4) and (5) are the only steps in the fracture algorithm that have not already been discussed or that are not executable in their given form. For convenience, these steps shall be repeated here along with a discussion of how the steps were accomplished in the analysis of the beam and the disk.

(3) Divide the structure into n convenient subvolumes $V_1, V_2, \ldots V_n$. No subvolume should be smaller than the gage volume of the tension specimen: $V_j \geq \bar{v}$, $j = 1,2,\ldots n$. Subvolumes should be selected with approximately homogeneous stress states.

The volume of the tension specimen is 0.0982 $in.^3$ The depth of the beam was divided into 20 equal segments thereby creating identical subvolumes of volume 0.100 $in.^3$ The disk was subdivided into 69 ring type subvolumes, each with a volume of 0.0996 $in.^3$. By selecting the smallest volumes possible in each case, the homogeneity of the stress state in each subvolume was optimized.

(4) For each value of time t determine the "worst" risk of rupture for each subvolume V_j:

$$B_{ij}(t) = \frac{V_i}{v}\left\{\max_{D_j} f\left[\sigma_i(x,y,z,t);\ m(T),\sigma_u(T),\sigma_o(T)\right]\right\}, \quad i=1,2 \tag{4}$$

where

$$f = \left[\frac{\sigma_i(x,y,z,t) - \sigma_u(T)}{\sigma_o(T)} \right]^{m(T)} \quad \text{for } \sigma_i > \sigma_u$$

$$= 0 \text{ for } \sigma_i \leq \sigma_u \tag{5}$$

and where $T = T(x,y,z,t)$ and D_j is the region in space occupied by V_j.

In the computer programs, it was assumed that the maximum value of f always occurred on the boundary of the subvolume in both the case of the beam and disk. Regarding the beam subvolume, the value of f was computed at the top and bottom surfaces and the largest was selected to be the maximum value in the subvolume. In the case of the disk, f was computed on the inside radius and outside radius with largest being taken for the maximum in the ring.

Strictly speaking, the maximum value of f will not always lie on the boundary of the subvolume. Now Equation (4) is itself a conservative statement and thus, when the assumption that f is maximum on the boundary is valid, the results are still conservative. However, when the assumption is not valid the results are not conservative. Therefore it is assumed that, by making the subvolumes small enough, more often than not the maximum values will be attained on the boundary and in this manner the cumulative results for the risk of rupture for the entire structure will remain conservative.

(5) Determine the maximum value of each $B_{ij}(t)$ in the interval $0 \leq t \leq \tau$

$$B^*_{ij}(\tau) = \max_{0 \leq t \leq \tau} B_{ij}(t) \tag{6}$$

In the computer programs, the value of time is iterated by finite amounts so the problem of determining the maximum value of $B_{ij}(t)$ with respect to time is similar to finding the maximum of f in D_j. The value of B_{ij} is computed at each value of time

and the largest value is selected as the maximum value. Now the true maximum value may have occurred at some intermediate value of time. So, again, an appeal is made to small increments in order to minimize the error. In the case of the beam and disk, the B_{ij}'s increased fairly monotonically with time and thus the problem was alleviated since the maximums tended to occur at the current value of time.

The remainder of the task of placing the analyses on the computer was very straightforward. The stress analyses were programmed exactly as presented earlier in this section. The material properties that entered into the analyses were incorporated into the computer programs as functions of temperature. Data in tabular form was read into the computer and whenever a value between entries was desired, it was obtained by linear interpolation. The temperature distributions were read into the computer as two-dimensional tables and linear interpolation was again used for intermediate values. In all cases, the tables were constructed so as to tend to minimize errors arising from the use of linear interpolation.

Figure 35 is the comparison between the experiments and the "predictions" obtained from the fracture algorithm. These curves were made using the computer programs described in Appendices II and III in conjunction with the material property curves described earlier in this section. The agreement in both cases between the experiments and the theory employing the tension data is fairly remarkable in that, to our knowledge, no other investigators have achieved as good an agreement between two sets of experiments - much less three sets as is the case here.

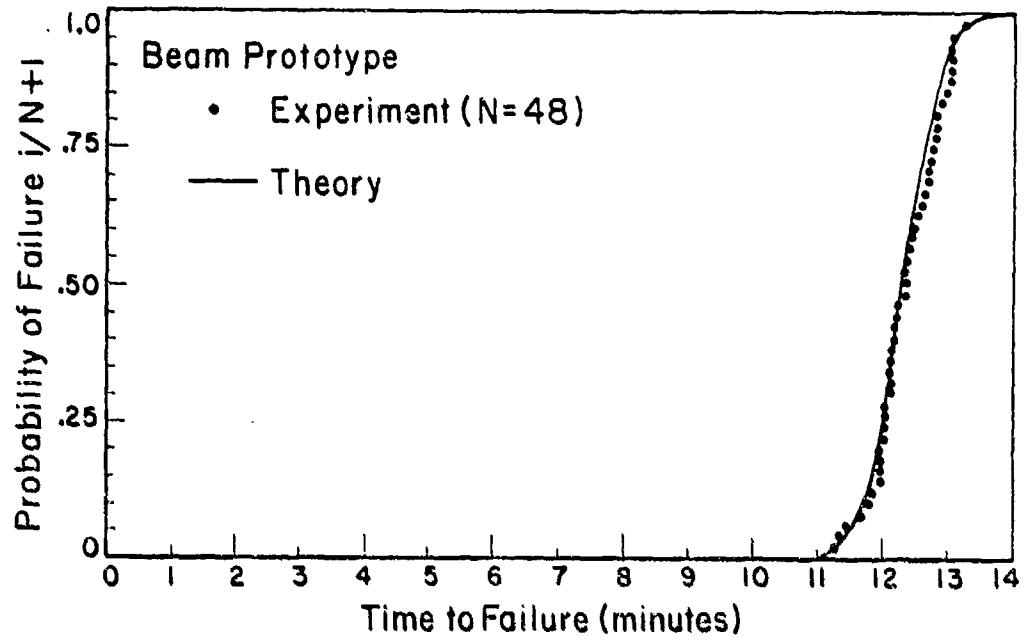

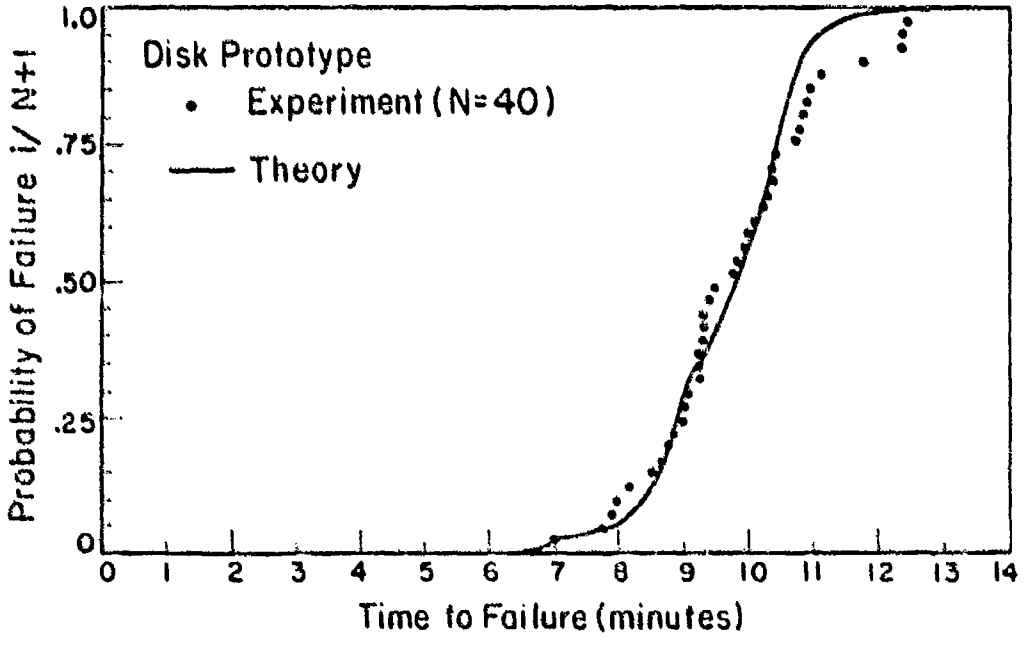

Figure 35 Comparison of Theory and Experiment for Beam and Disk (Using Weibull Tensile Strength Distribution with $m = 3.3$, $\sigma_u = 19{,}700$ psi, $\sigma_o = 7{,}000$ psi, and $V_e = 0.0982\,\text{in.}^3$

SECTION V
DISCUSSION OF RESULTS

1. RELIABILITY OF RESULTS

We have taken the position in this investigation that we have not proved the applicability of our fracture algorithm, but, that we have established its potential for predicting thermal/mechanical response. To justify this viewpoint in the light of the amazingly close predictions, we are obliged to expose a few of the scientific shortcomings of our program. The following unanswered questions all raise doubts concerning the veracity of our results.

(a) Have all the materials used in the beams, disks, and tension specimens been drawn from the same statistical population?

(b) Is high purity aluminum oxide a series material?

(c) Temperature dependent elastic and thermal properties and statistical strength parameters were taken from the literature. Do they represent the material used in this investigation?

(d) What is the magnitude and character of the various parasitic stresses present in the different test specimens?

(e) Was the material used in our specimens homogeneous; for example, is the surface and volume material identical?

Without dwelling on the desirability of resolving these points, let us say that a more ambitious program should address itself to such questions.

2. SENSITIVITY OF RESULTS

Due to the small disparity between the predicted and measured response of the beam and disk prototype structures, it is now unnecessary to conduct the error analysis originally contemplated

at the beginning of the program. Instead, a variation of parameters study was performed which yields more general information. Specifically, variations of plus and minus 10 percent ($\pm$ 10%) were introduced into each material property versus temperature curve entering into the response analyses. The resulting theoretical curves are compared with the data in Figures 36 through 41.

Referring to these figures, it is readily observed that the beam is virtually insensitive to the mechanical properties $\varepsilon_T(T)$, $E(T)$ and $\nu(T)$. Poisson's ratio was recognized to be unimportant in the stress analysis of the beam. However, the fact that the thermal strain and modulus of elasticity do not play a large role in the case of the beam is probably due to the fact that the temperature distribution is too linear. With respect to the Weibull parameters m, σ_u and σ_o the beam is observed to behave fairly sensitively.

The effect of Poisson's ratio was included in the stress analysis of the disk. Consequently, it is interesting that the $\pm$ 10% variations in $\nu(T)$ do not significantly alter the theoretical curve in Figure 38. The other figures indicate that the disk is fairly sensitive to m and very sensitive to $\varepsilon_T(T)$, $E(T)$, σ_u and σ_o. It is also interesting to note that the disk curves for $\pm$ 10% $\varepsilon_T(T)$ and $\pm$ 10% $E(T)$, Figures 36 and 37, are identical. This would be explained if the parameters always occurred as a product, $\varepsilon_T E$, as is the case in the stress analysis of the beam Equation (23). That this is not the situation in the case of the disk is readily observed by inspecting Equations (25) through (34) for the stress analysis of the disk. A simple example, however, will clear things up.

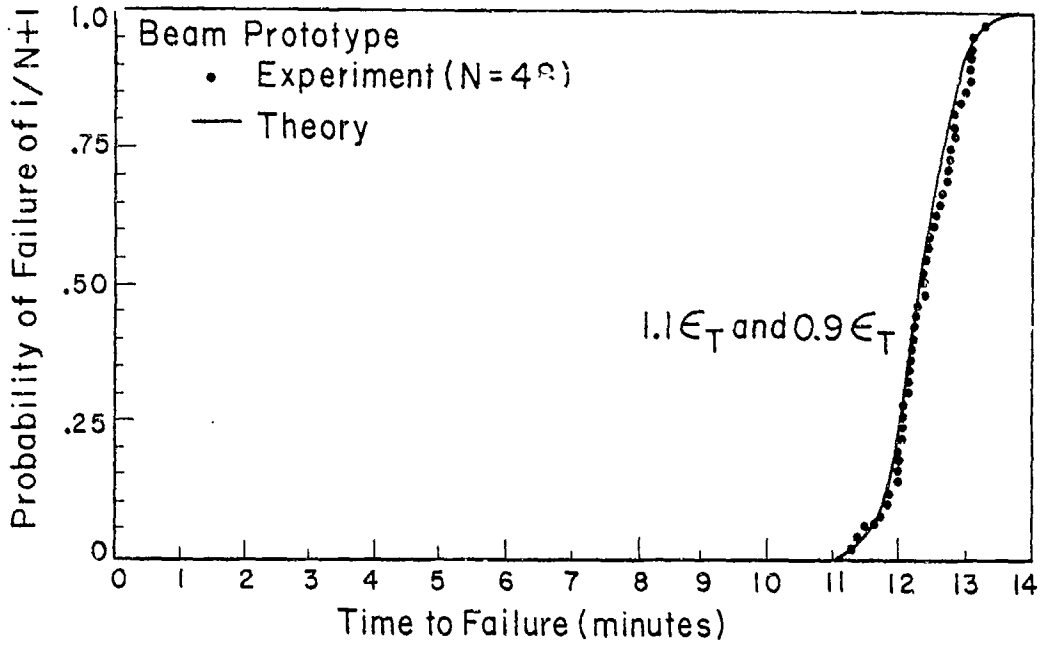

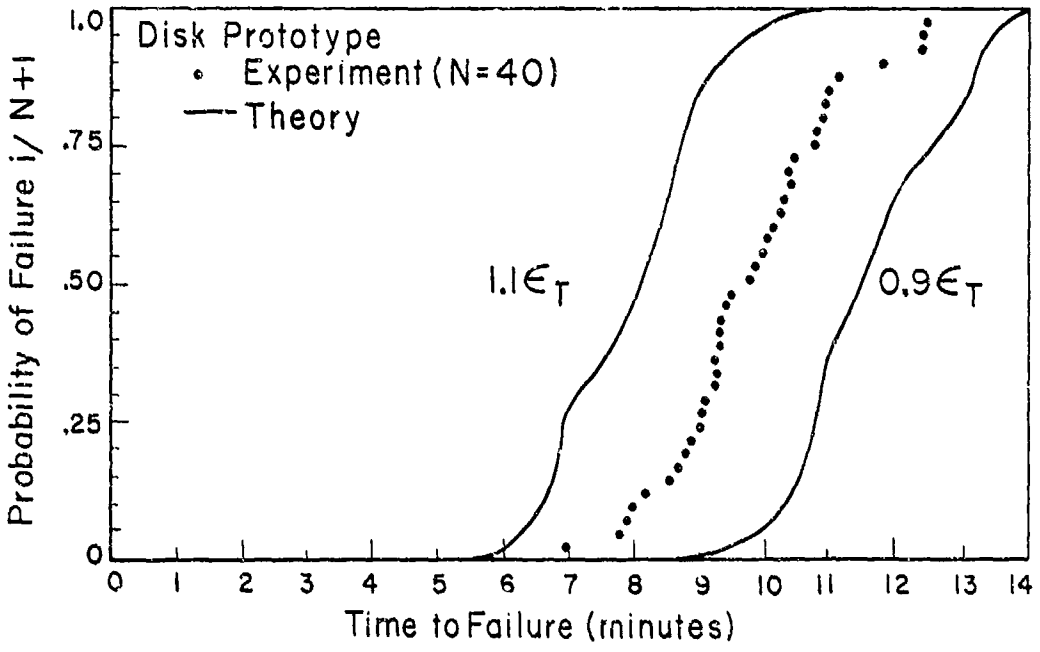

Figure 36 Effect of 10 Percent Variation in Thermal Strain Upon the Predicted Cumulative Distributions for the Beam and Disk

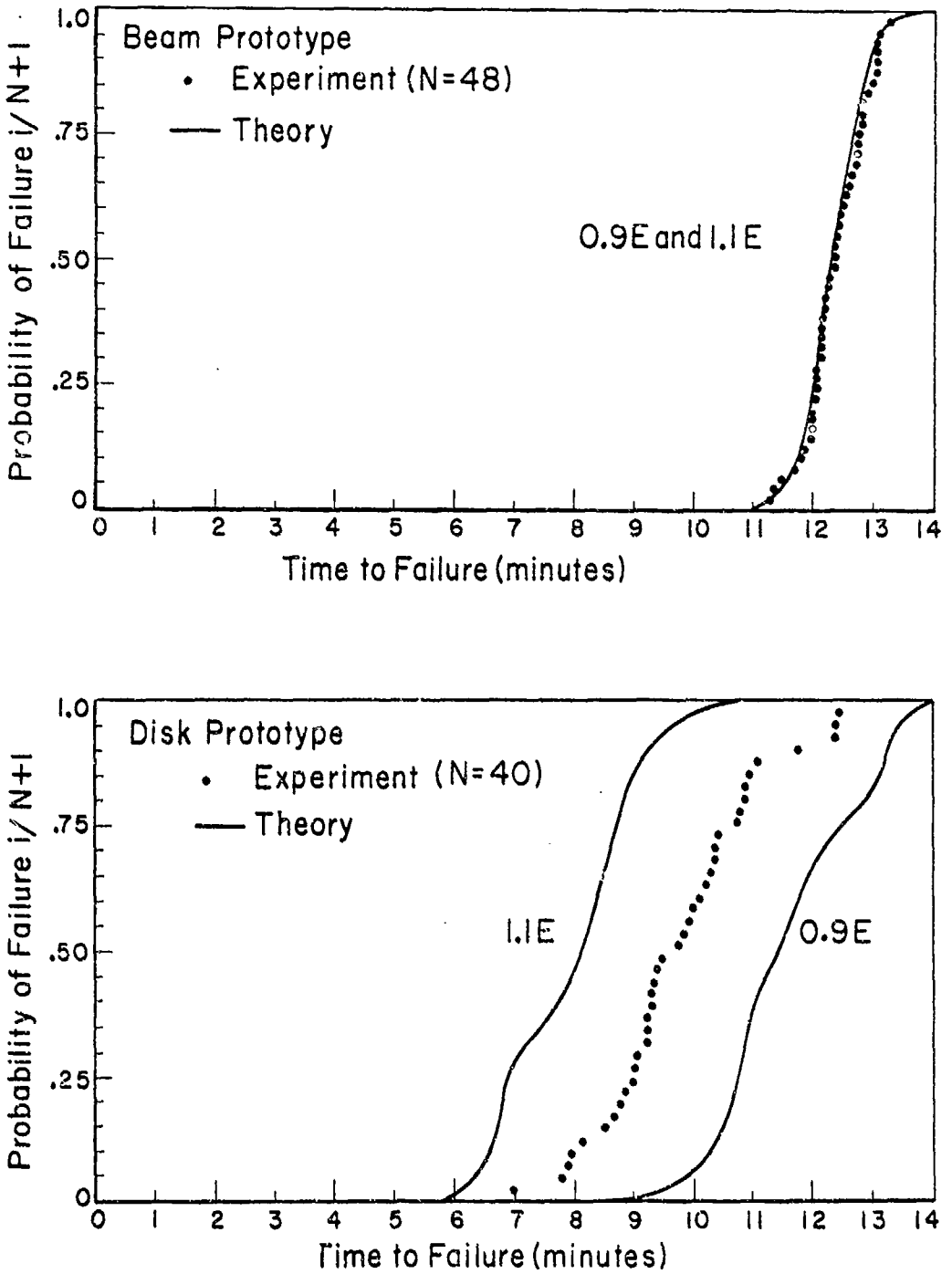

Figure 37 Effect of 10 Percent Variation in Modulus of Elasticity Upon the Predicted Cumulative Distributions for the Beam and Disk

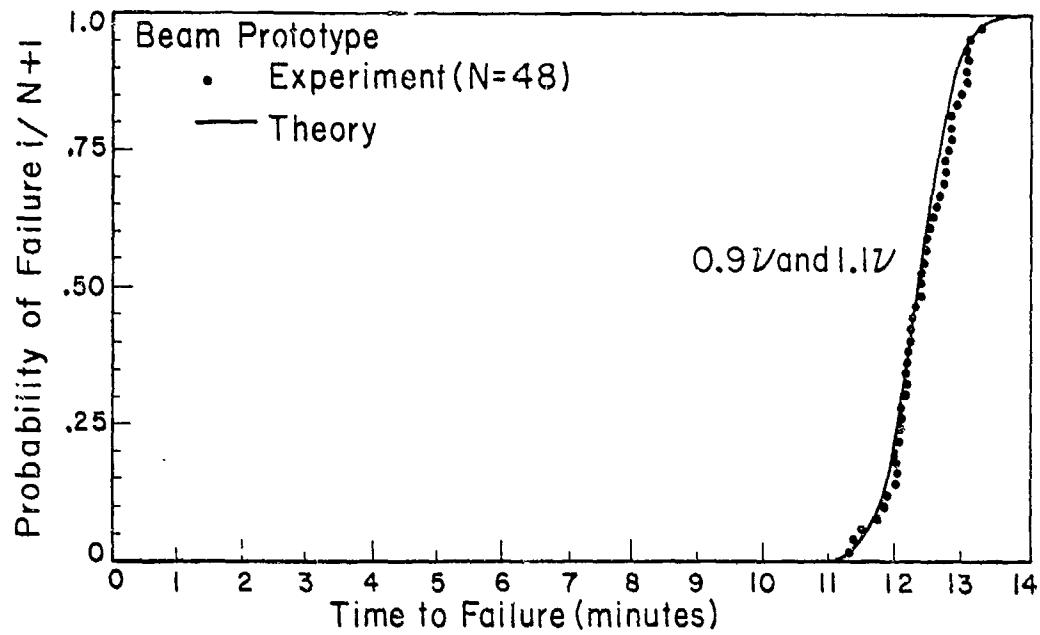

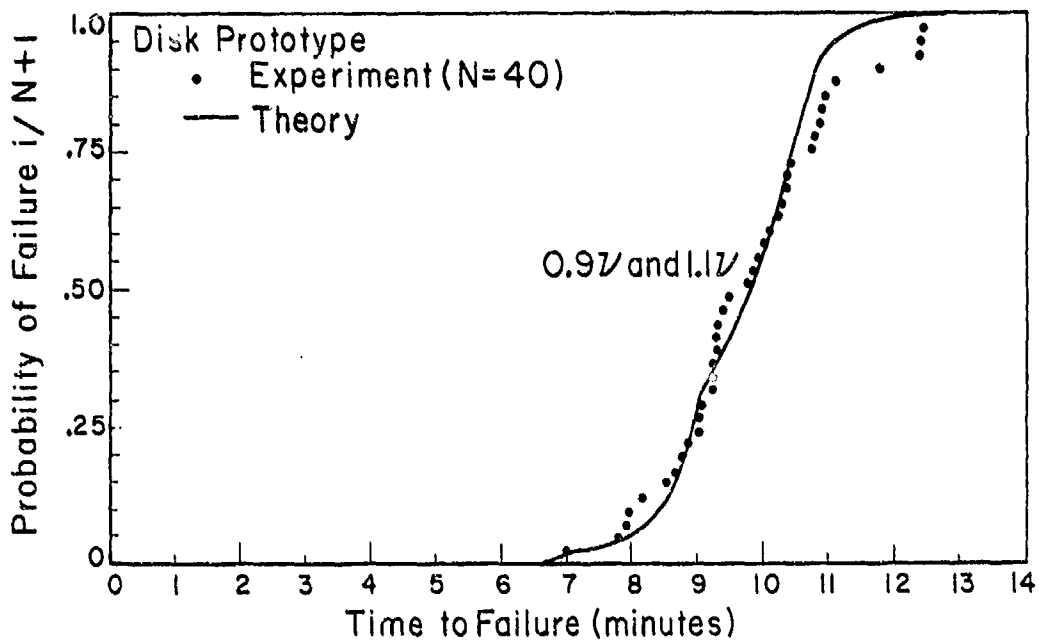

Figure 38 Effect of 10 Percent Variation in Poisson's Ratio Upon the Predicted Cumulative Distributions for the Beam and Disk

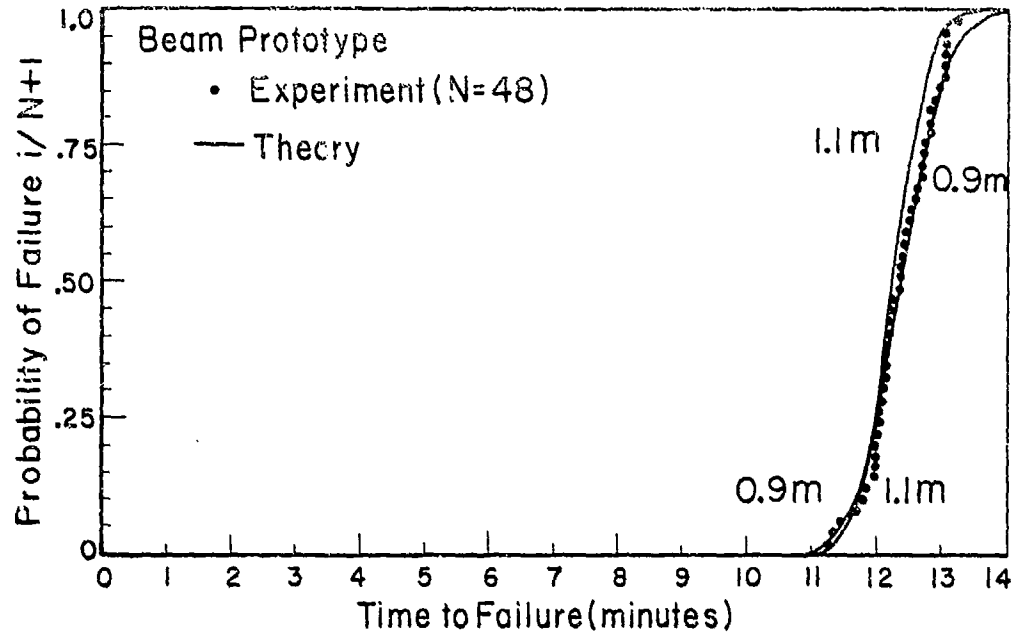

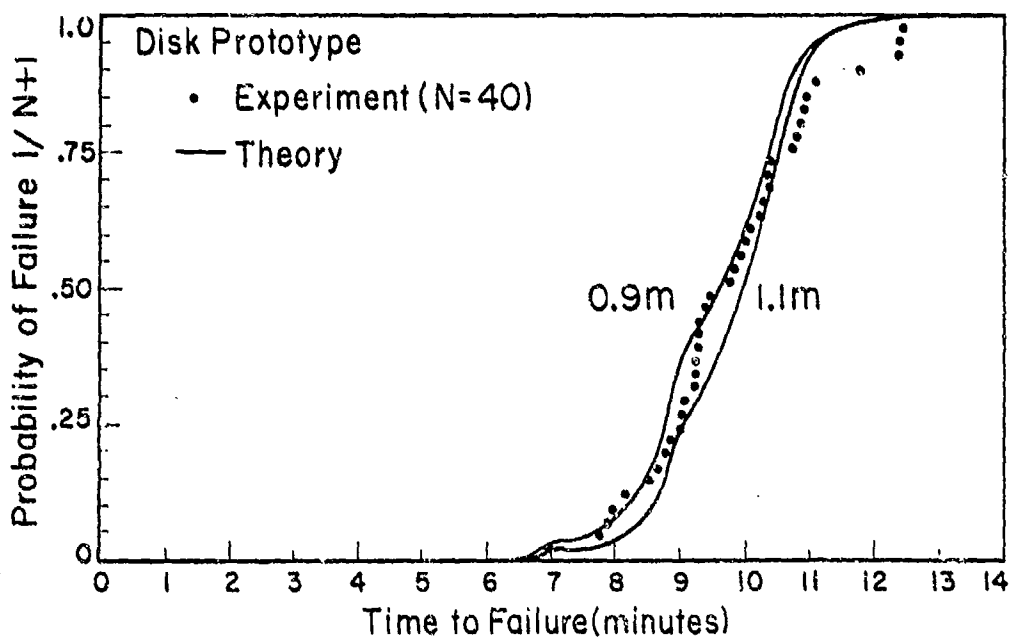

Figure 39 Effect of 10 Percent Variation in Weibull Parameter m Upon the Predicted Cumulative Distributions for the Beam and Disk

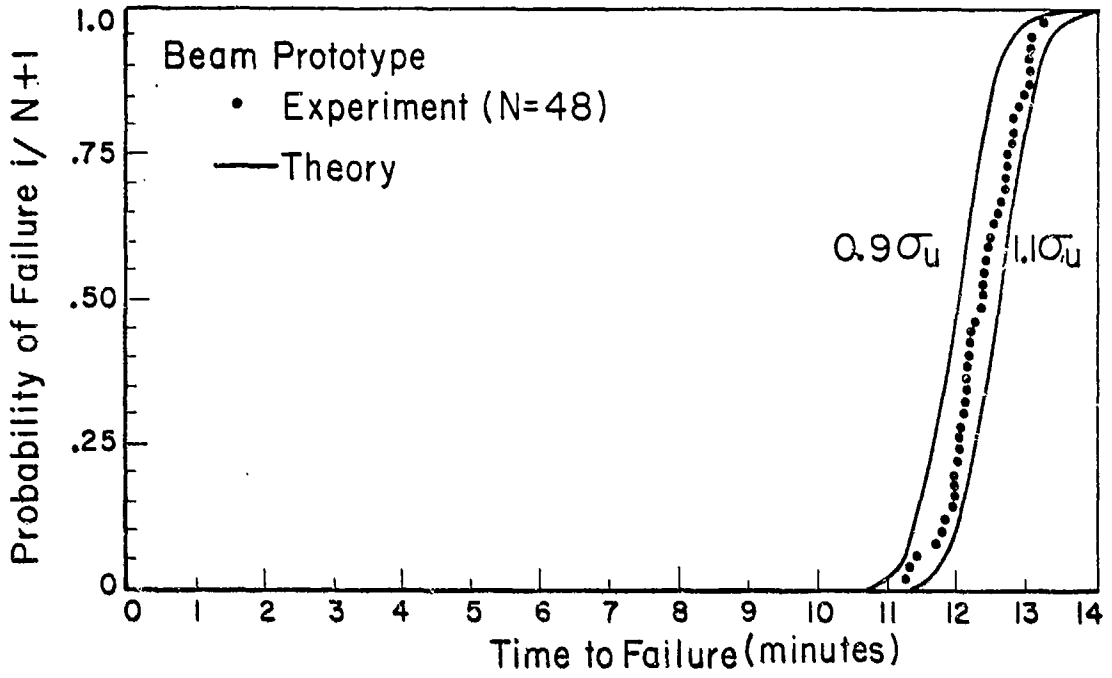

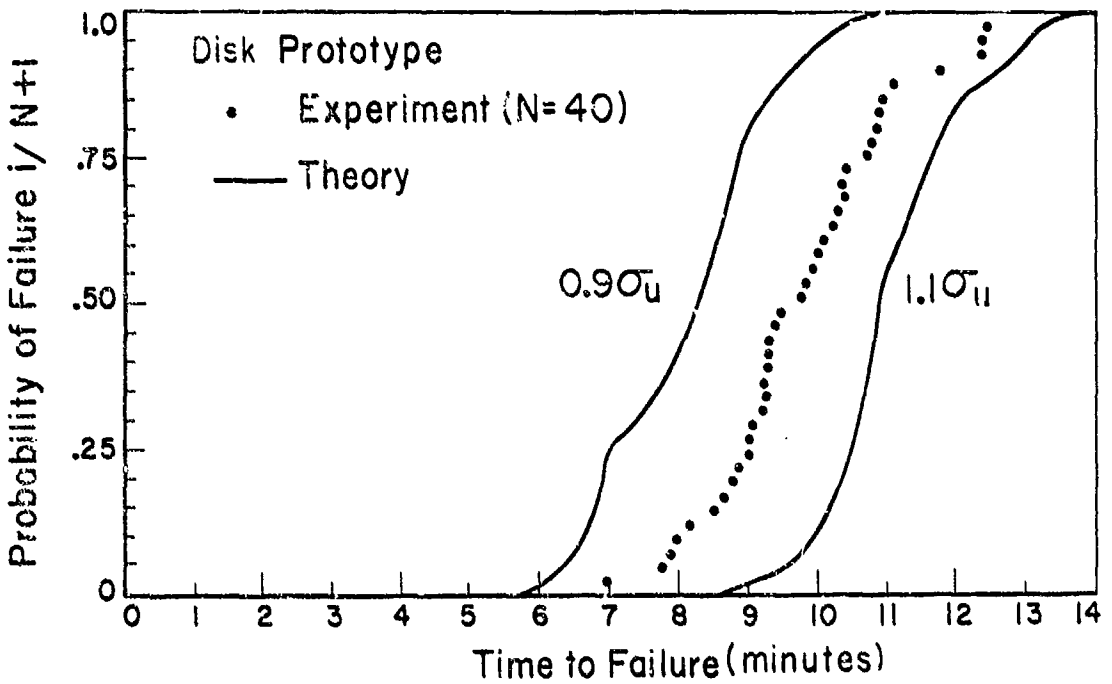

Figure 40 Effect of 10 Percent Variation in Weibull Parameter σ_u Upon the Predicted Cumulative Distributions for the Beam and Disk

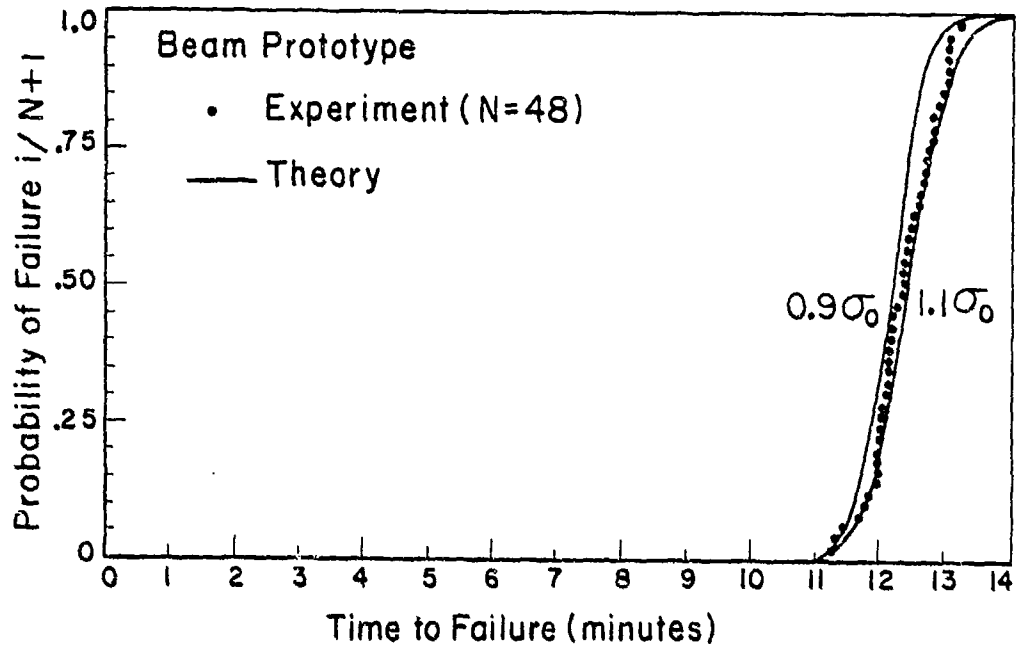

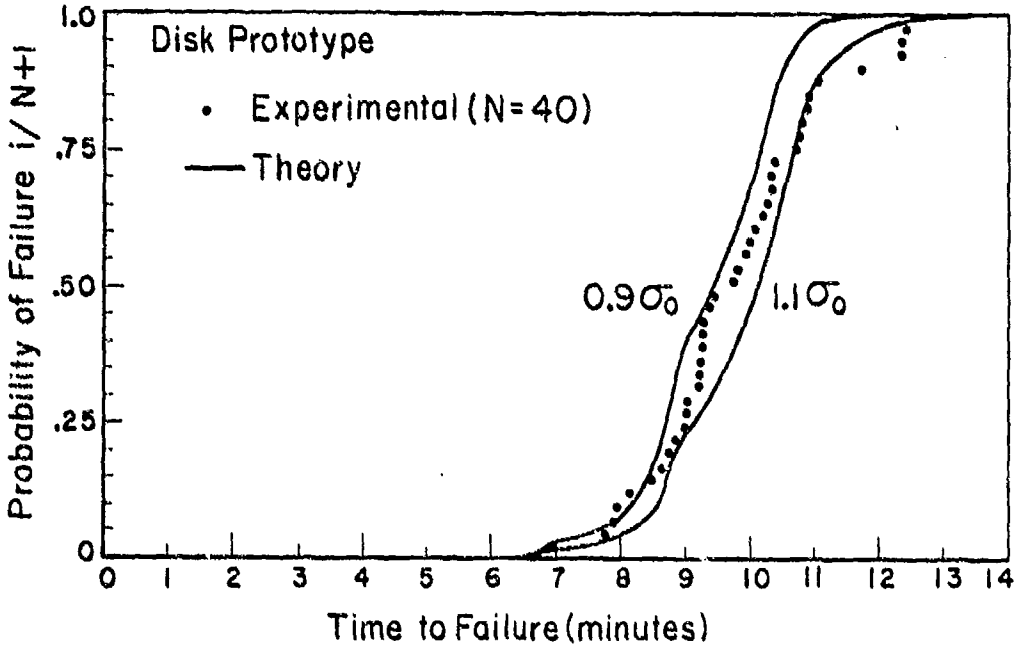

Figure 41 Effect of 10 Percent Variation in Weibull Parameter σ_o Upon the Predicted Cumulative Distributions for the Beam and Disk

Consider two singly fitting concentric rings of the same material. Assume that when both rings are at the reference temperature T_o, the rings are free from stress. Also, assume that both ε_T and F are functions of temperature. Now, let us examine what happens when the inside ring (number 1) is heated to T_1 and the outside ring (number 2) is heated to T_2. If the thickness of the ring δ is small, the radius of both rings may be taken as R and thus, after being heated to T_1 and T_2 respectively, the stresses in the rings can be computed from elementary theory to be

$$\sigma_1 = - \frac{\varepsilon_T(T_1) - \varepsilon_T(T_2)}{\frac{1}{E(T_1)} + \frac{1}{E(T_2)}} \tag{35}$$

$$\sigma_2 = - \sigma_1 \tag{36}$$

The form of Equation (35) demonstrates that the effect of a $\pm$ N% variation in $\varepsilon_T(T)$ will be identical to a $\pm$ N% variation in E(T)

3. FUTURE RESEARCH

Almost all of the work which has been done in the field of statistical fracture theory has concerned itself with the analysis problem as contrasted with the design problem. The present study is no exception since we attempt to predict the behavior of a known element under a specified environment. If we are to deal effectively with the problems of how to modify an inadequate structure or how to proportion a brittle component for minimum weight when operating under severe temperatures, we must address ourselves directly to the problem of design. Our fracture algorithm provides, to be sure, a basic tool for design; but, it does not constitute a design procedure.

To improve our analysis capabilities, there are two situations to consider. In the first, we must extend our capability so that we may predict the performance of simple materials (linear,

homogeneous, isotropic, series) in more severe temperature environments. In the second, we must try to characterize the behavior of more complicated materials (nonlinear, anisotropic, parallel) under room temperature and steady state elevated temperature environments.

APPENDIX I

STATISTICAL FRACTURE THEORY FOR COMBINED STRESS CONDITIONS

1. INTRODUCTION

In his classic paper of 1939 (Reference 14), Weibull developed an expression for the fracture probability of a brittle material under a polyaxial stress state. Using a different point of view, we shall expand on his brief statistical treatment of this combined stress problem and we shall extend our results to cases of varying mechanical and thermal loading and to materials which cannot be represented by the Weibull distribution function.

Briefly, it is our objective to establish a fracture surface, i.e., to find a relationship among the strengths achieved under various stress states. The usual approach to this problem in either brittle or ductile materials is to find a property common to all stress states that will indicate failure or nonfailure. In ductile materials the distortion energy represents such a property since incipient flow occurs in any stress state in which the distortion energy is equal to the distortion energy obtained in a tension specimen at yield. Stated in another way, we can correlate yielding under any stress state with the distortion energy. Our approach for brittle materials is completely analogous - we shall try to find a property that will correlate with the reliabilities associated with the various possible combined stress conditions.

To avoid the "size effect" problem observed in the strength of brittle elements, i.e., increasing fracture stress with decreasing volume, we shall confine our study to finite volumes ΔV of fixed size. We assume that both the material and the stress state in these basic volumes are homogeneous and that the materials used in all the volumes to be considered have been

drawn from the same population. In addition, we shall restrict the study to brittle materials that are statistically isotropic, i.e., the distribution of strengths obtained from an indefinitely large number of basic volumes will be identical in every direction.

We shall assume that the principal stresses S_1, S_2, S_3 which act on a basic volume are proportional to a load factor S, i.e.,

$$\begin{aligned} S_1 &= \alpha S \\ S_2 &= \beta S \\ S_3 &= \gamma S \end{aligned} \tag{37}$$

where α,β,γ are constants which define the stress state. Then, the strength of a basic element will be taken as the maximum load factor that it can equilibrate. Failure of the element is represented by its inability to equilibrate the applied loading. It is important to point out that it is possible for cracks to initiate and propagate within the basic volume without causing its failure. Materials in which cracks can be arrested or which provide alternative load paths when local failures occur are classified as parallel or series-parallel materials. If a local failure necessarily leads to overall failure, the associated material is called a series or "weakest link" material. One can advantageously adopt an infinitesimal basic volume for the series material and, as we shall subsequently discuss, combined stress testing is greatly simplified in this case.

Only the tensile or cohesive mode of failure will be considered in this investigation. We shall ignore the influence of compressive or shear stresses on the strength of a brittle material. The potential usefulness of this tension criterion is a consequence of two observations; first, that the shear strength of brittle materials is usually an order of magnitude greater than the tensile strength and, second,

that it is extremely difficult to eliminate tensile stresses from prototype or laboratory elements. Almost every structural failure of a brittle component can be attributed to the presence of some distribution of tensile stresses.

2. TWO-DIMENSIONAL THEORY

a. Heuristic Development-Single Loading

When we attempt to describe the statistical fracture strength of a finite volume of material under a uniaxial stress state, the axial stress (strain) is the only reasonable choice for the statistical variate. Taking a general form for any cumulative distribution function, we can write the fracture probability F for the uniaxial stress state as

$$F(\sigma) = 1 - \exp\left[-\frac{\Delta V}{v} g(\sigma)\right] \tag{38}$$

where ΔV is the specified volume of the basic element, v is a volume of unity and σ is the axial stress. The delineation of the constant $\Delta V/v$ does not affect the generality of this expression and in the special case of a series material it provides a convenient representation. If we examine the strength of a basic volume of an isotropic material under a general homogeneous stress state, it follows that failure will depend only on the three principal stresses acting on the unit. Thus, the probability of failure of the basic volume can be designated as $F(S_1, S_2, S_3)$ where the three principal stresses are taken as the statistical variates. For this case we shall take Equation (38) in the form

$$\frac{-\log\left[1-F(S_1,S_2,S_3)\right]}{\Delta V/v} = g(S_1,S_2,S_3) \tag{39}$$

For a specified reliability (1-F), Equation (39) becomes $g(S_1,S_2,S_3)$ equals constant, which defines our fracture surface.

On the basis that failure is caused only by tensile stresses, it seems reasonable to look for the function g within the collection of all possible tensile stresses which can occur at any point in the basic volume. In the plane stress problem, we can relate the normal stress σ_n acting in any direction to the principal stresses through the expression

$$\sigma_n = S_1 \cos^2\theta + S_2 \sin^2\theta \qquad (40)$$

where θ is the angle between σ_n and S_1. As θ sweeps through all values from $-\pi/2$ to $\pi/2$, Equation (40) describes every possible normal stress acting at a point. The normal stresses associated with the various directions described by θ are shown in Figure 42 for several different stress states. The question, now, is what are the distinguishing features of these figures which will reflect the differences they cause in a material's response?

The most obvious first guess is to differentiate among these stress states by comparing the areas associated with the tensile normal stresses. However, this approach does not reflect the possibility that the magnitude of the stresses may have a different influence than their extent or distribution. For example, hydrostatic tension and pure tension stress states which lead to the same area are depicted in Figure 42a where we observe that one peak stress is twice the other. Experience indicates that the pure tension state is the more critical. On the other hand, when the maximum hydrostatic tension and pure tension stresses are equal, as indicated in Figure 43b , our intuition would select the hydrostatic state as the more critical. Unlike pure tension, oriented flaws such as cracks cannot avoid exposure to high normal stresses by assuming a preferred direction since all directions experience the same stress under hydrostatic tension. This implies that a maximum stress theory is inapplicable and unconservative, and indeed, evidence exists to support this contention (Reference 15).

The two examples depicted in Figure 43 suggest that we "weight" the ordinates of the normal stress-theta diagrams for different stress states and then compare their areas. Assuming a statistically isotropic material, the weighting should be independent of the orientation of the normal stress, θ. We might use, for example, a power function to modify the normal stresses, i.e.,

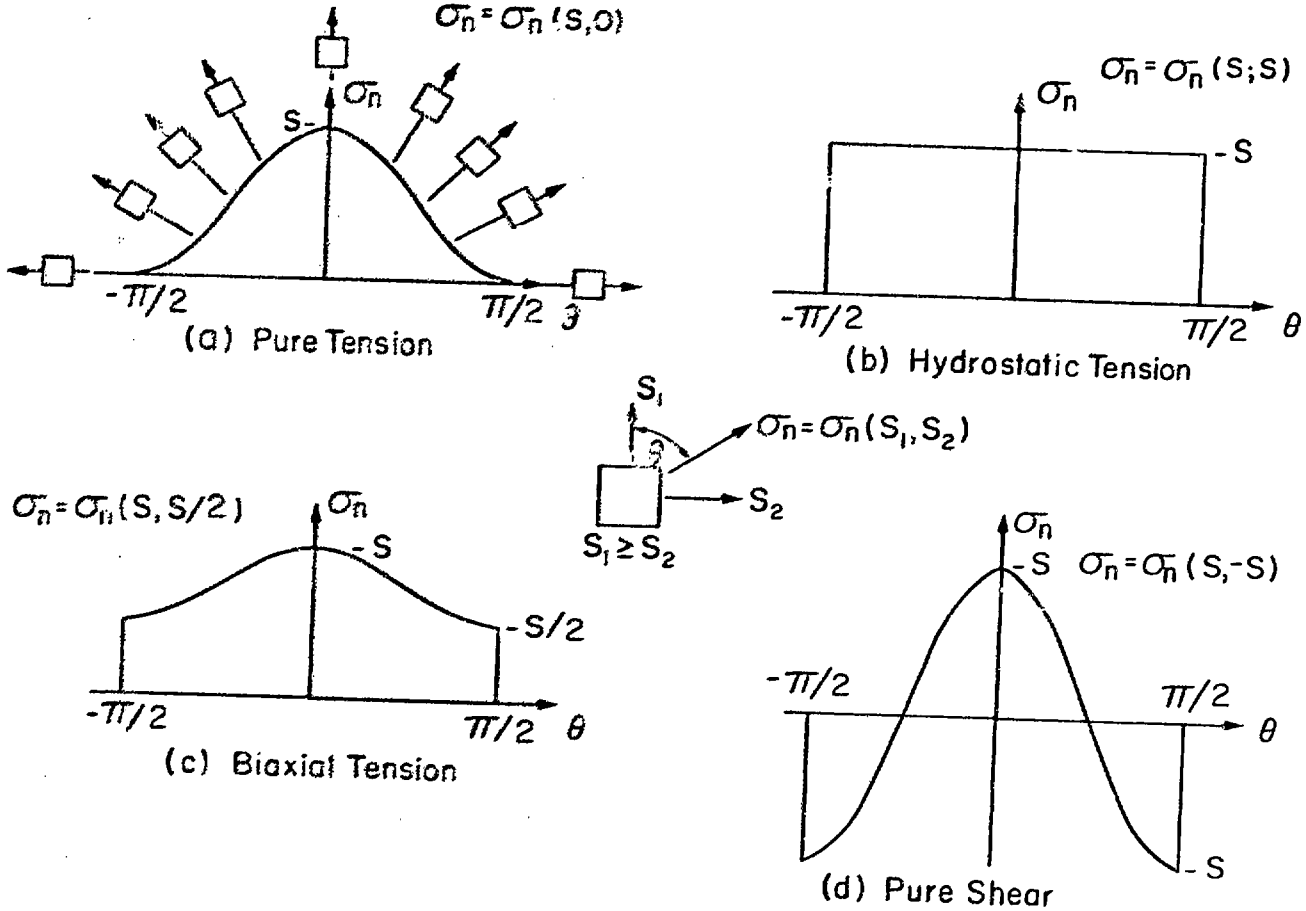

Figure 42 Normal Stress Distributions for Various Stress States, Two-Dimensional

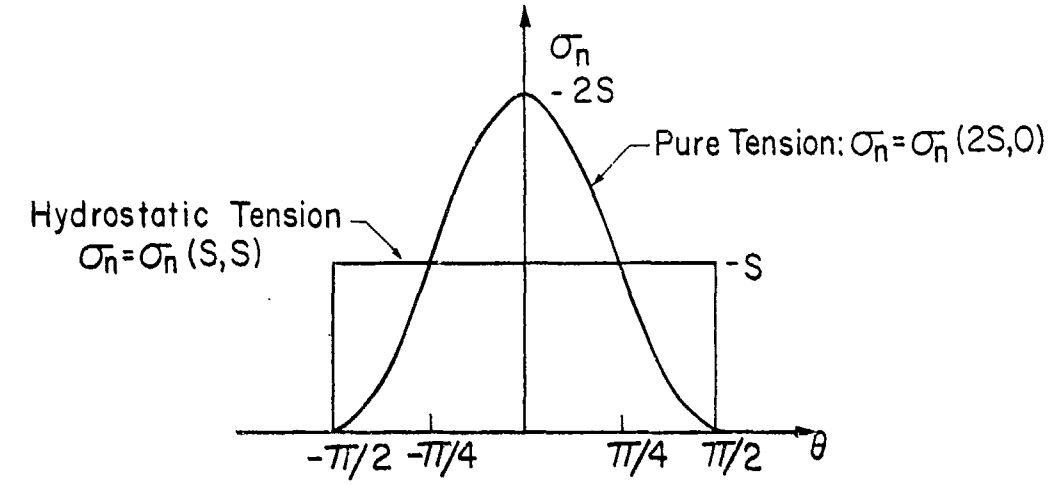

(a) Equal Areas - Unequal Maximum Stresses

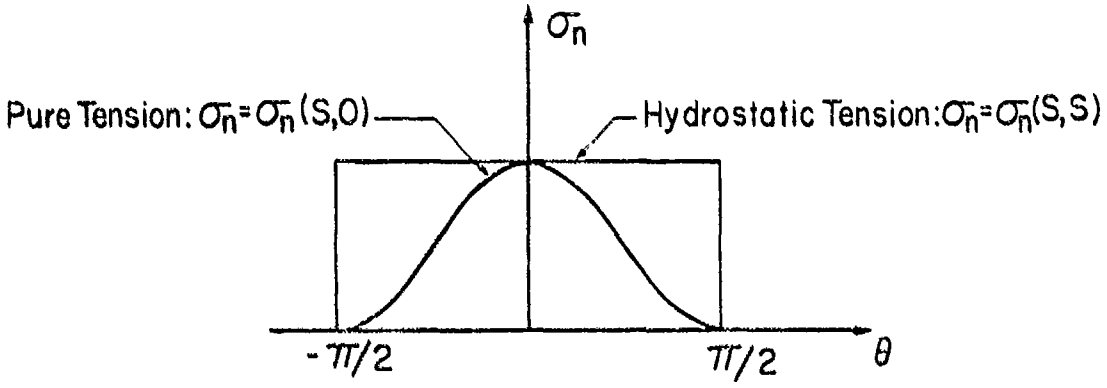

(b) Equal Maximum Stresses - Unequal Areas

Figure 43 Comparison of Hydrostatic Tension and Pure Tension States

$$D\ \sigma_n^k \tag{41}$$

where D and k are constants. This alteration results in the dashed curve shown in the left side of Figure 44 . If the normal stress distribution for several stress states are weighted in this fashion, we could compare the areas of the resulting curves, i.e.,

$$g(S_1,S_2) = \text{Area} = D\int_{\sigma_n \geq 0} \sigma_n^k \, d\theta \tag{42}$$

where the integration extends over those values of θ where the normal stress is non-negative. Because of symmetry we need consider only the positive normal stresses in the interval zero to $\pi/2$. To account for the possibility that tensile stresses below a certain magnitude σ_ℓ may not cause failure, we may choose to weight the difference $(\sigma_n - \sigma_\ell)$ as shown in the right half of Figure 44. The associated area is given by

$$g(S_1,S_2) = \text{Area} = D\int_{\sigma_n \geq \sigma_\ell} (\sigma_n - \sigma_\ell)^k \, d\theta \tag{43}$$

Certainly, the use of a power function to weight the normal stress-theta diagrams is completely arbitrary and there are many other ways of manipulating and distorting such curves. Our problem is to find a weighting function that will reflect the influence of stress state on the reliability of a basic volume. Denoting the weighting function by f, the fracture probability becomes

$$F(S_1,S_2) = 1 - \exp\left[\frac{-\Delta V}{V}\int_0^{\pi/2} f(\sigma_n)\, d\theta\right] \tag{44}$$

We are now in a position to describe certain guidelines for the selection of f. First, to account for the possible existence of a zero fracture probability stress σ_ℓ, we must take

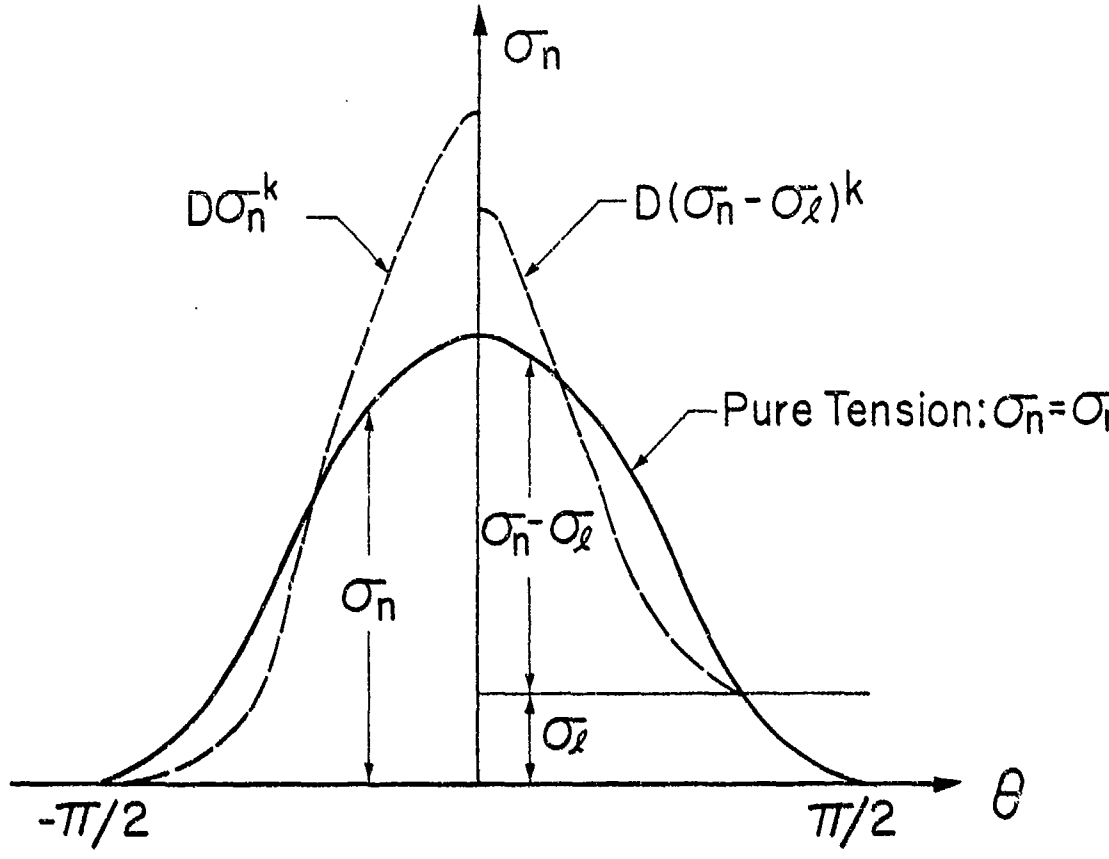

Figure 44 "Weighted" Normal Stress Diagram

$$f = f(\sigma_n - \sigma_\ell) \qquad \sigma_n \geq \sigma_\ell \geq 0$$

$$f = 0 \qquad \sigma_n \leq \sigma_\ell \tag{45}$$

The latter condition implies that both $S_1 \leq \sigma_\ell$ and $S_2 \leq \sigma_\ell$ and that in such cases $F = 0$. At the other extreme, we expect that fracture is a certainty when either S_1 or S_2 is positive and unbounded; hence, $F = 1$ implies that

$$f \to \infty \quad \text{when} \quad S_1, S_2 \to +\infty$$

Furthermore, we would expect on physical grounds that the failure probability would increase continuously with increasing principal tensile stresses; thus,

f...continuous and monotone increasing.

Finally, f must be chosen in such a way that the associated $F(S_1,S_2)$ fits the cumulative distribution curves obtained from fracture tests conducted using various stress states. In particular, it is necessary that fracture data obtained under pure tension be represented by $F(S_1,0)$ or $F(0,S_2)$ and that hydrostatic tension data be represented by $F(S_1,S_1)$. This is a standard problem in curve fitting and one proceeds by selecting a reasonable and versatile form for f which contains σ_ℓ and n additional parameters a_i; i.e., $f = f\left[(\sigma_n - \sigma_\ell); a_1, a_2, \ldots a_n\right]$. These parameters are chosen so that the curve for F passes "as close as possible" to each data point. For a series material, we note that the parameters which provide an exact fit to an infinite amount of data are intrinsic phenomenological strength properties of the material. Otherwise, they characterize approximately the strength of the basic volume.

The following typical functions may be useful candidates for $f(S_1,S_2,S_3)$:

For $\sigma_n \leq \sigma_\ell$:

$$f = 0$$

For $\sigma_n \geq \sigma_\ell$:

$$f = \left(\frac{\sigma_n - \sigma_\ell}{\sigma_c}\right)^k \equiv X^k \; ; \quad k > 0 \; ; \quad X \equiv \left(\frac{\sigma_n - \sigma_\ell}{\sigma_c}\right) \tag{46}$$

$$f = X + a_1 X^k \qquad a_1 > 0 \; ; \; k \geq 0 \tag{47}$$

$$f = a_1 X + a_2 X^2 + a_3 X^3 + \ldots + a_n X^n \; ; \; a_i \geq 0 \tag{48}$$

$$f = \exp X - 1 \tag{49}$$

$$f = \exp X^k - 1 \quad ; \quad k > 0 \tag{50}$$

$$f = \exp (\exp X - 1) - 1 \tag{51}$$

where k, σ_ℓ, σ_c, and the a_i's are statistical parameters and where σ_n is the normal stress. The first of these functions, $f = X^k$, is the one adopted by Weibull (Reference 14). We shall interpret f as the generalized normal stress and $\bar{f}$ as the generalized normal stress vector; in two dimensions $\bar{f} = \bar{f}(f,\theta)$.

b. Specific Formulas

In two dimensions the fracture probability is given by

$$F(S_1,S_2) = 1 - \exp\left[-\frac{\Delta V}{V}\int_0^{\theta_o} f(\sigma_n - \sigma_\ell)\, d\theta\right] \tag{52}$$

where the integration extends over the region where $\sigma_n > \sigma_\ell$; specifically,

$$\sigma_n = S_1 \cos^2\theta + S_2 \sin^2\theta \geq \sigma_\ell \tag{53}$$

Theta is the angle between $\bar{\sigma}_n$ and $\bar{S}_1$.

This inequality leads to three distinct cases:

(1) $S_1 \geq S_2 \geq \sigma_\ell \geq 0$:

$$\theta_o = \pi/2$$

(2) $S_1 \geq \sigma_\ell$; $S_2 \leq \sigma_\ell$:

$$\theta_o = \cos^{-1}\sqrt{\frac{\sigma_\ell - S_2}{S_1 - S_2}}$$

(3) $S_1 \leq \sigma_\ell$; $S_2 \leq \sigma_\ell$:

$$\theta_o = 0 \quad (F = 0)$$

Selecting the Weibull form for f given by Equation (46) we shall determine the failure probability for pure tension and for hydrostatic tension.

Pure Tension: $S_1 = \sigma_t > \sigma_\ell$; $S_2 = 0$

$$F(\sigma_t) = 1 - \exp\left[-\frac{\Delta V}{v}\int_0^{\cos^{-1}\sqrt{\sigma_\ell/\sigma_t}} \left(\frac{\sigma_t\cos^2\theta - \sigma_\ell}{\sigma_c}\right)^k d\theta\right] \quad (54)$$

When $\sigma_\ell = 0$, $F(\sigma_t)$ becomes

$$F(\sigma_t) = 1 - \exp\left[-\frac{\Delta V}{v}\frac{\sqrt{\pi}}{2}\frac{\Gamma(k+\frac{1}{2})}{\Gamma(k+1)}\left(\frac{\sigma_t}{\sigma_c}\right)^k\right] \quad (55)$$

Hydrostatic Tension: $S_1 = S_2 = \sigma_h > \sigma_\ell$

$$F(\sigma_h) = 1 - \exp\left[-\frac{\Delta V}{v}\frac{\pi}{2}\left(\frac{\sigma_h - \sigma_\ell}{\sigma_c}\right)^k\right] \quad (56)$$

This expression has the same form as the Weibull distribution function; consequently, the estimation of σ_ℓ, σ_c, and k can follow well developed procedures for this purpose (References 2, 14, and 16). If biaxial hydrostatic tension data can be obtained the parameter determination for all of the forms indicated in Equation (46) through (51) will be greatly simplified since all the f's become independent of theta.

c. Multiple Loadings

If our basic volume is subjected to a number of different loadings, we shall attempt to correlate fracture with the "worst" conditions that can arise. It is assumed that stresses which act on the basic volume prior to fracture do not significantly effect the resistance of the material. Now then, we shall separately consider every possible direction in our basic volume and identify the largest normal tensile stress which acts throughout the load history; i.e., $\max_t \sigma_n(t)$. Each of these maximum normal stresses will be weighted to form the maximum generalized normal stress f_{max} which will then be summed over theta in the usual way to form g. For example, consider three distinct loadings which give rise to the same principal directions such as illustrated in Figure 45a. The collection of maximum normal stresses is indicated as the envelop of the three solid curves and the weighted envelop curve is shown as a dashed curve. We note that symmetry is preserved across the σ_n and the θ axes. The fracture probability may then be written as

$$F\left[S_1(t),\ S_2(t)\right] = 1 - \exp\left\langle - \frac{\Delta V}{V} \int_0^{\pi/2} f\left\langle \left[\max_t \sigma_n(t)\right] - \sigma_\ell,\ a_i \right\rangle d\theta \right\rangle \tag{57}$$

where we recall that the constants σ_ℓ and the a_i's are statistical parameters.

Although we have chosen in our previous work to represent the σ_n - θ relationship in cartesian coordinates, there is no

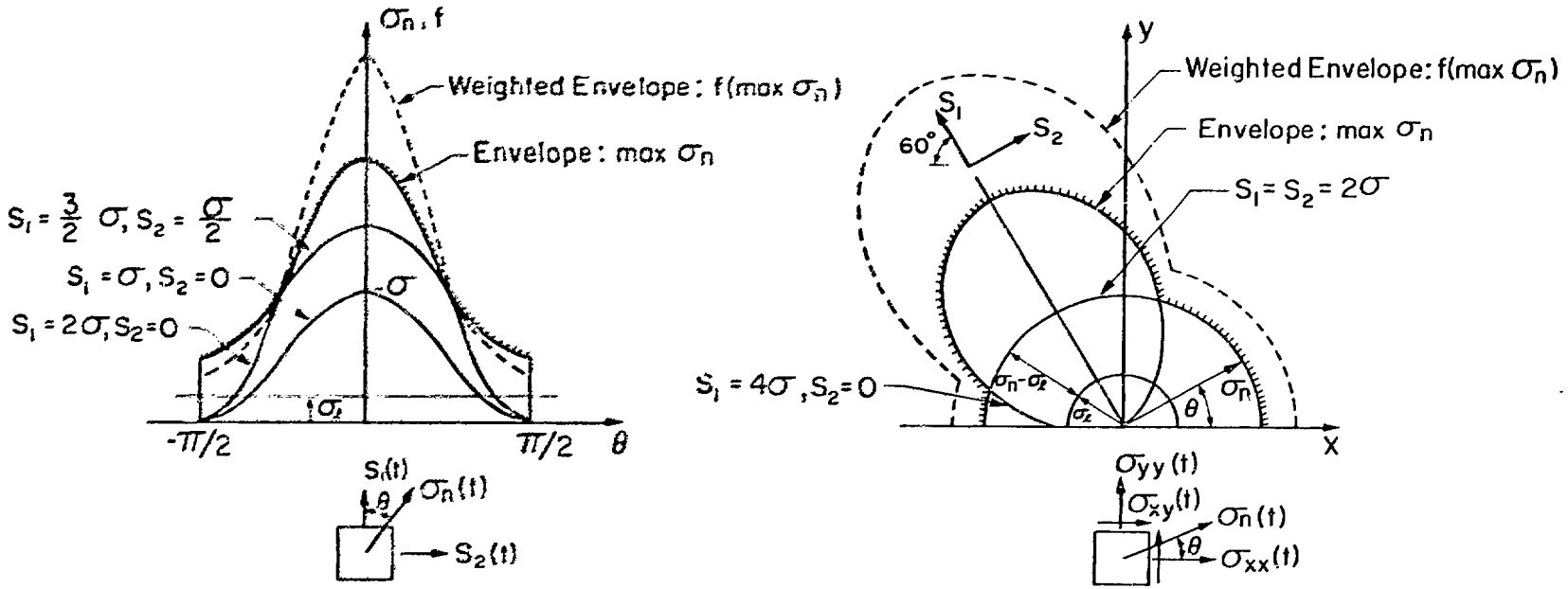

(a) Fixed Principal Directions - Cartesian Coordinates

(b) Variable Principal Directions - Polar Coordinates

Figure 45 Normal Stresses and Generalized Normal Stresses for Multiple Loadings

fundamental reason for doing so. For the multiple loading problem it is more convenient to use a polar representation as shown in Figure 45b where the normal stress vector $\bar{\sigma}_n$ and the generalized normal stress vector $\bar{f}$ are represented in a natural way. The x-y axes are assumed to be fixed in the body and both the principal stresses and directions are taken as time dependent. Calculating the area under the weighted maximum normal stress envelop, f_{max}, to establish g, the fracture probability in two-dimensional polar coordinates becomes

$$F\left[\sigma_{xx}(t),\ \sigma_{yy}(t),\ \sigma_{xy}(t)\right] = 1 - \exp\left[\frac{-\Delta V}{v}\int_0^{\pi}\int_0^{f_{max}} r\ dr\ d\theta\right]$$

or

$$F\left[\sigma_{xx}(t),\ \sigma_{yy}(t),\ \sigma_{xy}(t)\right] = 1-\exp\left\langle -\frac{\Delta V}{v}\int_0^{\pi}\frac{1}{2}\ f^2\left\{\left[\max_t\ \sigma_n(t)\right] - \sigma_i\ ,\ a_i\right\} d\theta\right\rangle \qquad (58)$$

where we note that symmetry is available only through the origin and where the normal stress is given by

$$\sigma_n = \sigma_{xx}(t)\ \cos^2\theta + \sigma_{yy}(t)\ \sin^2\theta + \sigma_{xy}(t)\ \sin 2\theta \qquad (59)$$

Comparing Equations (58) and (57), we find that the polar representation integrates f^2 rather than f over theta. This does not lead to an essential difference in the fracture probability expressions since in each case we must find an f that fits our data. For example, if f is given by Equation (46) the exponent is absorbed by the parameter k and differences in multiplicative constants are absorbed by σ_c.

d. Thermal Loading

It has tacitly been assumed throughout this study that under fixed environmental conditions (temperature, atmosphere, humidity) the cumulative strength distributions for our basic volume do

not vary with time. We do not account, for example, for the possible effects of static fatigue, creep, or continuous chemical changes in our material. Where this assumption holds we can associate a unique function f with every environmental condition. Specifically, for a uniformly distributed temperature T in our basic volume, we shall designate the generalized normal stress by $f_T(\sigma_n-\sigma_\ell;\ a_i)$. In practical situations one usually tries to use as few different forms of f as possible. For a given form, however, the statistical parameters must be taken as temperature dependent. Thus, f_T, can be written,

$$f_T = f_1\left[\sigma_n - \sigma_1(T);\ \ a_i(T)\right] \qquad T_o \leq T \leq T_1$$

$$f_T = f_2\left[\sigma_n - \sigma_2(T);\ \ b_j(T)\right] \qquad T_1 \leq T \leq T_2 \qquad (60)$$

$$f_T = f_m\left[\sigma_n - \sigma_m(T);\ \ c_k(T)\right] \qquad T_{m-1} \leq T \leq T_m$$

where the temperature range of interest is $T_o \leq T \leq T_m$ and where the symbols σ_1, σ_2, σ_m, a_i, b_j, c_k represent temperature dependent statistical parameters.

When a basic volume is subjected to a temperature history T(t) and a stress history $\sigma_{ij}(t)$, we once again identify the "worst" condition in every direction. Here, we should recognize that the largest normal tensile stress in a given direction does not necessarily lead to the largest generalized normal stress. What we must find is the maximum combination of normal stress and weighting. For a single stress state, the envelop of maximum generalized normal stresses is given by

$$f_{max} = \max_T f\left[\sigma_n - \sigma_\ell(T);\ a_i(t)\right] \qquad (61)$$

When the stress state varies, this maximum envelop is defined by

$$f_{max} = \max_t f_{T(t)}\left\{\sigma_n(t) - \sigma_\ell\left[T(t)\right];\ a_i\left[T(t)\right]\right\} \qquad (62)$$

where the statistical parameters σ_ℓ and a_i depend explicitly on the temperature and implicitly on the time parameter t. Adopting polar coordinates with fixed axes x-y in the basic volume, we form the function g by summing this f_{max} over theta; thus,

$$F\left[\sigma_{xx}(t),\ \sigma_{yy}(t),\ \sigma_{xy}(t)\right] = 1-\exp\left\{-\frac{\Delta V}{V}\int_0^{\pi}\frac{1}{2}\left\langle \max_t f_{T(t)}\left\langle \sigma_n(t) - \sigma_\ell\left[T(t)\right]\ ;\ a_i\left[T(t)\right]\right\rangle^2 d\theta\right\rangle\right\} \tag{63}$$

where f_T is defined by Equation (60) and σ_n is given by Equation (59). This expression predicts the fracture probability of a basic volume under biaxial time varying stresses and subjected to a changing temperature environment.

3. THREE-DIMENSIONAL THEORY

a. Single Loading

Following the two-dimensional development, we propose to correlate the behavior of the basic volume under a general stress state with some function of the totality of normal tensile stresses in three dimensions. In the belief that any tensile normal stress can occasionally cause a fracture by virtue of its magnitude and relative orientation with respect to a random flaw, we once again assume isotropy and weight each normal stress vector $\bar{\sigma}_n$ according to its magnitude only. Using the polar coordinates defined in Figure 46a, the normal stress in three dimensions can be written in terms of the three principal stresses; thus,

$$\sigma_n = \cos^2\phi \, (S_1 \cos^2\psi + S_2 \sin^2\psi) + S_3 \sin^2\phi \quad (64)$$

The normal stress diagrams associated with several important stress states are sketched in Figure 46 where we observe the following:

(1) Symmetry makes it possible to consider only one quadrant.

(2) The hydrostatic stress state gives rise to a spherical surface.

(3) The zero probability stress σ_ℓ can be represented as a sphere of radius σ_ℓ which can be subtracted from each diagram to yield $\sigma_n - \sigma_\ell$.

(4) If the three principal stresses are positive, the volume of the normal stress diagram is given by

$$V = \frac{\pi}{210}\left[5(S_1^3+S_2^3+S_3^3) + 3(S_1^2S_2+S_1^2S_3+S_2^2S_1+S_2^2S_3+S_3^2S_1+S_3^2S_2) + 2S_1S_2S_3\right] \quad (65)$$

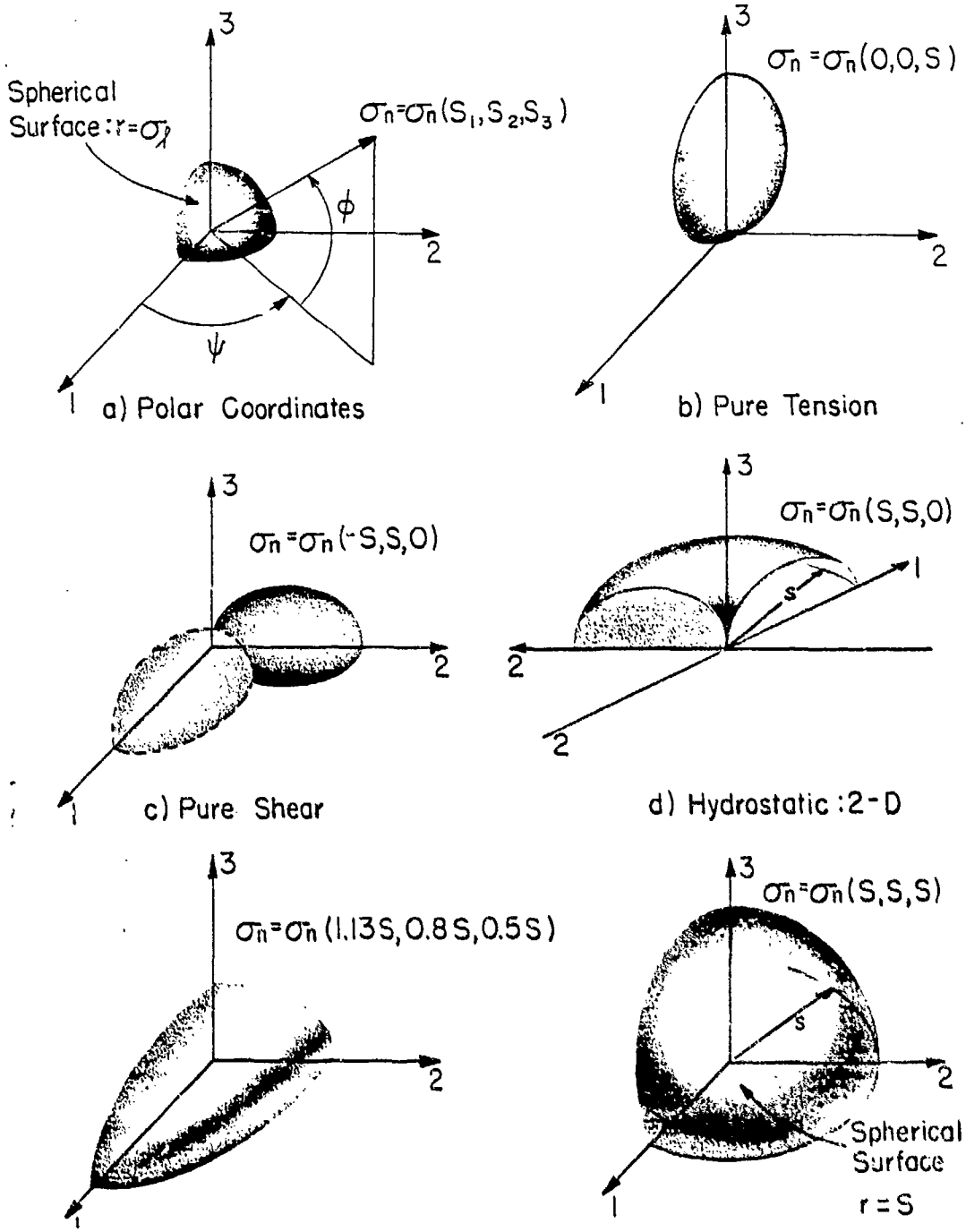

Figure 46 Normal Stress Diagrams, Three-Dimensional

This expression is useful as a computer check.

Now, adopting the same types of weighting functions f described in Section 2-a, we can write an expression for the fracture probability of a basic volume subjected to a three-dimensional stress state; thus,

$$F(S_1,S_2,S_3) = 1 - \exp\left\{ - \frac{\Delta V}{v} \iiint_{\sigma_n \geq \sigma_\ell^o}^{f} r^2 \, dr \cos\phi \, d\phi \, d\psi \right\} \quad (66)$$

where the integration extends over that portion of the first quadrant where the normal stress is greater than the zero probability stress. More specifically,

$$F(S_1,S_2,S_3) = 1-\exp\left\{ - \frac{\Delta V}{v} \int_0^{\pi/2} d\psi \int_{\phi_L}^{\phi_U} \frac{1}{3} f^3 \left[\sigma_n-\sigma_\ell^o;\ a_i\right] \cos\phi \, d\phi \right\} \quad (67)$$

where we delineate four distinct cases:

(1) $S_1 \geq S_2 \geq S_3 \geq \sigma_\ell$

$$\phi_L = 0$$

$$\phi_U = \pi/2$$

(2) $S_1 \geq S_2 \geq S_3 \geq \sigma_\ell$

$$\left.\begin{aligned} \phi_L &= 0 \\ \phi_U &= 0 \end{aligned}\right\} F = 0$$

(3) $S_1 \geq S_2 \geq \sigma_\ell$, $S_3 \leq \sigma_\ell$

$$\phi_L = 0$$

$$\phi_U = \cos^{-1} \sqrt{\frac{\sigma_\ell - S_3}{S_1\cos^2\psi + S_2\sin^2\psi - S_3}}$$

(4) $S_3 \geq \sigma_\ell$, $S_1 \leq S_2 \leq \sigma_\ell$

$$\phi_L = \cos^{-1} \sqrt{\frac{S_3 - \sigma_\ell}{S_3 - S_1\cos^2\psi - S_2\sin^2\psi}}$$

$$\phi_U = \pi/2$$

The integration limits in cases 3 and 4 are derived in Figure 47.

Using the Weibull form for f given by Equation (46), we shall determine the failure probabilities for several important cases.

Pure Tension:

Case 4; $\sigma_n = \sigma_n(0,0,\sigma_t)$; $\phi_L = \cos^{-1}\sqrt{(\sigma_t-\sigma_\ell)/\sigma_t}$; $\phi_U = \pi/2$

$$F(0,0,\sigma_t) = 1-\exp\left\{ - \frac{\Delta V}{v} \int_0^{\pi/2} d\psi \int_{\cos^{-1}\sqrt{(\sigma_t-\sigma_\ell)/\sigma_t}}^{\pi/2} \frac{1}{3} \left| \frac{\sigma_t\sin^2\phi-\sigma_\ell}{\sigma_c} \right|^{3k} \cos\phi \, d\phi \right\} \quad (68)$$

For $\sigma_\ell = 0$,

$$g(0,0,\sigma_t) = \frac{\pi}{6(6k+1)} \left| \frac{\sigma_t}{\sigma_c} \right|^{3k} \quad (69)$$

Comment: This formula for g is much simpler than the corresponding g in the two-dimensional case described by Equation (55). It has the same form as that found in the conventional Weibull distribution function and, consequently, the estimation techniques described in References 2, 14 and 16 can be used to establish the statistical parameters σ_c and k.

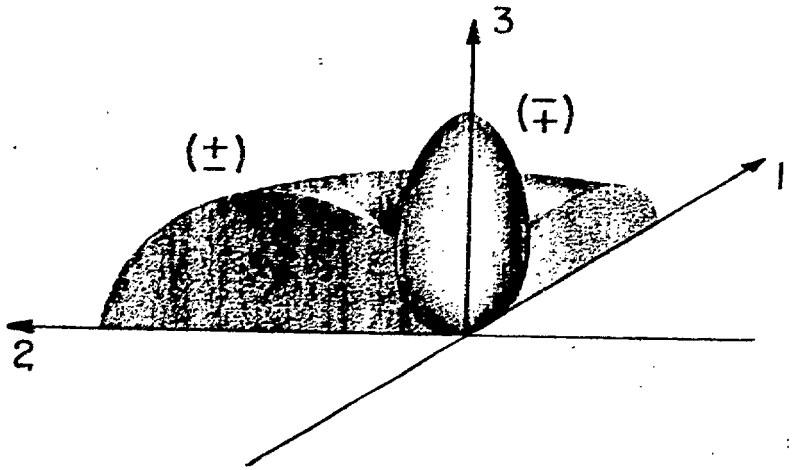

(a) $S_1 \lesseqgtr 0, S_2 \lesseqgtr 0, S_3 \gtreqless 0$

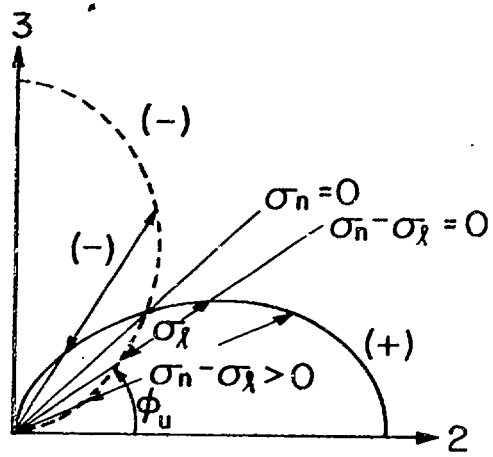

(b) $S_1 \geq \sigma_\ell, S_2 \geq \sigma_\ell, S_3 \leq 0$

$$\sigma_n = \cos^2\phi\,(S_1\cos^2\psi + S_2\sin^2\psi) + S_3(1-\cos^2\phi) \geq \sigma_\ell$$

$$\left(\frac{\sigma_\ell - S_3}{S_1\cos^2\psi + S_2\sin^2\psi - S_3}\right) \leq \cos^2\phi \leq \left(\frac{S_3 - \sigma_\ell}{S_3 - S_1\cos^2\psi - S_2\sin^2\psi}\right)$$

$$S_1 \geq \sigma_\ell, S_2 \geq \sigma_\ell, S_3 \leq \sigma_\ell: \ \phi_u \leq \cos^{-1}\sqrt{\frac{\sigma_\ell - S_3}{S_1\cos^2\psi + S_2\sin^2\psi - S_3}}$$

$$S_1 \leq \sigma_\ell, S_2 \leq \sigma_\ell, S_3 \geq \sigma_\ell: \ \phi_L \geq \cos^{-1}\sqrt{\frac{S_3 - \sigma_\ell}{S_3 - S_1\cos^2\psi - S_2\sin^2\psi}}$$

NOTE: $\cos\phi \geq A \Diamond \phi \leq \cos^{-1}A$

(c) Limits on ϕ

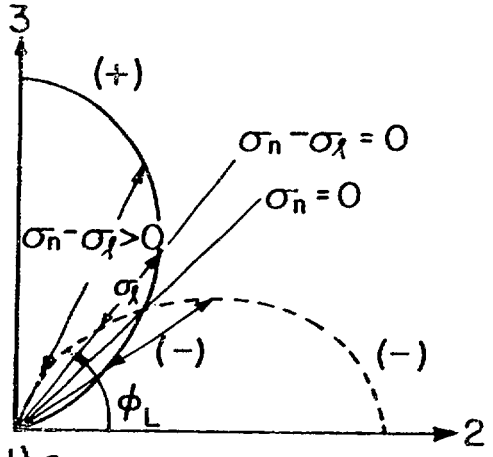

(d) $S_1 \leq \sigma_\ell, S_2 \leq \sigma_\ell, S_3 \geq 0$

Figure 47 Integration Limits on PHI

Hydrostatic Tension: 3-D

Case 1; $\sigma_n = \sigma_n(S_h,S_h,S_h)$; $S_h \geq \sigma_\ell$; $\phi_L = 0$; $\phi_U = \pi/2$

$$F(S_h,S_h,S_h) = 1-\exp\left\{-\frac{\Delta V}{v}\int_0^{\pi/2} d\psi \int_0^{\pi/2} \frac{1}{3}\left(\frac{S_h-\sigma_\ell}{\sigma_c}\right)^{3k} \cos\phi \, d\phi\right\} \quad (70)$$

$$g(S_h,S_h,S_h) = \frac{\pi}{6}\left(\frac{S_h-\sigma_\ell}{\sigma_c}\right)^{3k} \quad (71)$$

Comment: We can compare the magnitudes of hydrostatic tension S_h and pure tension σ_t when each produces the same failure probability in a basic volume ΔV. Equating the two functions g given by Equations (69) and (71) and taking $\sigma_\ell = 0$, we obtain

$$\left(\frac{S_h}{\sigma_t}\right) = \left(\frac{1}{6k+1}\right)^{1/3k} \quad (72)$$

Hydrostatic Tension: 2-D

Case 3; $\sigma_n = \sigma_n(\sigma_h,\sigma_h,0)$; $\sigma_\ell = 0$; $\phi_L = 0$ ' $\phi_U = \pi/2$

$$F(\sigma_h,\sigma_h,0) = 1-\exp\left[-\frac{\Delta V}{v}\int_0^{\pi/2} d\psi \int_0^{\pi/2} \frac{1}{3}\left(\frac{\sigma_h\cos^2\phi}{\sigma_c}\right)^{3k} \cos\phi \, d\phi\right] \quad (73)$$

$$g(\sigma_h,\sigma_h,0) = \frac{\pi^{3/2}}{12(3k+\frac{1}{2})} \frac{\Gamma(3k+1)}{\Gamma(3k+\frac{1}{2})}\left(\frac{\sigma_h}{\sigma_c}\right)^{3k} \quad (74)$$

Comment: The expression for $g(\sigma_h,\sigma_h,0)$ is more complicated than the corresponding $g(\sigma_h,\sigma_h)$ obtained from Equation (56) in our two-dimensional treatment of the hydrostatic tension plane stress problem. For equal reliabilities we can compare the biaxial hydrostatic state with the pure tension state by equating the functions g given by Equations (69) and (74); thus,

$$\left(\frac{\sigma_h}{\sigma_t}\right) = \left[\frac{1}{\sqrt{\pi}} \frac{\Gamma(3k+\frac{1}{2})}{\Gamma(3k+1)}\right]^{1/3k} \qquad \text{3-D Theory} \qquad (75)$$

We form the corresponding expression, using the two-dimensional theory, by equating Equations (55) and (56) and replacing the letter k by k'; thus,

$$\left(\frac{\sigma_h}{\sigma_t}\right) = \left[\frac{1}{\sqrt{\pi}} \frac{\Gamma(k'+\frac{1}{2})}{\Gamma(k'+1)}\right]^{1/k'} \qquad \text{2-D Theory} \qquad (76)$$

To compare the (2-D) and (3-D) theories, the same input data must be used to establish the respective parameters. Therefore, if each theory is fit to the same tension data, we can equate Equations (55) and (68) to obtain the relationships among the various parameters, i.e.,

$$\frac{\sqrt{\pi}}{2} \frac{\Gamma(k'+\frac{1}{2})}{\Gamma(k'+1)} \left(\frac{\sigma_t}{\sigma_c'}\right)^{k'} = \frac{\pi}{6(6k+1)} \left(\frac{\sigma_t}{\sigma_c}\right)^{3k} \qquad (77)$$

The equivalence is established if

$$k' = 3k \qquad (78)$$

$$\sigma_c' = \sigma_c \left[\frac{3(2k'+1)}{\sqrt{\pi}} \frac{\Gamma(k'+\frac{1}{2})}{\Gamma(k'+1)}\right]^{1/k'} \qquad (79)$$

Since only one parameter appears in Equation (75) we simply replace 3k by k' to see that Equations (75) and (76) are identical. In general, the (2-D) and (3-D) theories both predict the same fracture curve for the plane stress problem when the Weibull f is used.

$S_1=S_2=S, S_3=-S$:

Case 3; $\sigma_n = S\cos 2\phi$; $\sigma_\ell = 0$; $\phi_L = 0$; $\phi_U = \pi/4$

$$F(S,S,-S) = 1-\exp\left[-\frac{\Delta V}{v}\int_0^{\pi/2} d\psi \int_0^{\pi/4} \frac{1}{3}\left|\frac{S\cos 2\phi}{\sigma_c}\right|^{3k}\cos\phi\, d\phi\right] \tag{80}$$

$$k=1: \qquad g(S,S,-S) = \frac{\pi}{6}\left|\frac{8\sqrt{2}}{35}\right|\left(\frac{S}{\sigma_c}\right)^3 \tag{81}$$

$$k=2: \qquad g(S,S,-S) = \frac{\pi}{6}\left|\frac{512\sqrt{2}}{3003}\right|\left(\frac{S}{\sigma_c}\right)^6 \tag{82}$$

Comment: In situations where an axial prestress is brought onto a beam or column member, it may be important to know the increased tensile resistance in the transverse directions. The transverse integrity without prestressing can be estimated by the biaxial hydrostatic tension case. Comparing Equation (74) with Equations (81) and (82) we find,

for k=1,

$$\frac{\pi^{3/2}}{12(3+\frac{1}{2})}\frac{\Gamma(3+1)}{\Gamma(3+\frac{1}{2})}\left|\frac{\sigma_h}{\sigma_c}\right|^3 = \frac{\pi}{6}\left|\frac{8\sqrt{2}}{35}\right|\left(\frac{S}{\sigma_c}\right)^3 \tag{83}$$

$$S = 1.1222\,\sigma_h \tag{84}$$

for k=2,

$$\frac{\pi^{3/2}}{12(6+\frac{1}{2})}\frac{\Gamma(6+1)}{\Gamma(6+\frac{1}{2})}\left|\frac{\sigma_h}{\sigma_c}\right|^6 = \frac{\pi}{6}\left|\frac{512\sqrt{2}}{3003}\right|\left(\frac{S}{\sigma_c}\right)^6 \tag{85}$$

$$S = 1.0594\,\sigma_h \tag{86}$$

Thus, our axial prestress increases the transverse strength by 12.3 percent when k=1 and by 5.9 percent when k=2.

$S_1=S_2=-S, S_3=S$:

Case 4: $\sigma_n = -S\cos 2\phi$; $\sigma_\ell = 0$; $\phi_L = \pi/4$; $\phi_U = \pi/2$

$$F(-S,-S,S) = 1-\exp\left[-\frac{\Lambda V}{V}\int_0^{\pi/2} d\psi \int_{\pi/4}^{\pi/2} \frac{1}{3}\left|\frac{-S\cos 2\phi}{\sigma_c}\right|^{3k}\cos\phi\, d\phi\right] \quad (87)$$

$$k=1: \qquad g(-S,-S,S) = \frac{\pi}{6}\left|\frac{8\sqrt{2}-9}{35}\right|\left(\frac{S}{\sigma_c}\right)^3 \quad (88)$$

$$k=2: \qquad g(-S,-S,S) = \frac{\pi}{6}\left|\frac{835-512\sqrt{2}}{3003}\right|\left(\frac{S}{\sigma_c}\right)^6 \quad (89)$$

Comment: It is possible to increase the axial tensile strength of a member by applying a transverse compression loading. The problem arises, for example, in certain collet type grips for tension members. Such grips produce a radial compression state which is proportional to the tensile loading. The resulting increase in resistance at any reliability level can be determined by comparing Equation (69) with Equations (88) and (89); hence,

for k=1,

$$\frac{\pi}{6(6+1)}\left(\frac{\sigma_t}{\sigma_c}\right)^3 = \frac{\pi}{6}\left|\frac{8\sqrt{2}-9}{35}\right|\left(\frac{S}{\sigma_c}\right)^3 \quad (90)$$

$$S = 1.2924\,\sigma_t \quad (91)$$

for k=2,

$$\frac{\pi}{6(12+1)}\left(\frac{\sigma_t}{\sigma_c}\right)^6 = \frac{\pi}{6}\left|\frac{835-512\sqrt{2}}{3003}\right|\left(\frac{S}{\sigma_c}\right)^6 \quad (92)$$

$$S = 1.1299\,\sigma_t \quad (93)$$

Hence, an increase of 29.2 percent in the tensile strength is obtained when k=1; 13 percent when k=2.

b. Mechanical and Thermal Load History

Following the development of Section 2-d, we shall once again consider a basic volume subjected to a temperature history $T(t)$ and a stress history $\sigma_{ji}(t)$. The extension of our previous treatment of this problem to three dimensions requires that we use the three-dimensional form for the normal stress and the appropriate summation of the maximum generalized stress f_{max} given by Equation (62).

Using cartesian tensor notation, the components of the stress vector $\underline{T}$ acting on a plane with unit normal $\underline{n}$ can be written in terms of the stresses.

$$T_i = \sigma_{ji} n_j \qquad i,j = 1,2,3 \tag{94}$$

The magnitude of the normal stress vector, σ_n, is given by the scalar product of the stress vector and the unit normal vector; thus,

$$\sigma_n = T_i\, n_i = \sigma_{ji}\, n_j\, n_i \tag{95}$$

Interpreting the components of the unit normal vector n_i as the direction cosines of $\underline{n}$, we can relate the n_i's to the polar coordinates shown in Figure 46a.

$$\begin{aligned} n_1 &= \cos\phi \cos\psi \\ n_2 &= \cos\phi \sin\psi \\ n_3 &= \sin\phi \end{aligned} \tag{96}$$

Substituting Equations (96) into (95) we obtain

$$\begin{aligned} \sigma_n = \cos^2\phi(\sigma_{11}\cos^2\psi + \sigma_{22}\sin^2\psi) + \sigma_{33}\sin^2\phi \\ + \sigma_{12}\cos^2\phi \sin 2\psi + \sigma_{23}\sin 2\phi \sin\psi + \sigma_{31}\sin 2\phi \cos\psi \end{aligned} \tag{97}$$

For the most general loading, we can expect only that the normal stress vectors will be symmetic with respect to the origin; consequently, we must consider all of the normal stresses above the 1-2 plane. On this basis we can write down the fracture probability; thus,

$$F\left[\sigma_{ij}(t)\right] = 1-\exp\left\{-\frac{\Delta V}{V}\int_0^{2\pi}\int_0^{\pi/2}\frac{1}{3}\left\langle \max_t f_{T(t)}\left[\sigma_n(t)-\sigma_\ell\left[T(t)\right]\right]\right\rangle^3 \cos\phi\, d\phi\, d\psi\right\} \tag{98}$$

where σ_n is given by Equation (97) and f_T by Equation (60). The function f contained in the definition of f_T should meet the conditions described in Section 2-a.

4. THE FRACTURE SURFACE

a. Exact Theory

For a specified reliability (1-F) and a given basic volume ΔV, Equation (39) defines the fracture surface which describes the resistance of the basic volume under various stress states. We customarily normalize such surfaces by relating all behavior to that under pure tension. Then, the fracture surface becomes

$$\frac{g(S_1, S_2, S_3)}{g(0, 0, \bar{\sigma}_t)} = 1 \tag{99}$$

All points on this fracture surface have the same fracture probability; points falling inside have lower fracture probabilities and points falling outside have higher ones.

In the two-dimensional problem the fracture surface can be represented as a curve defined by

$$\frac{g(S_1,\ S_2)}{g(\sigma_t,0)} = 1 \tag{100}$$

Specializing this formula to the Weibull power function with $\sigma_\ell = 0$ we obtain,

$$\int_{\sigma_n \geq 0} \left[\left\langle \frac{S_1}{\sigma_t} \right\rangle \cos^2\theta + \left\langle \frac{S_2}{\sigma_t} \right\rangle \sin^2\theta \right] d\theta = \frac{\sqrt{\pi}}{2} \frac{\Gamma(k+\frac{1}{2})}{\Gamma(k+1)} \tag{101}$$

We have already evaluated this expression for the hydrostatic tension case in Equation (76). Numerical results for this case are tabulated in Table VI together with two other stress states. We should point out once again that, when the power form of f is used, the stress ratios can also be computed from Equation (99) when S_3 is set equal to zero.

Table VI

STRENGTH RATIOS FOR TWO-DIMENSIONAL STRESS STATES

Stress State	Strength Ratio	k=1	k=2	k=3	k=∞
Pure Tension $(\sigma_t,0)$	$\sigma_t/\sigma_t =$	1	1	1	1
Hydrostatic Tension (σ_h,σ_h)	$\sigma_h/\sigma_t =$	1/2	$(3/8)^{1/2}$	$(5/16)^{1/3}$	1
Biaxial Tension $(\sigma_b,\sigma_b/2)$	$\sigma_b/\sigma_t =$	2/3	$(12/19)^{1/2}$	$(40/63)^{1/3}$	1
Pure Shear $(\sigma_s,-\sigma_s)$	$\sigma_s/\sigma_t =$	$\pi/2$	$(3/2)^{1/2}$	$(15\pi/32)^{1/3}$	1

The fracture curve associated with Table VI is shown in Figure 48. We observe that the maximum stress theory, $\max(S_1,S_2) \leq \sigma_t$, coincides with the case k=∞. It was pointed out by Weibull (Ref. 14) that k=∞ corresponds to a classical deterministic material with an ultimate strength equal to σ_c. We also find in Figure 48 that the tensile

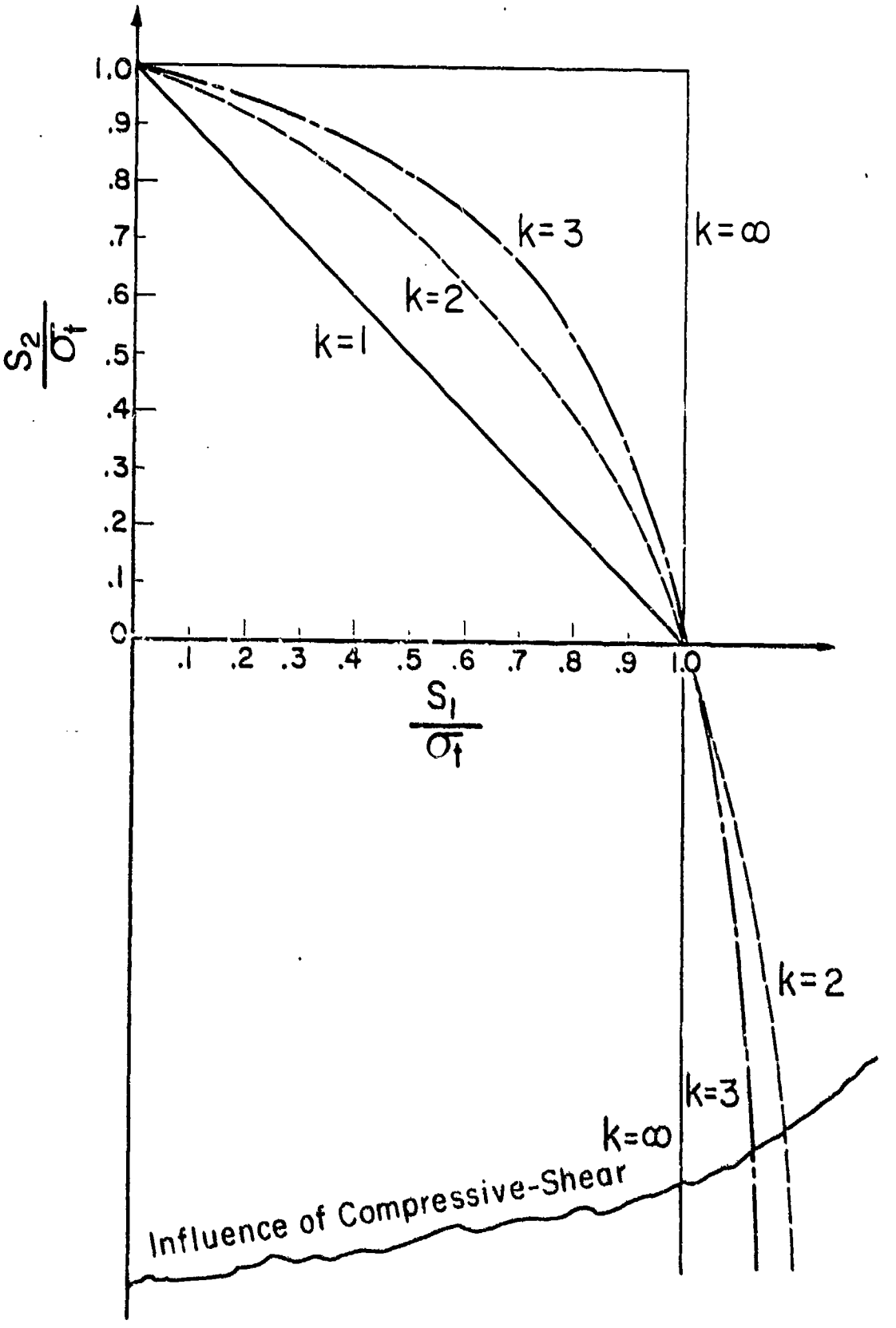

Figure 48 Combined Stress Theory (Weibull Form)

strength increases as the transverse compressive stress becomes greater. Physically, the compressive stress can be attributed with closing up some of the cracks which might otherwise be critical under the tensile loading.

As the compressive stress increases indefinitely, our theory indicates that the tensile strength becomes unbounded. This is clearly contrary to reality; but, it is not a surprising result since no provision has been made in our theory to account for compressive-shear failures. The emergence of another failure mode provides a limitation on the range of applicability of our theory. The ragged line in Figure 48 is meant to indicate such a limitation.

b. Approximate Theory

If the behavior of a basic volume under a general stress state was equivalent to the behavior of three basic volumes each under a distinct principal stress, the survival of the basic volume would require the simultaneous survival of each unit. Under these conditions the reliability of the basic volume would be given by

$$1-F_a = \left[1-F(S_1)\right]\ \left[1-F(S_2)\right]\ \left[1-F(S_3)\right] \qquad (102)$$

where $F(S)$ is the fracture probability of a basic volume under a pure tensile stress S.

For a Weibull material subjected to pure tension, the reliability is expressed as

$$1-F(\sigma_t) = \exp\left[-\frac{V}{v}\left(\frac{\sigma_t-\sigma_u}{\sigma_o}\right)^m\right] \qquad \sigma_t > \sigma_u$$

$$= 1 \qquad \sigma_t \le \sigma_u \qquad (103)$$

where σ_u, σ_o, m are the Weibull statistical parameters.

The associated approximate combined stress theory

$$\left[1-F_a(S_1,S_2,S_3)\right] = \exp\left\{-\frac{\Delta V}{V}\left[\left(\frac{R_1-\sigma_u}{\sigma_o}\right)^m + \left(\frac{R_2-\sigma_u}{\sigma_o}\right)^m + \left(\frac{R_3-\sigma_u}{\sigma_o}\right)^m\right]\right\} \quad (10$$

where

$$R_i = S_i \quad \text{when} \quad S_i > \sigma_u$$

$$R_i = \sigma_u \quad \text{when} \quad S_i \leq \sigma_u$$

Comparing the combined stress case with the pure tension case at the same reliability, we obtain the fracture surface

$$\left(\frac{S_1-\sigma_u}{\sigma_t-\sigma_u}\right)^m + \left(\frac{S_2-\sigma_u}{\sigma_t-\sigma_u}\right)^m + \left(\frac{S_3-\sigma_u}{\sigma_t-\sigma_u}\right)^m = 1 \quad (105)$$

This results in the two-dimensional fracture diagram shown in Figure 49 when S_3 is set equal to σ_u. To compare the approximate results to the exact theory, we select the parameters in both theories to match the same tension data. Here, we need only note that $m=k$ and that the k's used in Figure 49 correspond to those used in Figure 48

We can observe from Figures 48 and 49 that the approximate and exact theories are identical for the cases $k=1$ and $k=\infty$. Between these values, the exact theory will be found to be the more conservative. We shall determine the largest deviation between the theories by examining the case of hydrostatic tension which lies along a 45 deg line.

In two dimensions, the approximate reliability for the hydrostatic case is found by setting $R_1 = \sigma_h$, $R_2 = \sigma_h$, and $R_3 = \sigma_u$. Then, comparing this reliability with that of the tension case, we find

$$\left(\frac{\sigma_h}{\sigma_t}\right)_{approx} = (1/2)^{1/m} \quad (106)$$

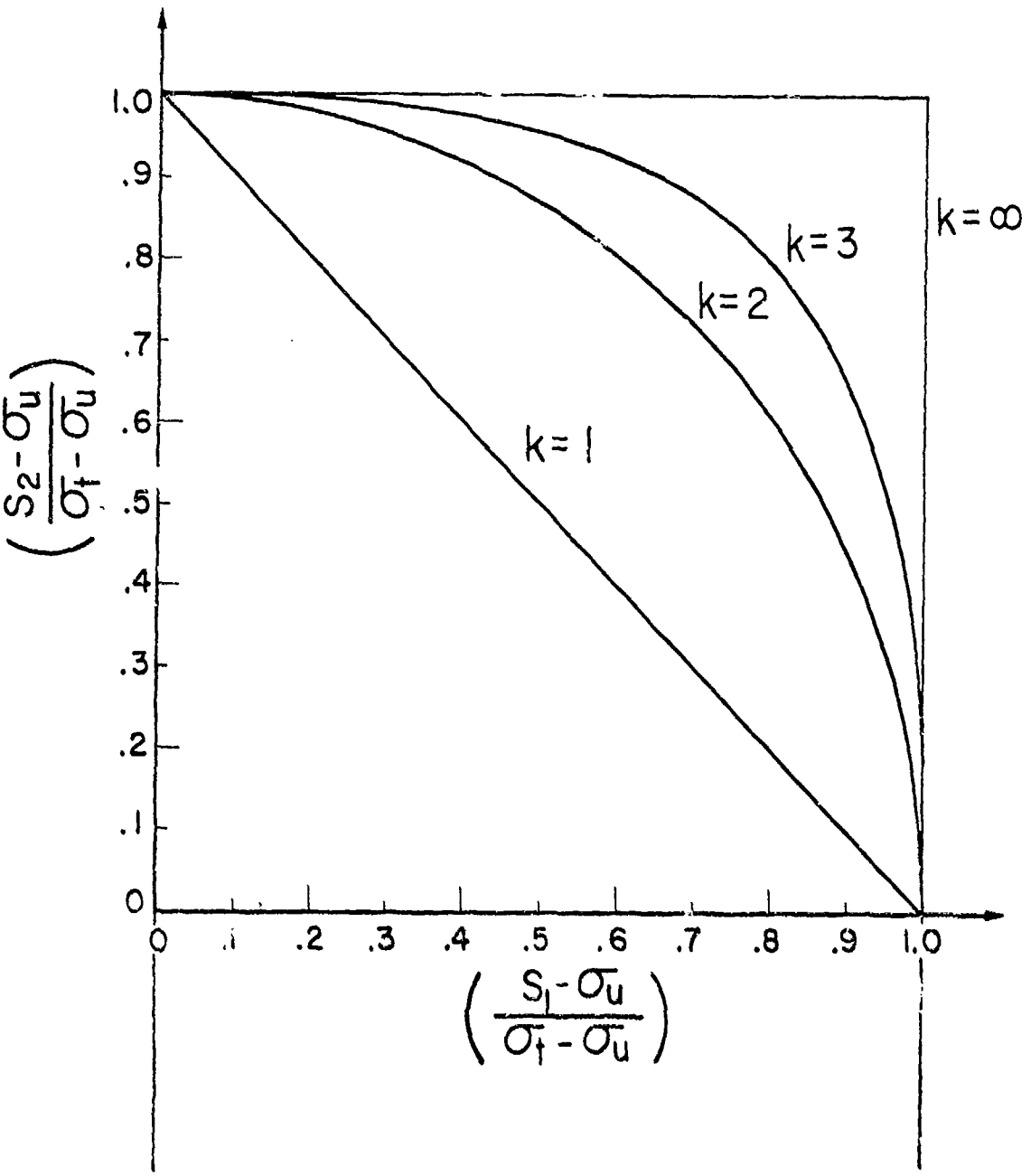

Figure 49 Approximate Combined Stress Theory

Forming the ratio between this expression and that described by Equation (76) for the exact case, we obtain

$$\frac{(\sigma_h/\sigma_t)_{approx}}{(\sigma_h/\sigma_t)_{exact}} = \left[\frac{\sqrt{\pi}}{2}\frac{\Gamma(m+1)}{\Gamma(m+\frac{1}{2})}\right]^{1/m} \qquad m=k \qquad (107)$$

This ratio is tabulated in Table VII for different values of m. The largest value occurs at near m=3 and shows a deviation from the exact theory of 16.9 percent. This discrepancy is smaller at all other m's and for all other stress states.

Table VII

COMPARISON OF EXACT AND APPROXIMATE COMBINED STRESS THEORIES

m	Two Dimensions $\frac{(\sigma_h/\sigma_t)_{approx}}{(\sigma_h/\sigma_t)_{exact}}$	Three Dimensions $\frac{(\sigma_h/\sigma_t)_{approx}}{(\sigma_h/\sigma_t)_{exact}}$
1	1.000	1.000
2	1.154	1.291
3	1.16935	1.32635
4	1.163	1.316
5	1.153	1.297
10	1.110	1.215
∞	1.000	1.000

Setting $S_1=S_2=S_3=S_h$ in Equation (105), we obtain the approximate ratio of hydrostatic strength to tensile strength for equal reliability; thus,

$$\left(\frac{S_h - \sigma_u}{\sigma_h - \sigma_u}\right)_{approx} = (1/3)^{1/m} \qquad (108)$$

When $\sigma_u = 0$, we can compare this expression to the exact ratio given in Equation (72).

$$\frac{(S_h/\sigma_t)_{approx}}{(S_h/\sigma_t)_{exact}} = \left(\frac{2m+1}{3}\right)^{1/m} \qquad 3k=m \tag{109}$$

where we have taken $3k=m$ so that both theories describe the same tension behavior. This ratio is tabulated in Table VII; it assumes its maximum value at $m=3.04$. For this value of m the deviation from the exact theory is 32.6 percent; furthermore, this discrepancy persists over a wide range of important values of m.

5. OBSERVATIONS AND REMARKS

a. Experimental Verification

1. The integrity of a basic volume is not generally an intrinsic property of the material, but rather, a complicated combination of crack initiations, propagations, and arrestments. For this reason, we must try to characterize the behavior of a particular basic volume. To do this, nominally identical volumes must be used for all the tests designed to establish a fracture surface.

2. The theory assumes that a basic volume is subjected to a homogeneous stress state; consequently, its verification requires that we meet this condition experimentally. Furthermore, the loading on a basic volume must be increased proportionally throughout the test. We note, for example, that the case of hydrostatic tension produces no shear stress unless the loading is incremented sequentially.

3. If the definition of failure is taken as the inability of a basic volume to equilibrate the applied loading, we must take pains to identify the fracture load. We must not, for example, allow a crack from outside the basic volume to propagate into the unit and cause its failure. Furthermore, we must not terminate our test because a fracture has occurred outside of the basic volume. When the entire specimen is the basic volume, this latter problem does not exist; if not, we face a problem in the interpretation of data which has not presently been solved. With low strength materials it is sometimes possible to mend (cement, glue) a fracture outside of the gage length and proceed with the test.

4. The construction of a fracture diagram requires that strength values be used with the same reliability level. Often, however, one finds that such diagrams plot the average strength values. Unfortunately, the average strengths from tests using different stress ratios do not generally represent the same reliability. It is permissible, for instance, to use the median stress for each type of loading.

5. The elimination of parasitic stresses from brittle tension specimens is one of the most exacting problems in the area of material testing (Reference 17). One can anticipate that the problem will be magnified for combined stress testing.

b. Weakest Link Materials

1. When failure at any point in a body necessarily constitutes overall failure of the body, the material is classified as a series or weakest link material. Now, if we define overall failure as failure at a point, we create in effect a series material. In this instance, the problem is to find some way of measuring the first pointwise failure. For example, if the incipient mobilization of the first crack in a body could be detected, we could use this feature as an overall failure criterion and thereby obtain a series material.

Because the behavior of a series material is understood, we can separate the volume and geometry aspects from the behavior of a test specimen and, thereby, make it possible to identify an intrinsic property of the material. Anticipation of this possibility prompted us to single out the volume ratio $\Delta V/v$ in all our studies.

2. Consider a component which is constructed from a series material. To establish its reliability we can divide it into n imaginary basic volumes and recognize that the overall survival of the component requires the simultaneous survival of each basic volume. Thus, the reliability of the body, $(1-F_b)$, can be written

$$1 - F_b = \prod_{i=1}^{n} (1-F_i) = \prod_{i=1}^{n} \exp\left[- \frac{\Delta V_i}{v} g_i(S_1,S_2,S_3) \right] \quad (110)$$

where the reliability of the basic volume, $1-F_i$, has been taken from Equation (39). For an infinitesimal basic volume we obtain,

$$1 - F_b = \exp\left[\frac{-1}{v} \iiint_V g(S_1,S_2,S_3)dV \right] \quad (111)$$

3. A very large basic volume of a series material follows the maximum stress theory. To see this we can take the limit of F in Equation (67) as $\Delta V \to \infty$. If this is done we observe that $F = 0$ when $f = 0$ and that $F = 1$ when $f \neq 0$. But, f becomes different from zero only when $\sigma_n > \sigma_\ell$; consequently, if the normal stress in any direction becomes slightly greater than σ_ℓ, fracture is a certainty. This is, of course, a statement of the maximum stress theory.

APPENDIX II

BEAM ANALYSIS COMPUTER PROGRAM

In this appendix, the computer program which was employed in the analysis of the beam prototype structure shall be described. The program combines the fracture algorithm of Section II with the beam thermal and stress analyses and material property curves of Section IV into a single package. A listing of the program as written in Fortran II for the IBM 7094 is included in this appendix.

The program consists of a main program containing the thermal, stress and statistical analyses and of function subprograms for describing the functions $T(z,t)$, $E(T)$, $\varepsilon_T(T)$, $k(t)$, $m(T)$, $\sigma_u(T)$ and $\sigma_0(T)$. The program has been specialized to some extent by specifying the geometry of the beam and its loading. However, the temperature distribution and the material property versus temperature curves are entered into the program via tables and hence the effects of variations in these curves may be readily obtained.

As an aid in using the program, a listing describing some of the more important variables entering into the program is also included in this appendix.

Listing of Significant Program Variables:

DEPTH (I)	i^{th} depth in beam, measured from the bottom
DTIME	size of time interval between computations
E(I)	i^{th} entry in table of modulus of elasticity vs. temperature
ET(I)	temperature corresponding to E(I)
FBTEMP(Z,TIME)	function subprogram for computing the temperature in the beam at depth Z and time TIME
FE(T)	function subprogram for computing the modulus of elasticity at the temperature T

FSO(T)	function subprogram for computing the Weibull parameter σ_o at the temperature T
FSU(T)	function subprogram for computing the Weibull parameter σ_u at the temperature T
FTK(T)	function subprogram for computing the thermal conductivity k at the temperature T
FTS(T)	function subprogram for computing the thermal strain ε_T at the temperature T
FXM(T)	function subprogram for computing the Weibull parameter m at the temperature T
HIMP	gross heat flux impingent upon the bottom of the beam
NE	number of entries in E(T) input table
NJ	number of entries with respect to t in T(z,t) input table
NPRINT	number of time increments between occurrences of detailed output printouts
NSO	number of entries in σ_o(T) input table
NSU	number of entries in σ_u(T) input table
NTK	number of entries in k(T) input table
NTS	number of entries in ε_T(T) input table
PFL(I)	probability of failure of the i^{th} subvolume up to current value of time
PINT	initial load on beam
POF	probability of failure of entire beam up to current value of time.
PRATE	rate at which load increases after t = TIMEP
RISK	risk of rupture of entire beam up to current value of time
RR(I)	risk of rupture in the i^{th} subvolume at current value of time

RRMAX(I) maximum value of RR(I) up to current value of time

RRT(I) risk of rupture computed using the values of stress, temperature, etc. at DEPTH (I) and at current value of time

SMAX(I) maximum value of STR(I) up to current value of time

STR(I) total stress acting at DEPTH(I)

STRM(I) mechanical component of STR(I)

STRT(I) thermal component of STR(I)

TIMEM maximum value of time for which computations are to be carried out

TIMEP value of time at which load begins to increase

TK(I) i^{th} entry in table of thermal conductivity vs. temperature

TKT(I) temperature corresponding to TK(I)

TRRM(I) time at which RRMAX(I) is achieved

TS(I) i^{th} entry in table of thermal strain vs. temperature

TST(I) temperature corresponding to TS(I)

TT(J) j^{th} value of time corresponding to WSO(I)

TTAB(I,J) temperature at depth ZT(I) and time TT(J)

WSO(I) i^{th} entry in table of Weibull σ_o vs. temperature

WSOT(J) temperature corresponding to WSO(I)

WSU(I) i^{th} entry in table of Weibull σ_u vs. temperature

WSUT(I) temperature corresponding to WSU(I)

WXM(I) i^{th} entry in table of Weibull m vs. temperature

WXMT(I) temperature corresponding to WXM(I)

ZT(I) i^{th} value of depth corresponding to TTAB(I,J)

PROGRAM LISTING

```
CM     UNIAXIAL STATISTICAL STRENGTH ANALYSIS PROGRAM
       DIMENSION TTAB(10,100),ZT(10),TS(10),TST(10),E(10),ET(10),TK(10),T
      1KT(10),WXM(10),WXMT(10),WSU(10),WSUT(10),WSO(10),WSOT(10),TT(40)
       COMMON TTAB,ZT,TS,TST,E,ET,TK,TKT,WXM,WXMT,WSU,WSUT,WSO,WSOT,TT,JJ
      1,DTIME
       DIMENSION RR(20),DEPTH(21),STR(21),STRM(21),STRT(21),SMAX(21),RRMA
      1X(20),TRRM(20),RRT(21),PFL(20)
       DIMENSION ZSTEP(102),TSTRA(102),YOUMO(102),TEMP(102)
     5 WRITE OUTPUT TAPE 6,7
     7 FORMAT (48H1ALUMINA BEAM UNDER MECHANICAL + THERMAL LOADING )
       READ INPUT TAPE 5,10,PINT,PRATE,TIMEP
    10 FORMAT (3F10.8)
       WRITE OUTPUT TAPE 6,12,PINT,PRATE,TIMEP
    12 FORMAT (6HOPINT=,F10.2,3X,6HPRATE=,F10.2,3X,6HTIMEP=,F5.3)
       READ INPUT TAPE 5,17,STIME,DTIME,TIMEM,NPRINT
    17 FORMAT (3F10.5,I5)
       WRITE OUTPUT TAPE 6,19,DTIME,TIMEM,NPRINT
    19 FORMAT (7HODTIME=,F5.3,3X,6HTIMEM=,F7.3,3X,7HNPRINT=,I3)
    20 READ INPUT TAPE 5,22,NJ,NTS,NE,NTK,NAM,NSU,NSO
    22 FORMAT (7I5)
       WRITE OUTPUT TAPE 6,24,NJ,NTS,NE,NTK,NAM,NSU,NSO
    24 FORMAT (4HONJ=,I3,3X,4HNTS=,I3,3X,3HNE=,I3,3X,4HNTK=,I3,3X,4HNXM=,
       IF(NJ)40,40,30
    30 DO 35 J=1,NJ
       READ INPUT TAPE 5,32,(TTAB(I,J),I=1,8)
    32 FORMAT (8F10.4)
    35 CONTINUE
    40 READ INPUT TAPE 5,42,(ZT(I),I=1,8)
    42 FORMAT (8F10.8)
    45 IF(NTS) 55,55,47
    47 DO 52 I=1,NTS
       READ INPUT TAPE 5,49,TST(I),TS(I)
    49 FORMAT (F10.4,F10.8)
    52 CONTINUE
    55 IF(NE) 65,65,57
    57 DO 62 I=1,NE
       READ INPUT TAPE 5,59,ET(I),E(I)
    59 FORMAT (F10.4,F10.2)
    62 CONTINUE
    65 IF(NTK) 75,75,67
    67 DO 72 I=1,NTK
       READ INPUT TAPE 5,69,TKT(I),TK(I)
    69 FORMAT (F10.4,F10.6)
    72 CONTINUE
    75 DO 90 I=1,NJ
    90 TT(I)=FLOAT(I-1)*.5
       WRITE OUTPUT TAPE 6,95,(ZT(I),I=1,8)
    95 FORMAT (5HOZT= ,F9.4,7F10.4)
       WRITE OUTPUT TAPE 6,97
    97 FORMAT (5H TIME)
       DO 102 J=1,NJ
       WRITE OUTPUT TAPE 6,100,TT(J),(TTAB(I,J),I=1,8)
```

```
  100 FORMAT (1H ,F5.2,F8.2,7F10.2)
  102 CONTINUE
      WRITE OUTPUT TAPE 6,105
  105 FORMAT (27HOTEMP (R)   TSTRAIN (IN/IN))
      DO 110 I=1,NTS
      WRITE OUTPUT TAPE 6,107,TST(I),TS(I)
  107 FORMAT (1H ,F8.2,5X,1PE14.6)
  110 CONTINUE

      WRITE OUTPUT TAPE 6,115
  115 FORMAT (35HOTEMP (R)   MOD OF ELASTICITY (PSI))
      DO 120 I=1,NE
      WRITE OUTPUT TAPE 6,107,ET(I),E(I)
  120 CONTINUE
      WRITE OUTPUT TAPE 6,125
  125 FORMAT (38HOTEMP (R)   THERMAL COND (BTU/FT*HR*R))
      DO 130 I=1,NTK
      WRITE OUTPUT TAPE 6,107,TKT(I),TK(I)
  130 CONTINUE
      IF(TIMEM-TT(NJ))135,135,132
  132 TIMEM=TT(NJ)
  135 TIMEM=-DTIMF+STIME
      J=0
      KZ=0
      II=1
      JJ=2
      DO 137 I=1,21
      DLPTH(I)=0.05*FLOATF(I-1)
      SMAX(I)=0.
      RRMAX(I)=0.
      PFL(I)=0.
  137 THRM(I)=0.
      DO 141 I=1,NXM
      READ INPUT TAPE 5, 69,WXMT(I),WXM(I)
      WRITE OUTPUT TAPE 6,140,I,WXMT(I),I,WXM(I)
  140 FORMAT (6HOWXMT(,I2,2H)=,F10.2,3H(R),5X,4HWXM(,I2,2H)=,F5.4)
  141 CONTINUE
      DO 145 I=1,NSU
      READ INPUT TAPE 5,59,WSUT(I),WSU(I)
      WRITE OUTPUT TAPE 6,143,I,WSUT(I),I,WSU(I)
  143 FORMAT (6HOWSUT(,I2,2H)=,F10.2,3H(R),5X,4HWSU(,I2,2H)=,F10.2,5H(PS
     1I))
  145 CONTINUE
      DO 148 I=1,NSO
      READ INPUT TAPE 5,59,WSOT(I),WSO(I)
      WRITE OUTPUT TAPE 6,147,I,WSOT(I),I,WSO(I)
  147 FORMAT (6HOWSOT(,I2,2H)=,F10.2,3H(R),5X,4HWSO(,I2,2H)=,F10.2,5H(PS
     1I))
  148 CONTINUE
  150 TIME=TIME+DTIME
      J=J+1
      IF(TIME-TIMEM) 155,155,5
  155 IF(TIME-TIMEP) 156,156,157
  156 AL=PINT
      GO TO 158
```

```
157 AL=PINT+PRATE*(TIME-TIMEP)
158 BM=1.1875*AL
    D=0.5
    B=0.5
    NS=50
    NZ=101
    PNS=NS
    PNS1=1.0/PNS
    ZSTEP(1)=-1.0
    I1=2*NS
    DO 160 J=2,I1
160 ZSTEP(J)=ZSTEP(J-1)+PNS1
    ZSTEP(NZ)=1.0
    DO 170 J=1,NZ
    ZZ=-ZSTEP(J)*D+0.5
    T1=FNTEMP(ZZ,TIME)
    TEMP(J)=T1
    TSTRA(J)=FTS(T1)
170 YOUMO(J)=FE(T1)
    H=ZSTEP(NZ)-ZSTEP(NZ-1)
    PT=0.0
    BMT=0.0
    PT=H*B*(TSTRA(1)*YOUMO(1)+TSTRA(NZ)*YOUMO(NZ))*0.5*D
    BMT=H*B*(TSTRA(1)*YOUMO(1)*ZSTEP(1)+TSTRA(NZ)*YOUMO(NZ)*ZSTEP(NZ))
   1*0.5*D**2
    N=NZ-1
    DO 180 J=2,N
    PT=PT+H*B*TSTRA(J)*YOUMO(J)*D
180 BMT=BMT+H*B*TSTRA(J)*YOUMO(J)*ZSTEP(J)*D**2
    SECMOM=2.0*B*D**3/3.0
    DO 190 J=1,21
    DEP=-DEPTH(J)+0.5
    Q=DEPTH(J)
    T2=FNTEMP(Q,TIME)
    STR(J)=-FTS(T2)*FE(T2)+PT/(B*2.*D)+DEP*(BMT+BM)/SECMOM
    STRT(J)=-FTS(T2)*FE(T2)+PT/(B*2.*D)+DEP*BMT/SECMOM
190 STRM(J)=STR(J)-STRT(J)
200 T0=FNTEMP(0.0,TIME)
    T1=FNTEMP(0.05,TIME)
    TGRAD=(T1-T0)*240.
    HEATIN=-TGRAD*FTK(T0)/3600.
    HRAD=(1.7/10.**9)*(T)**4)/3600.
    HIMP=HEATIN+HRAD
    RISK=0.
    BSTR=12.E3
    DO 240 I=1,21
    Z=DEPTH(I)
    TEMP(I)=FNTEMP(Z,TIME)
    T=TEMP(I)
    XM=FXM(T)
    SU=FSU(T)
    SO=FSO(T)
    IF(STR(I)-SMAX(I)) 215,215,210
```

```
      SMAX(I)=STR(I)
      IF(STR(I)-SU) 220,220,225
  220 RRT(I)=0.
      GO TO 230
  225 RRT(I)=0.1*((STR(I)-SU)/S0)**XM
  230 CONTINUE
      DO 260 I=1,20
      IF(RRT(I)-RRT(I+1)) 240,240,245
  240 RR(I)=RRT(I+1)
      GO TO 250
  245 RR(I)=RRT(I)
  250 IF(RR(I)-RRMAX(I)) 260,260,255
  255 RRMAX(I)=RR(I)
      TRRM(I)=TIME
      C=RR(I)
      PFL(I)=1.-EXPF(-C)
  260 RISK=RISK+RRMAX(I)
      POF=1.-EXPF(-RISK)
      WRITE OUTPUT TAPE 6,300,TIME,AL,BM,TGRAD,BSTR
  300 FORMAT (6HOTIME=,F5.2,3HMIN,4X,13HAPPLIED LOAD=,F6.1,3HLBS,4X,12HB
     1END MOMENT=,F6.1,5HIN-LBS,4X,10HTEMP GRAD=,F7.1,4HR/FT,4X,5HBSTR=,
     2F8.2,3HPSI)
      WRITE OUTPUT TAPE 6,305,HEATIN,HIMP,RISK,POF
  305 FORMAT (15H NET HEAT FLUX=,F6.2,11HBTU/FT2*SEC,4X,16HGROSS HEAT FL
     1UX=,F6.2,11HBTU/FT2*SEC,4X,5HRISK=,1PE14.8,4X,10HFAIL PROB=,0PF10.
     29)
      K1=1+(J-1)/NPRINT
      IF(K1-K2) 150,150,310
  310 K2=K1
      WRITE OUTPUT TAPE 6,315
  315 FORMAT (68HODEPTH (IN)   TEMP (R)   STRESS (PSI)   MAX STR (PSI)
     1 RR TEMPORARY  )
      WRITE OUTPUT TAPE 6,320
  320 FORMAT (1H ,70X,50HRR LAYER    RR LAYER MAX   TIME (MIN)   FAIL PR
     1OB )
      I=0
  330 I=I+1
      IF(I-21) 335,335,360
  335 WRITE OUTPUT TAPE 6,340,DEPTH(I),TEMP(I),STR(I),SMAX(I),RRT(I)
  340 FORMAT (1H ,F7.3,7X,F7.2,6A,F8.1,7X,F8.1,7X,1PE12.6)
      IF(I-20) 350,350,330
  350 WRITE OUTPUT TAPE 6,355,RR(I),RRMAX(I),TRRM(I),PFL(I)
  355 FORMAT (1H ,69X,1PE12.6,3X,1PE12.6,5X,0PF6.3,4X,9F10.8)
      GO TO 330
  360 WRITE OUTPUT TAPE 6,365
  365 FORMAT (54HODEPTH (IN)   MECH STRESS (PSI)   THERMAL STRESS (PSI))
      DO 375 I=1,21
      WRITE OUTPUT TAPE 6,370,DEPTH(I),STRM(I),STRT(I)
  370 FORMAT (1H ,F5.3,10X,F8.1,15X,F8.1)
  375 CONTINUE
      GO TO 150
      END
```

```
CBT   BEAM TEMPERATURE DISTRIBUTION FUNCTION
      FUNCTION FBTEMP(Z,TIME)
      DIMENSION TTAB(10,100),ZT(10),TS(10),TST(10),E(10),ET(10),TK(10),T
     1KT(10),WAM(10),WAMT(10),WSU(10),WSUT(10),WSO(10),WSOT(10),TT(40)
      COMMON TTAB,ZT,TS,TST,E,ET,TK,TKT,WAM,WAMT,WSU,WSUT,WSO,WSOT,TT,JJ
     1,DTIME
      JJ=2
   10 IF(TIME-TT(JJ))30,30,20
   20 JJ=JJ+1
      GO TO 10
   30 II=2
   35 IF(Z-ZT(II)) 45,45,40
   40 II=II+1
      GO TO 35
   45 TIJ=TTAB(II,JJ)
      TI1J=TTAB(II-1,JJ)
      TIJ1=TTAB(II,JJ-1)
      TI1J1=TTAB(II-1,JJ-1)
      TZ1=TI1J+(TIME-TT(JJ-1))*(TIJ-TI1J1)/0.5
      TZ=TIJ1+(TIME-TT(JJ-1))*(TIJ-TIJ1)/0.5
      FBTEMP=TZ1+(Z-ZT(II-1))*(TZ-TZ1)/(ZT(II)-ZT(II-1))+459.6
      RETURN
      END

CFTS  THERMAL STRAIN AS A FUNCTION OF TEMPERATURE
      FUNCTION FTS(T)
      DIMENSION TTAB(10,100),ZT(10),TS(10),TST(10),E(10),ET(10),TK(10),T
     1KT(10),WAM(10),WAMT(10),WSU(10),WSUT(10),WSO(10),WSOT(10),TT(40)
      COMMON TTAB,ZT,TS,TST,E,ET,TK,TKT,WAM,WAMT,WSU,WSUT,WSO,WSOT,TT,JJ
     1,DTIME
      I=1
   10 IF(T-TST(I+1))20,20,15
   15 I=I+1
      GO TO 10
   20 FTS=TS(I)+(T-TST(I))*(TS(I+1)-TS(I))/(TST(I+1)-TST(I))
      RETURN
      END

CFE   MODULUS OF ELASTICITY AS A FUNCTION OF TEMPERATURE
      FUNCTION FE(T)
      DIMENSION TTAB(10,100),ZT(10),TS(10),TST(10),E(10),ET(10),TK(10),T
     1KT(10),WAM(10),WAMT(10),WSU(10),WSUT(10),WSO(10),WSOT(10),TT(40)
      COMMON TTAB,ZT,TS,TST,E,ET,TK,TKT,WAM,WAMT,WSU,WSUT,WSO,WSOT,TT,JJ
     1,DTIME
      I=1
   10 IF(T-ET(I+1)) 20,20,15
   15 I=I+1
      GO TO 10
   20 FE=E(I)+(T-ET(I))*(E(I+1)-E(I))/(ET(I+1)-ET(I))
      RETURN
      END
```

```
C FTK  THERMAL CONDUCTIVITY AS A FUNCTION OF TEMPERATURE
       FUNCTION FTK(T)
       DIMENSION TTAB(10,100),ZT(10),TS(10),TST(10),E(10),ET(10),TK(10),T
      1KT(10),WXM(10),WXMT(10),WSU(10),WSUT(10),WSO(10),WSOT(10),TT(40)
       COMMON TTAB,ZT,TS,TST,E,ET,TK,TKT,WXM,WXMT,WSU,WSUT,WSO,WSOT,TT,JJ
      1,DTIME
       I=1
    10 IF(T-TKT(I+1)) 20,20,15
    15 I=I+1
       GO TO 10
    20 FTK=TK(I)+(T-TKT(I))*(TK(I+1)-TK(I))/(TKT(I+1)-TKT(I))
       RETURN
       END

C FXM  WEIBULL M AS A FUNCTION OF TEMPERATURE
       FUNCTION FXM(T)
       DIMENSION TTAB(10,100),ZT(10),TS(10),TST(10),E(10),ET(10),TK(10),T
      1KT(10),WXM(10),WXMT(10),WSU(10),WSUT(10),WSO(10),WSOT(10),TT(40)
       COMMON TTAB,ZT,TS,TST,E,ET,TK,TKT,WXM,WXMT,WSU,WSUT,WSO,WSOT,TT,JJ
      1,DTIME
       I=1
    10 IF(T-WXMT(I+1)) 20,20,15
    15 I=I+1
       GO TO 10
    20 FXM=WXM(I)+(T-WXMT(I))*(WXM(I+1)-WXM(I))/(WXMT(I+1)-WXMT(I))
       RETURN
       END

C FSU  WEIBULL SU AS A FUNCTION OF TEMPERATURE
       FUNCTION FSU(T)
       DIMENSION TTAB(10,100),ZT(10),TS(10),TST(10),E(10),ET(10),TK(10),T
      1KT(10),WXM(10),WXMT(10),WSU(10),WSUT(10),WSO(10),WSOT(10),TT(40)
       COMMON TTAB,ZT,TS,TST,E,ET,TK,TKT,WXM,WXMT,WSU,WSUT,WSO,WSOT,TT,JJ
      1,DTIME
       I=1
    10 IF(T-WSUT(I+1)) 20,20,15
    15 I=I+1
       GO TO 10
    20 FSU=WSU(I)+(T-WSUT(I))*(WSU(I+1)-WSU(I))/(WSUT(I+1)-WSUT(I))
       RETURN
       END

C FSO  WEIBULL SO AS A FUNCTION OF TEMPERATURE
       FUNCTION FSO(T)
       DIMENSION TTAB(10,100),ZT(10),TS(10),TST(10),E(10),ET(10),TK(10),T
      1KT(10),WXM(10),WXMT(10),WSU(10),WSUT(10),WSO(10),WSOT(10),TT(40)
       COMMON TTAB,ZT,TS,TST,E,ET,TK,TKT,WXM,WXMT,WSU,WSUT,WSO,WSOT,TT,JJ
      1,DTIME
       I=1
    10 IF(T-WSOT(I+1)) 20,20,15
    15 I=I+1
       GO TO 10
    20 FSO=WSO(I)+(T-WSOT(I))*(WSO(I+1)-WSO(I))/(WSOT(I+1)-WSOT(I))
       RETURN
       END
```

APPENDIX III

DISK ANALYSIS COMPUTER PROGRAM

The computer program used in the analysis of the disk prototype will be described in this appendix. The program is similar to the one employed in the beam analysis - the greatest difference being due to the fact that the disk is under a biaxial state of stress while the beam was under only a uniaxial state of stress. Again, the fracture algorithm of Section II is combined with the thermal and stress analyses of the disk and the material property curves of Section IV. A listing of this program as written in Fortran II for the IBM 7094 is included in this appendix.

The program is composed of a main program consisting of the thermal, stress and statistical analyses and of function subprograms for describing the functions $T(r,t)$, $E(T)$, $\varepsilon_T(T)$, $\nu(T)$, $k(T)$, $m(T)$, $\sigma_u(T)$ and $\sigma_o(T)$. The dimensions of the disk along with an arbitrary applied uniform stress at the outside radius have been incorporated into the program. The temperature distribution and the material property versus temperature curves are entered into the program through the use of tables and hence the effects of variations in these curves may be readily obtained.

As an aid in using the program, a listing describing some of the more important variables entering into the program has been included in this appendix.

Listing of Significant Program Variables:

DTIME	size of time interval between computations
E(I)	i^{th} entry in table of modulus of elasticity vs. temperature
ET(I)	temperature corresponding to E(I)
FDTEMP (R,TIME)	function subprogram for computing the temperature in the disk of radius R and time TIME

FE(T)	function subprogram for computing the modulus of elasticity at the temperature T
FNU(T)	function subprogram for computing Poisson's ratio at the temperature T
FSO(T)	function subprogram for computing the Weibull parameter σ_o at the temperature T
FSU(T)	function subprogram for computing the Weibull parameter σ_u at the temperature T
FTK(T)	function subprogram for computing the thermal conductivity k at the temperature T
FTS(T)	function subprogram for computing the thermal strain ε_T at the temperature T
FXM(T)	function subprogram for computing the Weibull parameters m at the temperature T
HIMP	gross heat flux impingent upon the inside radius of the disk
NE	number of entries in E(T) input table
NJ	number of entries with respect to t in T(r,t) input table
NNU	number of entries in ν(T) input table
NPRINT	number of time increments between occurrences of detailed output printouts
NSO	number of entries in σ_o(T) input table
NSU	number of entries in σ_u(T) input table
NTK	number of entries in k(T) input table
NTS	number of entries in ε_T(T) input table
NXM	number of entries in m(T) input table
PFR(I)	probability of failure of the i^{th} ring type subvolume up to current value of time

POF probability of failure of entire disk up to current value of time

RAD(I) i^{th} radius for ring subvolume

RISK risk of rupture of entire disk up to current value of time

RRR(I) radial risk of rupture of i^{th} ring at current value of time

RRRMAX(I) maximum value of RRR(I) up to current time

RRTR(I) radial risk of rupture computed using stresses, temperatures, etc. at RAD(I)

RRTT(I) circumferential risk of rupture computed using stresses, temperatures, etc. at RAD(I)

RT(I) i^{th} radius corresponding to TTAB(I,J)

S uniform tensile stress applied at outside radius of disk

SRMAX(I) maximum value of STRR(I) up to current time

STMAX(I) maximum value of STRT(I) up to current time

STRR(I) total radial stress at RAD(I)

STRRM(I) mechanical component of STRR(I)

STRRT(I) thermal component of STRR(I)

STRT(I) total circumferential stress at RAD(I)

STRTM(I) mechanical component of STRT(I)

STRTT(I) thermal component of STRT(I)

TIMEM maximum value of time for which computations are to be carried out

TK(I) i^{th} entry in table of thermal conductivity vs. temperature

TKT(I) temperature corresponding to TK(I)

TRMAX(I) time at which RRRMAX(I) occurred

TS(I) i^{th} entry in table of thermal strain vs. temperature

TST(I) temperature corresponding to TS(I)

TT(J)	j^{th} value of time corresponding to TTAB(I,J)
TTAB(I,J)	temperature at radius RAD(I) and time TT(J)
TTMAX(I)	time at which RRTMAX(I) occurred
WSO(I)	i^{th} entry in table of Weibull σ_o vs. temperature
WSOT(I)	temperature corresponding to WSO(I)
WSU(I)	i^{th} entry in table of Weibull σ_u vs. temperature
WSUT(I)	temperature corresponding to WSU(I)
WXM	i^{th} entry in table of Weibull m vs. temperature
WXMT(I)	temperature corresponding to WXM(I)
XNU(I)	i^{th} entry in table of Poisson's ratio vs. temperature
XNUT(I)	temperature corresponding to XNU(I)

PROGRAM LISTING

```
CM     BIAXIAL STATISTICAL STRENGTH ANALYSIS PROGRAM
       DIMENSION TTAB(12,100),RT(12),TS(10),TST(10),E(10),ET(10),TK(10),T
      1KT(10),XNU(10),XNUT(10),WXM(10),WXMT(10),WSU(10),WSUT(10),WSO(10),
      2WSOT(10),TT(40)
       COMMON TTAB,RT,TS,TST,E,ET,TK,TKT,XNU,XNUT,WXM,WXMT,WSU,WSUT,WSO,W
      1SOT,TT,JJ
       DIMENSION RA(70),STRR(70),STRT(70),STRRM(70),STRRT(70),STRTM(70),
      1STRTT(70),SRMAX(70),STMAX(70),RRTR(70),RRTT(70),RRR(70),RRT(70),
      2RRRMAX(70),RRTMAX(70),TRMAX(70),TTMAX(70),PFR(70)
       DIMENSION RSTEP(52),POISS(52),TSTRA(52),YOUMO(52),TEMP(70),RA(52),
      1TPA(52,3,3),OVTPA(52,3,3),TOIPA(3,3),INIPA(3,3)
    5  WRITE OUTPUT TAPE 6,7
    7  FORMAT (48HALUMINA DISK UNDER MECHANICAL + THERMAL LOADING )
       READ INPUT TAPE 5,10,S,DTIME,TIMEM,NPRINT
   10  FORMAT (3F10.5,I5)
       WRITE OUTPUT TAPE 6,15,S,DTIME,TIMEM,NPRINT
   15  FORMAT (3HOS=,F9.2,3X,6HDTIME=,F5.3,3X,6HTIMEM=,F7.3,3X,7HNPRINT=,
      1I3)
   20  READ INPUT TAPE 5,22,NJ,NTS,NNU,NE,NTK,NXM,NSU,NSO
   22  FORMAT (8I5)
       WRITE OUTPUT TAPE 6,24,NJ,NTS,NNU,NE,NTK,NXM,NSU,NSO
   24  FORMAT (4HONJ=,I3,3X,4HNTS=,I3,3X,4HNNU=,I3,3X,3HNE=,I3,3X,4HNTK=,
      1I3,3X,4HNXM=,I3,3X,4HNSU=,I3,3X,4HNSO=,I3)
       IF(NJ)40,40,30
   30  DO 35 J=1,NJ
       READ INPUT TAPE 5,32,(TTAB(I,J),I=1,12)
   32  FORMAT (12F6.1)
   35  CONTINUE
   40  READ INPUT TAPE 5,42,(RT(I),I=1,12)
   42  FORMAT (12F6.3)
   45  IF(NTS)50,50,47
   47  DO 49 I=1,NTS
       READ INPUT TAPE 5,48,TST(I),TS(I)
   48  FORMAT (F10.4,F10.9)
   49  CONTINUE
   50  IF(NNU)55,55,51
   51  DO 53 I=1,NNU
       READ INPUT TAPE 5,48,XNUT(I),XNU(I)
   53  CONTINUE
   55  IF(NE)65,65,57
   57  DO 62 I=1,NE
       READ INPUT TAPE 5,59,ET(I),E(I)
   59  FORMAT(F10.4,F10.2)
   62  CONTINUE
   65  IF(NTK)75,75,67
   67  DO 72 I=1,NTK
       READ INPUT TAPE 5,69,TKT(I),TK(I)
   69  FORMAT(F10.4,F10.6)
   72  CONTINUE
```

```
   75 DO 90 I=1,NJ
   90 TT(I)=FLOATF(I-1)
      WRITE OUTPUT TAPE 6,95,(RT(I),I=1,12)
   95 FORMAT(5HORT=,12F9.3)
      WRITE OUTPUT TAPE 6,97
   97 FORMAT(5H TIME)
      DO 102 J=1,NJ
      WRITE OUTPUT TAPE 6,100,TT(J),(TTAB(I,J),I=1,12)
  100 FORMAT(1H ,F5.2,12F9.1)
  102 CONTINUE
      WRITE OUTPUT TAPE 6,105

  105 FORMAT(27HOTEMP (R)   TSTRAIN (IN/IN))
      DO 110 I=1,NTS
      WRITE OUTPUT TAPE 6,107,TST(I),TS(I)
  107 FORMAT(1H ,F8.2,5X,1PE14.8)
  110 CONTINUE
      WRITE OUTPUT TAPE 6,112
  112 FORMAT(25HOTEMP (R)   POISSON RATIO)
      DO 115 I=1,NNU
      WRITE OUTPUT TAPE 6,114,XNUT(I),XNU(I)
  114 FORMAT(1H ,F8.2,6X,F6.4)
  115 CONTINUE
      WRITE OUTPUT TAPE 6,119
  119 FORMAT(35HOTEMP(R)   MOD OF ELASTICITY (PSI) )
      DO 120 I=1,NE
      WRITE OUTPUT TAPE 6,107,ET(I),E(I)
  120 CONTINUE
      WRITE OUTPUT TAPE 6,125
  125 FORMAT(38HOTEMP (R)   THERMAL COND (BTU/FT*HR*R))
      DO 130 I=1,NTK
      WRITE OUTPUT TAPE 6,107,TKT(I),TK(I)
  130 CONTINUE
      IF(TIMEM-TT(NJ))135,135,132
  132 TIMEM=TT(NJ)
  135 TIME=-DTIME
      J=0
      K2=0
      II=1
      JJ=2
      LL=0
      RAD(1)=.5
      DO 137 I=2,70
  137 RAD(I)=SQRTF(RAD(I-1)**2+.12681159)
      DO 139 I=1,70
      SRMAX(I)=0.
      STMAX(I)=0.
      RRRMAX(I)=0.
      RRTMAX(I)=0.
      TRMAX(I)=0.
      TTMAX(I)=0.
```

```
      139 PFR(I)=0.
          DO 141 I=1,NXM
          READ INPUT TAPE 5,69,WXMT(I),WXM(I)
          WRITE OUTPUT TAPE 6,140,I,WXMT(I),I,WXM(I)
      140 FORMAT(6HOWXMT(,I1,2H)=,F10.2,3H(R),5X,4HWXM(,I1,2H)=,F6.4)
      141 CONTINUE
          DO 145 I=1,NSU
          READ INPUT TAPE 5,59,WSUT(I),WSU(I)
          WRITE OUTPUT TAPE 6,143,I,WSUT(I),I,WSU(I)
      143 FORMAT(6HOWSUT(,I1,2H)=,F10.2,3H(R),5X,4HWSU(,I1,2H)=,F10.2,5H(PSI
         1))
      145 CONTINUE
          DO 149 I=1,NSO
          READ INPUT TAPE 5,59,WSOT(I),WSO(I)
          WRITE OUTPUT TAPE 6,146,I,WSOT(I),I,WSO(I)
      146 FORMAT(6HOWSOT(,I1,2H)=,F10.2,3H(R),5X,4HWSO(,I1,2H)=,F10.2,5H(PSI
         1))
      149 CONTINUE
      150 TIME=TIME+DTIME
          LL=LL+1
          IF(TIME-TIMEM)155,155,5


      155 P=50.25
          RSTEP(1)=0.5
          NR=51
          NT=50
          RSTEP(NR)=3.0
          PNT=NT
          N=NT
          DO 160 J=2,N
      160 RSTEP(J)=RSTEP(J-1)+(2.5/PNT)
          H=.25
          DO 170 J=1,NT
          TR=(RSTEP(J+1)-RSTEP(J))/2.0+RSTEP(J)
          T=FUTEMP(TM,TIME)
          TEMP(J)=T
          YOUMO(J)=FF(T)
          TSTRA(J)=FS(T)
          POISS(J)=FNU(T)
      170 CONTINUE
          N=NT
          DO 175 J=1,N
          RA(J+1)=1.0-(RSTEP(J)/RSTEP(J+1))**2
          TPA(J+1,1,1)=(45*EP(J+1)/RSTEP(J))*(1.0-(1.0+POISS(J))/2.0*RA(J+1)
         1)
          TPA(J+1,1,2)=RSTEP(J+1)*(2.0-POISS(J)**2)*RA(J+1)/(YOUMO(J)*H*2.0)
          TPA(J+1,1,3)=(1.0+POISS(J))/2.0*TSTRA(J)*RSTEP(J+1)*PA(J+1)
          TPA(J+1,2,1)=(YOUMO(J)*RSTEP(J+1))/(2.*RSTEP(J))
          TPA(J+1,2,2)=1.0-(1.0-POISS(J))*RA(J+1)/2.0
          TPA(J+1,2,3)=-H*YOUMO(J)*TSTRA(J)*RA(J+1)/2.0
          TPA(J+1,3,1)=0.0
          TPA(J+1,3,2)=0.0
```

```
175 TPA(J+1,3,3)=1.0
    OVIPA(1,1,1)=1.0
    OVIPA(1,1,2)=0.0
    OVIPA(1,1,3)=0.0
    OVIPA(1,2,1)=0.0
    OVIPA(1,2,2)=1.0
    OVIPA(1,2,3)=0.0
    OVIPA(1,3,1)=0.0
    OVIPA(1,3,2)=0.0
    OVIPA(1,3,3)=1.0
    DO 180 K=1,3
    DO 180 L=1,3
180 OVIPA(2,K,L)=TPA(2,K,L)
    N=NT+1
    IF(N-3) 195,185,185
185 DO 190 J=3,N
    DO 190 L=1,3
    DO 190 M=1,3
190 OVIPA(J,L,M)=TPA(J,L,1)*OVIPA(J-1,1,M)+TPA(J,L,2)*OVIPA(J-1,2,M)+
   1TPA(J,L,3)*OVIPA(J-1,3,M)
195 TP=(P-OVIPA(NT+1,2,3))/OVIPA(NT+1,2,1)
    DO 240 K=1,T0
    J=1
    P1=PA(K)
200 R2=RSTEP(J)
    IF(R2-P1) 205,210,225
205 J=J+1
    GO TO 200
210 DO 215 I=1,3
    DO 215 L=1,3
215 TOIPA(I,L)=OVIPA(J,I,L)
    IF(J-1) 235,235,220
220 J=J-1
    GO TO 235
225 J=J-1
    RF1=1.0-(RSTEP(J)/R1)**2
    TNIPA(1,1)=(R1/RSTEP(J))*(1.0-(1.0-POISS(J))/2.0*RF1)
    TNIPA(1,2)=R1*1.0-POISS(J)**2)*RF1)/(YOUNG(J)*H*2.0)
    TNIPA(1,3)=(1.0-POISS(J))/2.0*STRA(J)*R1*RF1
    TNIPA(2,1)=(YOUNG(J)*H*RF1)/(2.0*RSTEP(J))
    TNIPA(2,2)=1.0-(1.0-POISS(J))*RF1/2.0
    TNIPA(2,3)=-H*YOUNG(J)*STRA(J)*RF1/2.0
    TNIPA(3,1)=0.0
    TNIPA(3,2)=0.0
    TNIPA(3,3)=1.0
    DO 230 L=1,3
    DO 230 I=1,3
230 TOIPA(L,I)=TNIPA(L,1)*OVIPA(J,1,I)+TNIPA(L,2)*OVIPA(J,2,I)+
   1TNIPA(L,3)*OVIPA(J,3,I)
235 DISP=TP*TOIPA(1,1)+TOIPA(1,3)
    T=FNTEMP(R1,TIME)
    STRR(K)= (TP*TOIPA(2,1)+TOIPA(2,3))/H
    STRT(K)=PE(T)*DISP/R1+FNU(T)*STRR(K)-PE(T)*PTS(T)
```

```
      TPO=-OVIPA(NT+1,2,3)/OVIPA(NT+1,2,1)
      DISPO=TPO*TOIPA(1,1)+TOIPA(1,3)
      STRRT(K)=(TPO*TOIPA(2,1)+TOIPA(2,3))/M
      STRTT(K)=FE(T)*DISPO/R1+FNO(T)*STRRT(K)-FE(T)*PTS(T)
      STRRM(K)=STRR(K)-STRRT(K)
      STRTM(K)=STRT(K)-STRTT(K)
  240 CONTINUE
  250 TO=FOTEMP(0.5,TIME)
      T1=FOTEMP(0.55,TIME)
      TGRAD=(T1-TO)*240.
      HEATIN=-TGRAD*PTY(TO)/3600.
      HRAD=(1./11./10.**9)*(TO**4)/3600.
      HIMP=HEATIN+HRAD
      RISK=0.
      RISKR=0.
      RISKT=0.
      DO 300 I=1,70
      TR=RAD(I)
      TEMP(I)=FOTEMP(TR,TIME)
      T=TEMP(I)
      XM=FXM(T)
      SO=FSO(T)
      SO=FSO(T)
      IF(STRR(I)-SRMAX(I))265,265,260
  260 SRMAX(I)=STRR(I)
  265 IF(STRR(I)-SO)270,270,275
  270 PRTR(I)=0.
      GO TO 278
  275 PRTR(I)=.09959765*((STRR(I)-SO)/SO)**XM
  278 IF(STRT(I)-STMAX(I))285,285,280
  280 STMAX(I)=STRT(I)
  285 IF(STRT(I)-SO)290,290,295
  290 PRTT(I)=0.
      GO TO 300
  295 PRTT(I)=.09959765*((STRT(I)-SO)/SO)**XM
  300 CONTINUE
      DO 350 I=1,69
      IF(PRTR(I)-PRTM(I+1))310,310,315
  310 PRR(I)=PRTM(I+1)
      GO TO 320
  315 PRR(I)=PRTM(I)
  320 IF(PRR(I)-PRRMAX(I))328,328,325
  325 PRRMAX(I)=PRR(I)
      TRMAX(I)=TIME
  328 CR=PRRMAX(I)
      IF(PRTT(I)-PRTT(I+1))330,335,335
  330 PRT(I)=PRTT(I+1)
      GO TO 340
  335 PRT(I)=PRTT(I)
  340 IF(PRT(I)-PRTMAX(I))348,348,345
  345 PRTMAX(I)=PRT(I)
      TTMAX(I)=TIME
```

```
348 CT=RRTMAX(I)
    PFR(I)=1.-EXPF(-CR-CT)
    RISKR=RISKR+RRRMAX(I)
350 RISKT=RISKT+RTIMAX(I)
    RISK=RISKR+RISKT
    POFR=1.-EXPF(-RISKR)
    POFT=1.-EXPF(-RISKT)
    POF=1.-EXPF(-RISK)
    WRITE OUTPUT TAPE 6,360,TIME,S,TU,TGRAD
360 FORMAT(6HOTIME=,F5.2,3HMIN,4X,15HAPPLIED STRESS=,F7.1,3HPSI,4X,10H
   1SURF TEMP=,F6.1,1HR,5X,10HTEMP GRAD=,F7.1)
    WRITE OUTPUT TAPE 6,365,HEATIN,HRAD,HIMP
365 FORMAT(15H NET HEAT FLUX=,F6.2,11HBTU/FT2*SEC,4X,9HHEAT RAD=,F4.2,
   111HBTU/FT2*SEC,4X,16HGROSS HEAT FLUX=,F6.1,11HBTU/FT2*SEC)
    WRITE OUTPUT TAPE 6,370,POFR,POFT,RISK,POF
370 FORMAT(15H RAD FAIL PROB=,F10.8,4X,15H TAN FAIL PROB=,F10.8,4X,13H
   1OVERALL RISK=,1PE14.8,19H OVERALL FAIL PROB=,0PF10.8)
    K1=1+(LL-1)/NPRINT
    IF(K1-K2)150,150,375
375 K2=K1
    WRITE OUTPUT TAPE 6,380
380 FORMAT(99HO   RADIUS     TEMP      STRRM      STRTM      STRRT      STR
   1TT       STRR       STRT       SRMAX      STMAX  )
    DO 390 I=1,70
    WRITE OUTPUT TAPE 6,385,RAD(I),TEMP(I),STRRM(I),STRTM(I),STRRT(I),
   1STRTT(I),STRR(I),STRT(I),SRMAX(I),STMAX(I)
385 FORMAT(1H ,F8.4,9F10.0)
390 CONTINUE
    WRITE OUTPUT TAPE 6,395
395 FORMAT(29HO RAD         RR*R          RRTT)
    WRITE OUTPUT TAPE 6,400
400 FORMAT(1H ,39X,76HRRR              RRT            RRRMAX       TRMAX
   1    RRTMAX     TTMAX       PFR )
    I=0
    OPFR=0.
    PFR(70)=-1.
410 I=I+1
    IF(PFR(I)-OPFR)420,410,420
420 WRITE OUTPUT TAPE 6,425,RAD(I),RRTR(I),RRTT(I)
425 FORMAT(1H ,F8.3,1PE14.6,F14.6)
    IF(I-69)430,430,150
430 IF(PFR(I))432,431,432
431 OPFR=0.
    GO TO 410
432 OPFR=PFR(I)

    WRITE OUTPUT TAPE 6,435,RRR(I),RR(I),RRRMAX(I),TRMAX(I),RRTMAX(I)
   1,TTMAX(I),PFR(I)
435 FORMAT(1H ,35X,1PE14.6,2F14.6,0PF7.3,1PE14.6,0PF7.3,1PE14.6)
    GO TO 410
    END
```

```
CDT   DISK TEMPERATURE DISTRIBUTION FUNCTION
      FUNCTION FDTEMP(R,TIME)
      DIMENSION TTAB(12,100),RT(12),TS(10),TST(10),E(10),ET(10),TK(10),T
     1KT(10),XNU(10),XNUT(10),WXM(10),WXMT(10),WSU(10),WSUT(10),WSO(10),
     2WSOT(10),TT(40)
      COMMON TTAB,RT,TS,TST,E,ET,TK,TKT,XNU,XNUT,WXM,WXMT,WSU,WSUT,WSO,W
     1SOT,TT,JJ
   10 IF(TIME-TT(JJ))30,30,20
   20 JJ=JJ+1
      GO TO 10
   30 II=2
   35 IF(R-RT(II))45,45,40
   40 II=II+1
      GO TO 35
   45 TIJ=TTAB(II,JJ)
      TI1J=TTAB(II-1,JJ)
      TIJ1=TTAB(II,JJ-1)
      TI1J1=TTAB(II-1,JJ-1)
      TR1=TI1J1+(TIME-TT(JJ-1))*(TI1J-TI1J1)
      TR=TIJ1+(TIME-TT(JJ-1))*(TIJ-TIJ1)
      FDTEMP=TR1+(R-RT(II-1))*(TR-TR1)/(RT(II)-RT(II-1))+459.6
      RETURN
      END

CFTS  THERMAL STRAIN AS A FUNCTION OF TEMPERATURE
      FUNCTION FTS(T)
      DIMENSION TTAB(12,100),RT(12),TS(10),TST(10),E(10),ET(10),TK(10),T
     1KT(10),XNU(10),XNUT(10),WXM(10),WXMT(10),WSU(10),WSUT(10),WSO(10),
     2WSOT(10),TT(40)
      COMMON TTAB,RT,TS,TST,E,ET,TK,TKT,XNU,XNUT,WXM,WXMT,WSU,WSUT,WSO,W
     1SOT,TT,JJ
      I=1
   10 IF(T-TST(I+1))20,20,15
   15 I=I+1
      GO TO 10
   20 FTS=TS(I)+(T-TST(I))*(TS(I+1)-TS(I))/(TST(I+1)-TST(I))
      RETURN
      END

CFE   MODULUS OF ELASTICITY AS A FUNCTION OF TEMPERATURE
      FUNCTION FE(T)
      DIMENSION TTAB(12,100),RT(12),TS(10),TST(10),E(10),ET(10),TK(10),T
     1KT(10),XNU(10),XNUT(10),WXM(10),WXMT(10),WSU(10),WSUT(10),WSO(10),
     2WSOT(10),TT(40)
      COMMON TTAB,RT,TS,TST,E,ET,TK,TKT,XNU,XNUT,WXM,WXMT,WSU,WSUT,WSO,W
     1SOT,TT,JJ
      I=1
   10 IF(T-ET(I+1)) 20,20,15
   15 I=I+1
      GO TO 10
   20 FE=E(I)+(T-ET(I))*(E(I+1)-E(I))/(ET(I+1)-ET(I))
      RETURN
      END
```

```
C FNU  POISSON RATIO AS A FUNCTION OF TEMPERATURE
       FUNCTION FNU(T)
       DIMENSION TTAB(12,100),RT(12),TS(10),TST(10),E(10),ET(10),TK(10),T
      1KT(10),XNU(10),XNUT(10),WXM(10),WXMT(10),WSU(10),WSUT(10),WSO(10),
      2WSOT(10),TT(40)
       COMMON TTAB,RT,TS,TST,E,ET,TK,TKT,XNU,XNUT,WXM,WXMT,WSU,WSUT,WSO,W
      1SOT,TT,JJ
       I=1
   10  IF(T-XNUT(I+1))20,20,15
   15  I=I+1
       GO TO 10
   20  FNU=XNU(I)+(T-XNUT(I))*(XNU(I+1)-XNU(I))/(XNUT(I+1)-XNUT(I))
       RETURN
       END

C FTK  THERMAL CONDUCTIVITY AS A FUNCTION OF TEMPERATURE
       FUNCTION FTK(T)
       DIMENSION TTAB(12,100),RT(12),TS(10),TST(10),E(10),ET(10),TK(10),T
      1KT(10),XNU(10),XNUT(10),WXM(10),WXMT(10),WSU(10),WSUT(10),WSO(10),
      2WSOT(10),TT(40)
       COMMON TTAB,RT,TS,TST,E,ET,TK,TKT,XNU,XNUT,WXM,WXMT,WSU,WSUT,WSO,W
      1SOT,TT,JJ
       I=1
   10  IF(T-TKT(I+1)) 20,20,15
   15  I=I+1
       GO TO 10
   20  FTK=TK(I)+(T-TKT(I))*(TK(I+1)-TK(I))/(TKT(I+1)-TKT(I))
       RETURN
       END

C FXM  WEIBULL M AS A FUNCTION OF TEMPERATURE
       FUNCTION FXM(T)
       DIMENSION TTAB(12,100),RT(12),TS(10),TST(10),E(10),ET(10),TK(10),T
      1KT(10),XNU(10),XNUT(10),WXM(10),WXMT(10),WSU(10),WSUT(10),WSO(10),
      2WSOT(10),TT(40)
       COMMON TTAB,RT,TS,TST,E,ET,TK,TKT,XNU,XNUT,WXM,WXMT,WSU,WSUT,WSO,W
      1SOT,TT,JJ
       I=1
   10  IF(T-WXMT(I+1)) 20,20,15
   15  I=I+1
       GO TO 10
   20  FXM=WXM(I)+(T-WXMT(I))*(WXM(I+1)-WXM(I))/(WXMT(I+1)-WXMT(I))
       RETURN
       END
```

```
C FSU  WEIBULL SU AS A FUNCTION OF TEMPERATURE
       FUNCTION FSU(T)
       DIMENSION TTAB(12,100),RT(12),TS(10),TST(10),E(10),ET(10),TK(10),T
      1KT(10),XNU(10),XNUT(10),WXM(10),WXMT(10),WSU(10),WSUT(10),WSO(10),
      2WSOT(10),TT(40)
       COMMON TTAB,RT,TS,TST,E,ET,TK,TKT,XNU,XNUT,WXM,WXMT,WSU,WSUT,WSO,W
      1SOT,TT,JJ
       I=1
    10 IF(T-WSUT(I+1)) 20,20,15
    15 I=I+1
       GO TO 10
    20 FSU=WSU(I)+(T-WSUT(I))*(WSU(I+1)-WSU(I))/(WSUT(I+1)-WSUT(I))
       RETURN
       END

C FSO  WEIBULL SO AS A FUNCTION OF TEMPERATURE
       FUNCTION FSO(T)
       DIMENSION TTAB(12,100),RT(12),TS(10),TST(10),E(10),ET(10),TK(10),T
      1KT(10),XNU(10),XNUT(10),WXM(10),WXMT(10),WSU(10),WSUT(10),WSO(10),
      2WSOT(10),TT(40)
       COMMON TTAB,RT,TS,TST,E,ET,TK,TKT,XNU,XNUT,WXM,WXMT,WSU,WSUT,WSO,W
      1SOT,TT,JJ
       I=1
    10 IF(T-WSOT(I+1)) 20,20,15
    15 I=I+1
       GO TO 10
    20 FSO=WSO(I)+(T-WSOT(I))*(WSO(I+1)-WSO(I))/(WSOT(I+1)-WSOT(I))
       RETURN
       END
```

REFERENCES

1. Barnett, R. L., "Utilization of Refractory Nonmetallic Materials in Future Aerospace Vehicles," Part 1, "Review of Structural Design Techniques for Brittle Components Under Static Loads," FDL-TDR-64-123, September, 1964.

2. Barnett, R. L.,Costello, J. F., Hermann, P. C. and Hofer, K.E., "The Behavior and Design of Brittle Structures," AFFDL-TR-65-165, September, 1965.

3. Schwartz, B., Thermal Stress Failure of Pure Refractory Oxides; J. Amer. Cer. Soc., 35 (12), 325-33, 1952, (S-950).

4. Hess, F. O., Investigation of Pure Oxide Ceramic Materials Intended for High Temperature and High Stress Applications; FIAT Final Report No. 924, September 1946, PB 47012, (S-434).

5. Ryshkewitsch, E., The Compressive Strength of Pure Refractories Ber. Deut. Keram. Ges., 22, 54-65, 1951, (S-905)

6. Ryshkewitsch, E. One Component Oxide Ceramics on the Basis of Physical Chemistry, Berlin, Springer-Verlag, 1948 (S-907).

7. Christian, W. J., et. al., "Evaluation of Thermal Protective Systems for Advanced Aerospace Vehicles," ML-TDR-64-204, Vol. II, April 1965.

8. Pears, C. D. and Starrett, ., "Experimental Studies of Weibull Volume Theory," AFML 66-228, 1966.

9. Goldsmith, A., Hirschhorn, H. J. and Waterman, T. E. "Thermophysical Properties of Solid Materials," WADC TR-58-476, Vol. III, November 1960.

10. Dally, J. W., "Design Data for Materials Employed in Thermal Protective Systems on Advanced Aerospace Vehicles," ML-TDR-64-204, Vol. III, August, 1965.

11. Coble, R. L. and Kingery, W. D., "Effect of Porosity on Physical Properties of Sintered Alumina," J. Amer. Cer. Soc., 39 (11), pp. 377-85, 1956.

12. Boley, B. A. and Weiner, J. H., Theory of Thermal Stresses, John Wiley and Sons, New York, 1960, pp. 288-311.

13. Pestel, E. and Leckie, F., Matrix Methods in Elastomechanics, McGraw Hill, New York, 1963.

14. Weibull, W., "A Statistical Theory of the Strength of Material: Ing. Vetenskaps Akad., 151, pp. 1-45, 1939.

15. Grassi, R. C. and Cornet, I., "Fracture of Gray-Cast-Iron Tubes Under Biaxial Stresses," J.A.M., June, 1949, pp. 178-182.

16. Gregory, L. D., and Spruill, C. E., "Structural Reliability of Re-entry Vehicles Using Brittle Materials in Primary Structure," IAS Aerospace Systems Reliability Symposium, Salt Lake City, April, 1962.

17. Barnett, R. L. and McGuire, R. L., "Statistical Approach to Analysis and Design of Ceramic Structures," Amer. Cer. Soc. Bull., Vol. 45, No. 6, June 7, 1966.